Numerical Study of the Parametrically Driven Damped Nonlinear Schrödinger Equation.

by

M. Bondila

Submitted in fulfilment of

the M.Sc. Degree

in the Applied Mathematics Department

at the University of Cape Town.

September 1995

Contents

Chapter 1

Introduction

"It does not say in the Bible that all laws of nature are expressible linearly!"
Enrico Fermi

1.1 About nonlinearity, attractors and all that

Two great discoveries, each of which was made with the aid of the computer, have completely reshaped mathematical physics over the past twenty years. These are the strange attractor and the soliton, with the link between the two being a powerful general principle: nonlinearity. Whenever the collective behaviour of a composite system is qualitativelly different from that of the sum of the individual parts (whether these components are neurons, bit strings, ants or normal oscillation modes), one may claim that the system is *nonlinear*.

Traditionally, a dynamicist would believe that to write down a system's equations is to understand the system. How better to capture the essential features? For a playground swing, the equations tie together the pendulum's angle, its velocity, friction, and the force driving it. But because of the little bits of nonlinearity in these equations, a dynamicist would find himself helpless to answer the easiest practical question about the future of the system. The tradition of looking at systems locally — isolating the mechanisms and then adding them together — broke down. For pendulums, for fluids, for electronic circuits, for lasers, knowledge of the fundamental equations no longer is the right kind of knowledge. The first to understand this was Henri Poincaré [1] who wrote at the turn of the century:

A very small cause which escapes our notice determines a considerable effect that we cannot fail to see, and then we say that the effect is due to chance. If we knew exactly the laws of nature and the situation of the universe at the initial moment, we could predict exactly the situation of the same universe at a succeeding moment. But even if it were the case that the natural laws had no longer secret for us, we could still know the situation approximatelly. If that enabled us to predict the succeeding situation with the same approximation, that is all we require, and we should say that the phenomenon had been predicted, that it is governed by the laws. But it is not always so; it may happen that small differences in the initial conditions

produce very great ones in the final phenomena. A small error in the former will produce an enormous error in the latter. Prediction becomes impossible...

Only lately, the scientists learned to look at their differential equations in the sense expressed by Poincaré, meaning not locally but globally. That is, they want to "vizualize" the full range of behaviours of a system exploring patiently the outcome from different starting conditions. And this is the idea that has been guiding us in the numerical study presented here [93].

But the starting conditions of a real system are never known precisely, and may be totally unknown: what initial conditions should be assumed for a complex model of the atmosphere, or an oilrig at sea in a developing storm? So since the motions of a nonlinear system can depend crucially on these conditions, a mammoth task begins to emerge. How can we hope to explore the responses from all possible starts?

Clearly we need some overview of what can happen in the evolution of a system, and how this is influenced by the starting conditions. Here we have our first major guidance from dynamical systems theory in the concept of *attractor*. By definition, attractors have the important property of stability — in a real system, where moving parts are subject to bumps and jiggles from the real-world noise, motion tends to return to the attractor. A bump may shove a trajectory away for a brief time, but the resultant start-up transient dies out and the motion settles down towards some form of long-term recurrent behaviour. Motions from adjacent starts tend to converge towards stable, attracting solutions [9].

The simplest is a stationary equilibrium point at which all motion has ceased. The archetypal example of this, studied experimentally by Newton, is the pendulum. From whatever starting values of position and velocity, this returns to its vertical hanging state, damped by air resistance and other forms of energy dissipation. In the two-dimensional abstract *phase space* whose coordinates are the displacement and velocity, all possible motions appear as non-crossing spirals converging asymptotically towards the resting state at the origin. This focus in the *phase portrait* of all possible motions is called a *point attractor*.

Secondly, we have the *periodic attractor*. If a thin steel strip is driven into resonance by an electromagnet carrying an alternating current, the strip will normally settle into a steady vibration at the frequency of the forcing. After a small knock, trasients will slowly decay, and the stable fundamental oscillation will be re-established. But given a bigger initial disturbance, an entirely new stable steady state may be observed. Different starts of a given system may thus lead to alternative final states, with multiple attractors coexisting in the phase portrait of a single dynamical system in a state of competition.

A third attractor whose unexpected features have generated an explosion of interest recently, is the *strange*, or *chaotic attractor*. It captures the solution of a perfectly deterministic and well defined equation into a steady but perpetual chaos. But although a single time history possesses an aspect of true randomness and a noisy broadband power spectrum, a comprehensive phase-space investigation reveals an underlying order in the ensemble of all trajectories [9].

Pendulum dynamics broadened to cover high technologies from lasers to superconducting Josephson junctions. Some chemical reactions displayed pendulum-like behaviour, as did

the beating heart. The unexpected possibilities extended to physiological and psychiatric medicine, economic forecasting, and perhaps evolution of the society. From microscopic particles to everyday complexity, nonlinear terms made their way into the governing equations. Just to illustrate this, without even trying to cover the full range of the fields of where they arise, we shall recall briefly some of the most important nonlinear evolution equations.

The KdV equation

$$q_t + 6qq_x + q_{xxx} = 0, \tag{1.1}$$

was first derived by Korteweg and deVries to describe the lossless propagation of shallow water waves, but also arises anywhere when one wishes to include (and balance) a weak nonlinearity and a weak dispersive effect. Such studies include ion acoustic waves in plasma, long waves in shear flows, pressure waves in liquid-gas bubble mixture, thermally excited phonon packets in low-temperature nonlinear crystals (see [24] and [25] for references) and a host of other situations. The anharmonic modes in lattices and molecules are described by the *modified* KdV (see, e. g., [24, 26] for references):

$$q_t + 6q^2q_x + q_{xxx} = 0. \tag{1.2}$$

A wide interest is still today granted to the *Toda lattice* equations,

$$\begin{aligned} m\frac{d^2y_n}{dt^2} &= a\Big(e^{-br_n} - e^{-br_{n+1}}\Big), \\ r_n &= y_n - y_{n+1},\ n = 1, 2, \ldots; \quad a, b = \text{const} \end{aligned} \tag{1.3}$$

which have been widely used as a model for the dynamical and statistical properties of a variety of physical systems, from nonlinear solids subject to shock waves [27] to complex biological molecules, as the protein and DNA [28].

The *sine-Gordon* equation,

$$q_{xx} - q_{tt} = \sin q, \tag{1.4}$$

appears in nonlinear optics where it describes the propagation of light pulses in resonant media. In condensed matter physics it is used to model charge density waves in periodic pinning potentials; spin waves in liquid He^3; magnetic flux propagation in a Josephson transmission line. It is related to the $O(3)$ σ-model (n-field) arising in the field theory; its solutions exhibit many properties of elementary particles. It is found in statistical mechanics where it is used in the description of the critical region of Ising-like models. For a list of the many contexts in which (1.4) arises, we refer to [24, 29, 4, 30].

If one could be impressed by all the places in which either the KdV, Toda or the sine-Gordon equation arise, he or she would be truly amazed at the universality and ubiquity of the *Nonlinear Schrödinger Equation* (NLS). It is an equation for a complex scalar field $\psi(x,t)$:

$$i\psi_t + \psi_{xx} \pm 2|\psi|^2\psi = 0. \tag{1.5}$$

the beating heart. The unexpected possibilities extended to physiological and psychiatric medicine, economic forecasting, and perhaps evolution of the society. From microscopic particles to everyday complexity, nonlinear terms made their way into the governing equations. Just to illustrate this, without even trying to cover the full range of the fields of where they arise, we shall recall briefly some of the most important nonlinear evolution equations.

The KdV equation

$$q_t + 6qq_x + q_{xxx} = 0, \tag{1.1}$$

was first derived by Korteweg and deVries to describe the lossless propagation of shallow water waves, but also arises anywhere when one wishes to include (and balance) a weak nonlinearity and a weak dispersive effect. Such studies include ion acoustic waves in plasma, long waves in shear flows, pressure waves in liquid-gas bubble mixture, thermally excited phonon packets in low-temperature nonlinear crystals (see [24] and [25] for references) and a host of other situations. The anharmonic modes in lattices and molecules are described by the *modified* KdV (see, e. g., [24, 26] for references):

$$q_t + 6q^2q_x + q_{xxx} = 0. \tag{1.2}$$

A wide interest is still today granted to the *Toda lattice* equations,

$$\begin{aligned} m\frac{d^2y_n}{dt^2} &= a\Big(e^{-br_n} - e^{-br_{n+1}}\Big), \\ r_n &= y_n - y_{n+1},\ n = 1, 2, \ldots; \quad a, b = \text{const} \end{aligned} \tag{1.3}$$

which have been widely used as a model for the dynamical and statistical properties of a variety of physical systems, from nonlinear solids subject to shock waves [27] to complex biological molecules, as the protein and DNA [28].

The *sine-Gordon* equation,

$$q_{xx} - q_{tt} = \sin q, \tag{1.4}$$

appears in nonlinear optics where it describes the propagation of light pulses in resonant media. In condensed matter physics it is used to model charge density waves in periodic pinning potentials; spin waves in liquid He^3; magnetic flux propagation in a Josephson transmission line. It is related to the $O(3)$ σ-model (n-field) arising in the field theory; its solutions exhibit many properties of elementary particles. It is found in statistical mechanics where it is used in the description of the critical region of Ising-like models. For a list of the many contexts in which (1.4) arises, we refer to [24, 29, 4, 30].

If one could be impressed by all the places in which either the KdV, Toda or the sine-Gordon equation arise, he or she would be truly amazed at the universality and ubiquity of the *Nonlinear Schrödinger Equation* (NLS). It is an equation for a complex scalar field $\psi(x,t)$:

$$i\psi_t + \psi_{xx} \pm 2|\psi|^2\psi = 0. \tag{1.5}$$

Herschel, he said "It is merely half of a common wave that has been cut off". But it is not so, because the common waves go partly above and partly below the surface level; and not only that but its shape is different. Instead of being half a wave it is clearly a whole wave, with this difference, that the whole wave is not above and below the surface alternately but always above it. So much for what a heap of water does: it will not stay where it is but travel to a distance [46].

Both the KdV and NLS equations arise as asymptotic solvability conditions. That is, they arise as the leading order approximation to the solution of a more complicated set of equations which ensures that the higher orders of the approximation remain uniformly bounded. We will exemplify this procedure by deriving the NLS in the next section. Some other universal equations, also derived by this process and which also admit soliton solutions, are the sine-Gordon (1.4) and the modified KdV equation (1.2), the derivative nonlinear Schrödinger equation,

$$i\psi_t + \psi_{xx} \pm i(|\psi|^2\psi)_x = 0; \tag{1.8}$$

the three-wave interaction equations,

$$(\partial_t + \vec{v_j} \cdot \vec{\nabla})q_j + \eta_j q_k^* q_l^* = 0, \quad (+j,k,l \text{ cycled over } 1,2,3); \tag{1.9}$$

the Boussinesq equation,

$$q_{tt} - q_{xx} - q_{xxxx} + 3(q^2)_{xx} = 0; \tag{1.10}$$

the Kadomtsev-Petviashvili (the "two-dimensional KdV") equation,

$$(q_t + q_{xxx} - 6qq_x)_x \pm q_{yy} = 0; \tag{1.11}$$

the Benjamino-Ono equation,

$$q_t + \mathbf{H}q_{xx} - 6qq_x = 0, \text{ where } \mathbf{H} \text{ is the Hilbert transform;} \tag{1.12}$$

the massive Thirring model,

$$\begin{aligned} iu_\eta &+ v + u|v|^2 = 0, \\ iv_\xi &+ u + v|u|^2 = 0; \end{aligned}$$

the Gross-Neveu model,

$$\begin{aligned} iu_\eta^{(n)} &= v^{(n)} \sum_{m=1}^{N} \left(v^{(m)*} u^{(m)} + u^{(m)*} v^{(m)} \right), \\ iv_\xi^{(n)} &= u^{(n)} \sum_{m=1}^{N} \left(u^{(m)*} v^{(m)} + v^{(m)*} u^{(m)} \right); \end{aligned}$$

the Vaks-Larkin-Nambu-Jona Lasinio model,

$$\begin{aligned} iu_x^{(n)} &= v^{(n)} \sum_{m=1}^{N} v^{(m)*} u^{(m)}, \\ iv_t^{(n)} &= u^{(n)} \sum_{m=1}^{N} u^{(m)*} v^{(m)}; \end{aligned}$$

the $O(3)$ sigma-model,

$$\vec{v}_{xt} + (\vec{v}_x \cdot \vec{v}_t)\vec{v} = 0, \quad (\vec{v} \cdot \vec{v}) = 1, \vec{v} = (v_1, v_2, v_3); \tag{1.13}$$

the Benney-Roskes-Davey-Stewartson (the "two-dimensional NLS") equation :

$$\begin{aligned} iu_t &- u_{xx} + u_{yy} + u|u|^2 - 2uv = 0, \\ v_{xx} &+ v_{yy} - (|u|^2)_{yy} = 0. \end{aligned}$$

What is remarkable and still unexplained, is that so many of the equations, derived as asymptotic solvability conditions under very general and widely applicable assumptions, are also integrable equations with soliton solutions. One of the key properties of such equations is that they have an infinite number of conservation laws and associated symmetries. It is certainly clear that, in developing mathematical models for physical situations, one naturally includes certain symmetries (like translational invariance) which discard the unnecessary and focus on the essential features of the process under investigation. But why should the process of finding the assymtotic solvability condition introduce so many symmetries, most of which are hidden and not readily accessible to physical interpretation? If one is given a hatful of equations and asked to pick one at random from this hat, it is very unlikely that it would be completely integrable. Yet in the hatful of equations that physics provides as asymptotic solvability conditions, there would appear to be a disproportionate share of ones with integrability properties and soliton solutions [6].

What one means by an integrable equation? We have hinted that this concept is intimately related with the concept of a soliton. All we have said so far is that a soliton is a solitary, travelling wave solution of a nonlinear partial differential equation with remarkable stability and particle-like properties. However, a true soliton, a solution to an equation with very special qualities, is much more than a solitary wave. Many equations admit solitary waves, i. e. travelling wave solutions with nonlinear stability properties. For example, if we change the cubic nonlinearity in (1.5) to the nonlinearity $-iq(1+2qq^*)^{-1}$ or the $6qq_x$ term in (1.6) to $6q^3q_x$, there are still travelling wave solutions which are stable to small disturbances.

The solitary wave solutions of *integrable* equations have additional properties, however. One property is that two such solitary waves pass through each other without any loss of identity. For example, observe that the solitary wave (1.7) has an amplitude-dependent velocity. Now, imagine that at some initial time, we start off two solitary waves very far apart with the one to the left having the larger amplitude and velocity. The larger one will eventually overtake the smaller. The interaction will be very nonlinear and will not at all resemble the interaction of two linear waves in which the composite solution is simply a sum of the two individual waves. Nevertheless, after the nonlinear interaction, two pulses again

will emerge, with the larger one in front, and each will regain its former identity (amplitude, width and velocity) precisely. There will be no radiation, no other mode created by the scattering process. The only interaction memory will be a phase shift; each pulse will be centered at a location different from where it would have been had it travelled unimpeded. It was Kruskal and Zabusky [47] who first noticed this remarkable phenomenon in their numerical experiment. And because of the particle-like behaviour they coined the term *soliton* for this special solitary wave.

Whereas this interaction property is remarkable and indeed often used as the test of integrability, it is not, by itself, sufficient. There are equations which admit solutions which are a nonlinear superposition of *two* solitary waves but which do not have all the properties enjoyed by an integrable equation. An integrable equation, when it admits solitary wave solutions, must admit a solution which is a nonlinear superposition of N solitary waves for arbitrary N. What is even more important, any arbitrary initial localized data, at sufficiently long times, must break up into N solitons plus some additional small-amplitude tail which dies out dispersively in time like $1/\sqrt{t}$.

As a matter of fact, through the famous inverse scattering method (see [45, 48, 7, 49, 50, 8]) the soliton parameters are being given by invariant eigenvalues of the associated linear operator. The stationary nature of eigenvalues provides the important property of the stability of the solitons when undergoing collisions. Hence, solitons are important not only as particular solutions of the integrable equations, but as unique solutions whose stability is guaranteed by the time-invariant property of the corresponding eigenvalues. The fact that the $t \to \infty$ asymptotic solutions of the integrable equation can be expressed in terms of N-sets of solitons indicates that solitons can be identified as *fundamental nonlinear modes* to the nonlinear equations, playing the role of the Fourier modes in a linear system.

An equation integrable in the above sense is also integrable in the sense of the infinite-dimensional extension of a completely integrable Hamiltonian system [51, 52]. A finite-dimensional ($2m$ variables) Hamiltonian system is said to be completely integrable if it admits m constants of motion $F_i (i = 1, \ldots, m)$ which are independent and in involution under the Poisson bracket associated with the Hamiltonian structure, and the level surface defined by the intersection of the surfaces $F_i = c_i$ is compact and connected [6]. There is a theorem that says that such a system can be canonically transformed (thereby preserving the Hamiltonian structure) to a set of new coordinates, the *action-angle variables* in which the system is completely separable. The action variables $J_i, 1 \leq i \leq m$ (which are functions of the integrals of motion F_i) are constant in time and the angle variables θ_i change linearly in time; i. e. $\theta_i = \omega_i t + a_i$, $1 \leq i \leq m$, a_i, ω_i constant. As a consequence of this, the motion must be quasiperiodic (i. e. the frequencies are not rationally related and the motion will never exactly repeat itself) and take place on an m-torus, topologically equivalent to the direct product of m circles. There is also a canonical transformation (the inverse scattering transform, which we mentioned earlier and which can be treated as the nonlinear analogue of the Fourier transform) which converts the integrable equation into an infinite sequence of decoupled equations for the action-angle variables, each member of which can be trivially integrated. It turns out that some of the action variables are the soliton parameters; as we pointed out above, this is the reason that a soliton's identity (its shape, speed, amplitude, internal frequency etc.) is preserved under collisions. Other action variables are connected

will emerge, with the larger one in front, and each will regain its former identity (amplitude, width and velocity) precisely. There will be no radiation, no other mode created by the scattering process. The only interaction memory will be a phase shift; each pulse will be centered at a location different from where it would have been had it travelled unimpeded. It was Kruskal and Zabusky [47] who first noticed this remarkable phenomenon in their numerical experiment. And because of the particle-like behaviour they coined the term *soliton* for this special solitary wave.

Whereas this interaction property is remarkable and indeed often used as the test of integrability, it is not, by itself, sufficient. There are equations which admit solutions which are a nonlinear superposition of *two* solitary waves but which do not have all the properties enjoyed by an integrable equation. An integrable equation, when it admits solitary wave solutions, must admit a solution which is a nonlinear superposition of N solitary waves for arbitrary N. What is even more important, any arbitrary initial localized data, at sufficiently long times, must break up into N solitons plus some additional small-amplitude tail which dies out dispersively in time like $1/\sqrt{t}$.

As a matter of fact, through the famous inverse scattering method (see [45, 48, 7, 49, 50, 8]) the soliton parameters are being given by invariant eigenvalues of the associated linear operator. The stationary nature of eigenvalues provides the important property of the stability of the solitons when undergoing collisions. Hence, solitons are important not only as particular solutions of the integrable equations, but as unique solutions whose stability is guaranteed by the time-invariant property of the corresponding eigenvalues. The fact that the $t \rightarrow \infty$ asymptotic solutions of the integrable equation can be expressed in terms of N-sets of solitons indicates that solitons can be identified as *fundamental nonlinear modes* to the nonlinear equations, playing the role of the Fourier modes in a linear system.

An equation integrable in the above sense is also integrable in the sense of the infinite-dimensional extension of a completely integrable Hamiltonian system [51, 52]. A finite-dimensional ($2m$ variables) Hamiltonian system is said to be completely integrable if it admits m constants of motion $F_i (i = 1, \ldots, m)$ which are independent and in involution under the Poisson bracket associated with the Hamiltonian structure, and the level surface defined by the intersection of the surfaces $F_i = c_i$ is compact and connected [6]. There is a theorem that says that such a system can be canonically transformed (thereby preserving the Hamiltonian structure) to a set of new coordinates, the *action-angle variables* in which the system is completely separable. The action variables $J_i, 1 \leq i \leq m$ (which are functions of the integrals of motion F_i) are constant in time and the angle variables θ_i change linearly in time; i. e. $\theta_i = \omega_i t + a_i$, $1 \leq i \leq m$, a_i, ω_i constant. As a consequence of this, the motion must be quasiperiodic (i. e. the frequencies are not rationally related and the motion will never exactly repeat itself) and take place on an m-torus, topologically equivalent to the direct product of m circles. There is also a canonical transformation (the inverse scattering transform, which we mentioned earlier and which can be treated as the nonlinear analogue of the Fourier transform) which converts the integrable equation into an infinite sequence of decoupled equations for the action-angle variables, each member of which can be trivially integrated. It turns out that some of the action variables are the soliton parameters; as we pointed out above, this is the reason that a soliton's identity (its shape, speed, amplitude, internal frequency etc.) is preserved under collisions. Other action variables are connected

with the energy in each of the nonlinear *radiation* modes, the nonlinear analogue of the continuum of Fourier modes of a linear system [6].

The first hints regarding the integrability of the soliton-bearing equation go back to the Fermi-Pasta-Ulam [53] experiment. Fermi, Pasta and Ulam studied the heat transfer problem (i.e. why do solids have finite heat conductivity) in a solid modelled by a one-dimensional lattice of equal masses connected by nonlinear springs. They examined the dynamical behaviour of a chain with nonlinear interactions between the atoms (mass points), expecting that the initial energy would eventually be shared among all the degrees of freedom of the lattice and the system would reach the thermal equilibrium (i. e. the system is ergodic on the energy shell). Much to their surprise, the energy did not spread throughout *all* the normal modes, but after being initially contained in the lowest mode and then flowing back and forth among several low-order modes, the energy recollected into the originally excited mode and from there on the process approximatelly repeated itself. The system seemed to behave like a system of linearly coupled harmonic oscillators whose motion on a torus is quasiperiodic.

But how this could be? Why didn't the nonlinearity excite *all* the Fourier modes? Could the answer be that the system, when viewed in the right coordinates, was equivalent to a separable system of harmonic oscillators? The answer came from Zabusky and Kruskal who used KdV to model this system [47, 54, 55]. The reason for the "almost recurrence" was that the initial profile decomposes into relatively few soliton shapes. The approximate recurrence time is the minimum time for pulses with different constant velocities to arrive once again at a common point on a cirle of length L. The strange interaction properties of the solitons together with the almost recurrence property seemed more and more to indicate that, in some sense, the KdV equation was integrable and there should be a lot of conserved quantities.

Let us contrast this behaviour with one would expect to occur in a mechanical system with strong coupling between many degrees of freedom. In general, one would not expect such a system to be separable. Consequently one would also not expect to see the power spectrum of the time series of any one of the dependent variables to consist of m distinct frequencies, as it would for example if it were a completely integrable Hamiltonian system with a compact structure. On the contrary, one would expect there to be at least some spectrum broadening indicating stochastic, although not necessarilly ergodic, behaviour. Indeed, the second great discovery referred to at the beginning of this section, is the realization that one can have chaotic time dependence in systems with few degrees of freedom. What counts is the qualitative nature of the system of equations and not the dimension of the system. If the equations are such that solutions depend sensitively on initial conditions, then small errors in initial data are exponentially magnified by the flow to the point where it becomes completelly impossible to predict the future state of the system. Even dissipative systems, in which a given volume in state space contracts under the flow, are not immune. It turns out that the motion can take place on a new kind of attractor called a *strange attractor*. The attractor is called strange not simply because of its structure (locally it can be thought as a Cantor set) but because motion on it depends sensitively on initial conditions. There is hope that in some cases the apparent stochastic time dependence of systems with many degrees of freedom may be explained by the motion of the state space point on a strange

attractor whose dimension is much smaller [13]. Analitically, this could be proved by what is known as the "inertial manifold" theory [57].

This digression on nonintegrable systems was intended to emphasize as strongly as possible that in order for an equation to be completely integrable it must have very special properties. Solutions of integrable systems do not depend sensitively on initial condition; initial errors are magnified in time by at most a linear rate (since action variables are constant in time and the angle variables change linearly in time). However, it is instructive to find out what happens to these properties as the integrability nature of an equation is destroyed either by the addition of terms (as it will happen in the equation to which this study is devoted) or by changing some of the crucial coefficients. It is expected that such a perturbation will give rise to some chaotic regions in the phase space. If the perturbation is small, one would expect that a Kolmogorov-Arnold-Moser (KAM) type result would hold. One recalls that in a completely integrable Hamiltonian system with a bounded Hamiltonian, the motion takes place on an invariant m-dimensional torus parametrized by the m values of the action variables. The celebrated KAM theorem states that under small perturbation most of the tori will only be distorted, while a few tori near the resonances (tori with rationally related frequencies) will be replaced by small chaotic layers [10, 11], in which the trajectories wander erratically.

If the perturbation is allowed to increase, the thickness of the chaotic layers increases, by merging adjacent chaotic layers. This merging coincides with destruction of a KAM torus between two chaotic layers. But as Arnold pointed out [12], the main difference between a two-degree-of-freedom Hamiltonian and a system with three or more degrees of freedom is of topological nature. A two-torus separates three-space into an interior and an exterior, but this is no longer true of a three-torus in a five-space. Thus even though KAM tori survive perturbation, they need not separate the chaotic layers. In fact, the chaotic layers form a single connected region, called the *Arnold web*. If motion starts in this web, it will spread over all the region. This *Arnold diffusion* is extremely slow, but takes place however small the nonlinearity. One might use these ideas to characterize turbulent or chaotic (stochastic) behaviour in models in physics, models which when unperturbed are exactly solvable, and which are intimately connected with integrable equations [6].

Here we must clarify the use of the term soliton in its broad sense (as it is common in the current physics literature). We mentioned that when used by mathematicians the term soliton has a precise meaning in the context of inverse scattering theory and carries with it the associated properties of a localised non-linear wave, elastic scattering amongst solitons, stability and being part of an integrable system. In a physics context where, stricly speaking, due to dissipation no integrable systems exist, the term *soliton* is used simply as a synonim for *solitary wave*. As this work is devoted to a nonintegrable system, we shall adopt this simplified terminology.

Since the equation we are interested in is a perturbed NLS, that is, a near integrable equation (by sending the perturbation parameters to zero we get the completely integrable NLS), we hope that the above discussion on nonintegrable systems gives some hints on what one could expect in the region where its soliton solution proves to be unstable. One might ask: why NLS? The aim of the next section is to explain the reasons for the ubiquity and

therefore the importance of the NLS equation.

1.3 The nonlinear Schrödinger equation

In order to achieve our goal it is best to derive the NLS starting with a simple example. Let us consider Scott's model consisting of a string of pendula suspended from and free to turn about a horizontal torsion wire. If the twist angle of the pendulum at x is denoted by $u(x,t)$, then its motion is given by the sine-Gordon equation

$$u_{tt} - c^2 u_{xx} + \omega_p^2 \sin u = 0, \tag{1.14}$$

where the $(-\omega_p^2 \sin u)$ force is due to gravity and the $c^2 u_{xx}$ force models the effect of the twist. Now imagine that we wiggle one end of the pendulum chain with a very small amplitude motion of frequency ω. Approximating $\sin u$ by its Taylor series about $u = 0$, and keeping the first two terms, one obtains

$$u_{tt} - c^2 u_{xx} + \omega_p^2 u = \frac{\omega_p^2}{6} u^3 + \cdots \tag{1.15}$$

The linearized equation admits sinusoidal solutions $u = e^{ikx - i\omega t}$ where k is real and given by the dispersion relation

$$\omega^2 = \omega_p^2 + c^2 k^2 \tag{1.16}$$

as long as $\omega > \omega_p$. For $\omega < \omega_p$, k is pure imaginary and the initial wiggle dies out exponentially in x. Let us suppose that $\omega > \omega_p$ so that real waves propagate down the string. Now it is also to be expected that eventually the nonlinear terms will cause some modulation of this motion as we know that the period of the nonlinear spring (same as a single pendulum) depends on amplitude. To find this modulation, let us seek solutions to (1.15) in the form

$$u = \varepsilon(u_0 + \varepsilon u_1 + \varepsilon^2 u_2 + \cdots), \tag{1.17}$$

where

$$u_0 = a e^{ikx - i\omega t} + a^* e^{-ikx + i\omega t} \tag{1.18}$$

and where we will allow a to be a slowly varying function of time :

$$a_t = \varepsilon A_1(a, a^*) + \varepsilon^2 A_2(a, a^*) + \cdots \tag{1.19}$$

The coefficients $A_j(a, a^*)$ in (1.19) are chosen in order to suppress secular behaviour in $u_1, u_2, \ldots$. This procedure is known as Krylov-Bogoliubov-Mitropolski method. Here we mainly follow the exposition of Newell [6]. Secular behaviour refers to a situation in which iterates $u_1, u_2, \ldots$ grow algebraically in the fast time or space variables. If this were allowed

to happen, the asymptotic series (1.17) would not be uniformly valid over long times and distances. In the jargon of multiple time scales we would write A_1 as $\partial a/\partial T_1$, $T_1 = \varepsilon t$; A_2 as $\partial a/\partial T_2$, $T_2 = \varepsilon^2 t$, and so on. Solving (1.15) iteratively leads to $u_1 = 0$,

$$\begin{aligned} A_1 &= 0, \quad A_2 = \frac{i}{4}\frac{\omega_p^2}{\omega} a^2 a^*, \\ u_2 &= -\frac{a^3}{48} e^{3i(kx-\omega t)} + (c.c.), \end{aligned}$$

whence

$$u_0 = a_0 \exp\left[ikx - it\left(\omega - \frac{\omega_p^2}{4\omega}\varepsilon^2 |a_0|^2\right)\right] + (c.c.). \tag{1.20}$$

Notice that the period of motion increases. In the context of water waves, the solution computed in this way is known as the *Stokes wave*. Note that in all this calculation e^{ikx} plays a passive role. Once ω is fixed, then so is k from (1.16). But it is impossible to wiggle a chain at a perfectly tuned frequency and so one might expect a small but finite band width μ of frequencies and wavenumbers to be excited. How can one incorporate this into the description? One way is to look for solutions u_0 which are a finite sum of waves

$$u_0 = \sum_{k_j = k + \mu K_j} a_j e^{i(k_j x - \omega_j t)} + (c.c.), \quad \omega_j^2 = \omega_p^2 + c^2 k_j^2, \tag{1.21}$$

but this approach is clumsy and leads to a set of coupled nonlinear equations for the amplitudes a_j which are cumbersome to handle. Another way, which is suggested by (1.21), is to look for solutions of a form in which the amplitude a is a slowly varying function of x as well as time, an idea originally introduced in [62]. The most interesting balance between the various effects occurs when $\mu = \varepsilon$.

Let us repeat the previous calculations where this time we allow A_1, A_2 to be functions of $a, a^*, a_X, a_X^*, a_{XX}, \ldots$, and $X = \varepsilon x$. At $\mathcal{O}(\varepsilon)$ we find

$$u_{1tt} - c^2 u_{1xx} + \omega_p^2 u_1 = (2i\omega a_{T_1} + 2ikc^2 a_X) e^{i(kx-\omega t)} + (c.c.), \tag{1.22}$$

where $\partial a/\partial T_1 = A_1$. In order to suppress secular growth in u_1, we must require that

$$\frac{\partial a}{\partial T_1} + \frac{c^2 k}{\omega} a_X = 0, \tag{1.23}$$

or that a moves with the group velocity $\omega' = d\omega/dk$, as calculated from (1.16), of the wave packet. Then $u_1 = 0$. At order ε^2,

$$\begin{aligned} u_{2tt} - c^2 u_{2xx} &+ \omega_p^2 u_2 = \frac{\omega_p^2}{6} a^3 e^{3i(kx-\omega t)} \\ &+ \left(2i\omega a_{T_2} - a_{T_1 T_1} + c^2 a_{XX} + \frac{1}{2}\omega_p^2 a^2 a^*\right) e^{i(kx-\omega t)} + (c.c.), \end{aligned}$$

and the suppression of secular terms requires that

$$\frac{\partial a}{\partial T_2} - \frac{i\omega''}{2} a_{\xi\xi} - \frac{i}{4}\frac{\omega_p^2}{\omega} a|a|^2 = 0. \tag{1.24}$$

In finding (1.24), one uses (1.23) in order to write $\partial^2 a/\partial T_1^2$ in terms of a_{XX}. Also, $\xi = \varepsilon(x - \omega' t), T_2 = \varepsilon^2 t$ and ω'' is the dispersion $d^2\omega/dk^2$ as calculated from (1.16). Equation (1.24) is nothing but the nonlinear Schrödinger equation. One observes that it contains as a special solution the "nonlocalised" solution (1.20). It is very important that it is unstable if the product of the coefficients in front of the dispersion term $\omega''/2$ and the nonlinear term $(\frac{1}{4}\omega_p^2/\omega)$ is positive, a situation which obtains in the present example. This is the instability which was discovered by Benjamin and Feir [59] when they tried to demonstrate experimentally the existence of the Stokes solution for surface water waves. It is a most important instability because it is widespread and plays an important role in various nonlinear wave phenomena, and it causes otherwise monochromatic wavetrains to evolve into a series of pulses. The sidebands of the carrier wave can draw on its energy via a resonance mechanism with the result that the envelope becomes modulated. In one space dimension, this envelope modulation continues to grow until the soliton shape is reached. At this point, nonlinearity and dispersion are in exact balance and no further distorsion ocurrs. In two-dimensions, the focusing process is never halted and continues until the pulse achieves locally an infinite amplitude which it does in a finite time. This focusing phenomenon was observed in plasmas in the form of Langmuir wave collapse and in nonlinear optics as filamentation [60, 61].

We return to the reasons for the ubiquity of the NLS equation and show how all the linear terms in the equation have a universal structure. Consider the class of equations

$$\mathbf{L}(\partial_t, \partial_x)u = \mathbf{N}(u^2, u^3, \ldots), \tag{1.25}$$

where $\mathbf{L}u$ and $\mathbf{N}(u^2, u^3, \ldots)$ are constant coefficient linear and nonlinear operators on u and its derivatives. Let the linear part of (1.25) admit sinusoidal solutions of the form

$$u = ae^{i(kx - \omega t)}, \tag{1.26}$$

where

$$\mathbf{L}(-i\omega, ik) = 0 \tag{1.27}$$

is the dispersion relation giving ω as function of k (and vice versa). At this point we emphasize that we are considering only strongly dispersive systems. Since (1.27) holds for all k, one can deduce that

$$-i\omega'\mathbf{L}_1 + i\mathbf{L}_2 = 0 \tag{1.28}$$

$$-i\omega''\mathbf{L}_1 - \omega'^2\mathbf{L}_{11} + 2\omega'\mathbf{L}_{12} - \mathbf{L}_{22} = 0 \tag{1.29}$$

by differentiating once and then twice with respect to k ($\mathbf{L}_j$ is the derivative of $\mathbf{L}$ with respect to j-th argument.). Now, let us seek solutions of (1.25) in the form

$$u(x,t) = \varepsilon(u_0 + \varepsilon u_1 + \varepsilon^2 u_2 + \ldots) \tag{1.30}$$

with u_0 given by (1.18) with a being a slowly varying function of position and time. We note that $\mathbf{L}(\partial_t, \partial_x)$, under the multiple time scale algorithm, formally becomes

$$\begin{aligned}\mathbf{L}(\partial_t + \varepsilon\partial_{T_1} + \varepsilon^2\partial_{T_2} \quad &, \quad \partial_x + \varepsilon\partial_X) \\ &= \mathbf{L}(\partial_t, \partial_x) + \varepsilon(\mathbf{L}_1\partial_{T_1} + \mathbf{L}_2\partial_X) \\ &+ \varepsilon^2\Big(\mathbf{L}_1\partial_{T_2} + \frac{1}{2}\mathbf{L}_{11}\partial_{T_1T_1} + \mathbf{L}_{12}\partial_{T_1X} + \frac{1}{2}\mathbf{L}_{22}\partial_{XX}\Big) + \cdots\end{aligned} \tag{1.31}$$

which we can write as $\mathbf{L}^{(0)} + \varepsilon\mathbf{L}^{(1)} + \varepsilon^2\mathbf{L}^{(2)} + \cdots$. Iteratively solving (1.25), we have

$$\mathbf{L}^{(0)}(\partial_t, \partial_x)u_0 = 0 \tag{1.32}$$

with solution

$$u_0 = a(X, T_1, T_2, ...)e^{i(kx-\omega t)} + (c.c.), \tag{1.33}$$

with (1.27) holding between ω and k. Next at order ε,

$$\mathbf{L}^{(0)}u_1 = -\mathbf{L}^{(1)}u_0 + \mathbf{N}(u_0^2). \tag{1.34}$$

The right-hand side of (1.34) can contain secular terms giving rise to a solution u_1 which grow algebraically in x and t. They can be recognized by the fact that they have an (x,t)-structure which belongs to the null space of $\mathbf{L}^{(0)}$. For example, $\mathbf{L}^{(1)}u_0$ belongs to this class as $\mathbf{L}^{(0)}\mathbf{L}^{(1)}u_0 = \mathbf{L}^{(1)}\mathbf{L}^{(0)}u_0 = 0$. The term u_0^2 itself contains second harmonics $a^2e^{2i(kx-\omega t)}$ and mean terms aa^*. But, since the system is strongly dispersive, for almost all $k, \omega(2k) \neq 2\omega(k)$ and therefore $\mathbf{L}^{(0)}e^{2i(kx-\omega t)} \neq 0$. Now, the constant solution aa^* may indeed belong to the null space of $\mathbf{L}^{(0)}$. If it does and if $\mathbf{N}(u_0^2)$ is nonzero, one must include in the zeroth order approximation u_0 a mean term which slowly varies with x and t.

What happens more often is that $\mathbf{N} \cdot aa^*$ is zero to this order. This occurs because the equation has underlying symmetries like Galilean invariance which makes it impossible to force a mean flow directly. On the other hand, due to the slow dependence of the envelope on x, a local mean flow, which has the form $\varepsilon^2(\partial_X)aa^*$, can arise, and unless removed, cause a secular response at the ε^2 level in u_2. Such a term need not violate any overall conservation property. In one ε^{-1} patch, it may increase the mean level; in the next patch its parity can change so that no net "mass" is added to the system. In order to account for this effect one must include a mean contribution as a homogenous solution b in u_1 (or simply in u_0 at order ε). This mean term b then will contribute to potential secular behaviour $e^{i(kx-\omega t)}$ at the $\mathcal{O}(\varepsilon^2)$ level in u_2 through the quadratic product $\mathbf{N}(u_0u_1)$. Removing secular terms at $\mathcal{O}(\varepsilon^2)$ then leads to a coupled system of equations in a, the wave envelope and b, the slowly varying mean.

For now let us assume that the mean flow is not in the null space of $\mathbf{L}^{(0)}$ as, for example, would be the case if $\mathbf{L} = \partial_{tt} - c^2\partial_{xx} + \omega_p^2$. Then the only secular term in (1.34) is $\mathbf{L}^{(1)}u_0$ and so one must choose the dependence of a on X and T_1 such that $\mathbf{L}^{(1)}u_0 = 0$, namely

$$\mathbf{L}_1\frac{\partial a}{\partial T_1} + \mathbf{L}_2\frac{\partial a}{\partial X} = 0. \tag{1.35}$$

But from (1.28), $\mathbf{L}_2 = \omega' \mathbf{L}_1$ and so if $\mathbf{L}_1 \neq 0$ (which is assumed)

$$a = a(X - \omega' T_1, T_2). \tag{1.36}$$

We then solve for u_1, which contains second harmonics and perhaps a mean term proportional to $|a|^2$. At order ε^2, the secular terms which are nonlinear in a and a^* arise from the quadratic product $u_0 u_1$ and the cubic product u_0^3. These lead to a term which we write as $\beta \mathbf{L}_1 a|a|^2$. The linear terms which are secular are of the form $\mathbf{L}_2 u_0$ which, when we take account of (1.36), may be written as a product of $e^{i(kx-\omega t)}$ with

$$\mathbf{L}_1 \frac{\partial a}{\partial T_2} + \left(\frac{1}{2} \omega'^2 \mathbf{L}_{11} - \omega' \mathbf{L}_{12} + \frac{1}{2} \mathbf{L}_{22} \right) a_{XX}. \tag{1.37}$$

But from (1.29), this is equal to

$$\mathbf{L}_1 \left(\frac{\partial a}{\partial T_2} - \frac{i\omega''}{2} a_{XX} \right), \tag{1.38}$$

and so the universal NLS equation is

$$\frac{\partial a}{\partial T_2} = \frac{i\omega''}{2} a_{\xi\xi} + i\beta a|a|^2, \tag{1.39}$$

where a is a function of $\xi = \varepsilon(x - \omega' t)$ and $T_2 = \varepsilon^2 t$.

The transformation

$$\xi = X, \qquad \frac{\omega'' T_2}{2} = \tau, \qquad q = \left| \frac{\beta}{\omega''} \right|^{1/2} a \tag{1.40}$$

puts it into canonical form

$$q_\tau = i q_{XX} \pm 2iq|q|^2, \tag{1.41}$$

where the sign is given by the sign of β/ω''.

The equation describes the evolution of the envelope of a wave train and, unlike its linear counterpart, contains within it the soliton solution embodying the concept of the wave packet. For the "+" sign in (1.41), the asymptotic solution of the initial value problem for (1.41) consists of a sequence of envelope solitons

$$q(X, \tau) = 2\eta \frac{\exp^{-2iv X - 4i(v^2 - \eta^2)\tau}}{\cosh[2\eta(X + 4v\tau)]} \tag{1.42}$$

and radiation modes. The circumstances necessary for the ocurrence of (1.41) are that the underlying wave packet is strongly dispersive, almost monochromatic and weakly nonlinear. The X is position measured with respect to reference frame moving with the (linear)

group velocity corresponding to the wave number of the carrier wave, and the equation itself represents a balance between linear dispersion which has a tendency to spread wave packets out and the focusing effect of the cubic nonlinearity produced by the self interaction of the wave with itself. The nonlinearity is not always as simple as $q|q|^2$, arising from a $q^2e^{2i\theta} \times q^*e^{-i\theta}, (\theta = kx - \omega t)$ interaction, but may also involve a mean (nonoscillatory) component.

Finally, we have shown in this section that there is a class of partial differential equations of the form (1.25) which yield the nonlinear Schrödinger equation as a *generic* envelope equation.

1.4 Real-world disturbances, perturbed NLS and our problem

The fact that an envelope of a wave which propagates in a strongly dispersive nonlinear medium admits a soliton solution is likely to have a tremendous impact in our daily life. It is the optical soliton, the solitary wave of a light envelope, which in the near future could revolutionize the world of telecommunications and computer technologies (we refer to the books by Hasegawa (1989) [15], Agrawal (1989) [16], Newell and Moloney (1991) [17], and Taylor (1992) [18], and references therein). And it is the NLS equation which describes that envelope of a light wave in a fiber. This time it takes the form

$$iq_z + q_{tt} + 2|q|^2q = 0, \tag{1.43}$$

where z represents the distance along the direction of propagation, and t the time in the group velocity frame. The second term originates from the dispersion of the group velocity, i. e., the fact that the group velocity is dependent on the wavelength, and the third term originates from the nonlinear effect, i. e., the fact that the wavelength depends on the intensity of the wave.

In an optical transmission system using linear pulses, the bit rate of transmission is limited by the dispersive character of the material, which causes the pulses to spread out and eventually overlap to such an extent that all the information is lost. To overcome this limitation, Hasegawa and Tappert [63] proposed to compensate the dispersive effect by the nonlinear change (the Kerr effect) of the refractive index of the fiber material. When the frequency shift due to Kerr effect is balanced with that due to dispersion, the initial optical pulse may tend to form the stable optical soliton.

However, in a real fiber, due to imperfect internal reflexion, the light propagates with some loss and one has to account for the effects of loss. This can of course be done, but if one does, one obtains a new governing equation, a perturbation of NLS which is no longer exactly integrable. Nevertheless, in some circumstances, it is necessary to forego the mathematical conveniences of exact integrability in order to capture the essential physics of the system. The standard way to take dissipation into account is to include the term $(-i\gamma q)$ in the

right-hand side of the equation. In this particular case,

$$iq_z + q_{tt} + 2|q|^2 q = -i\gamma q, \quad \gamma > 0, \tag{1.44}$$

where γ denotes the loss rate.

What happens to the soliton? Will it survive this perturbation? The answer is no. Assuming that the fiber loss is sufficiently small and using a perturbation technique [64] to obtain the one-soliton solution of equation (1.44), one can show (see, e. g., [15]) that the soliton amplitude decreases exponentially as $\exp(-2\gamma z)$, and the width increases as $\exp(2\gamma z)$. Also, the pulse energy, conserved by the pure NLS (the energy is an integral of motion), decreases in proportion to $\exp(-2\gamma z)$ which means that for sufficiently large distances and implicitly time, the soliton decays. Another way to study the effects of fiber loss, for *arbitrary* γ, is to integrate the equation (1.44) numerically for a range of values of γ and of the amplitude of an initial pulse. Blow and Doran [65] performed such a numerical experiment and observed the same behaviour.

This result indicates that in order to prevent attenuation, energy must be supplied from outside. For the optical soliton, the most promising methods are the amplification by the induced Raman effect and by means of erbium doped fibers. When compensating the effect of loss on optical fibers, an optical soliton can propagate without distorsion over an extremely long distance with important consequences for future long-distance high-bit-rate communications systems (see [66, 67]). To account for this energy pumping, one has to add the gain ($f(z)$ in this particular case) chosen to compensate for the losses :

$$iq_z + q_{tt} + 2|q|^2 q = -i\gamma q + if(z)q. \tag{1.45}$$

So far, we have seen that a little realism, in the form of dissipation, changes the picture. But the optical fiber is just one of the many damped systems (and the world is full of such systems, beginning with the weather, damped by the friction of the moving air and water and by the dissipation of the heat to outer space, and driven by the constant push of the sun's energy). Actually, all physically meaningful systems are dissipative and one has to account both for damping and driving when studying the behaviour of the system.

The problem of activation and stabilization of solitons in real systems with dissipation is a subject of currently growing interest (see, e. g., [72, 88, 69, 91, 92, 68, 78, 117]) all the more qualitatively new aspects are linked to this area : bifurcations, attractors, self-organization and chaos, everything that the new approach to nonlinear dynamics has in display.

Nozaki and Bekki [70] showed that the soliton may be a reasonable candidate for an attractor in a forced dissipative soliton system (when solitons and radiation persist as nearly separable nonlinear modes). They considered a plasma driven by an external rf field and derived from the fluid equations of plasma the following *externally* driven damped NLS equation :

$$iq_t + q_{xx} + 2|q|^2 q = -i\gamma q - ihe^{i\Omega t}, \tag{1.46}$$

where h is the driver's amplitude. By means of numerical and IST-based perturbational methods they studied a sequence of bifurcations of attractors and showed that direct interactions between soliton and a small pump field bring about a phase-locked soliton attractor (phase-locking means that the nonlinear frequency shift is in resonance with the driving frequency Ω). As the strength of the pump increases, the phase-locked soliton (a fixed point in the phase space) is bifurcated to an amplitude-oscillating soliton (a limit cycle). Subsequent period-doubling bifurcations of a limit cycle lead to a low-dimensional chaotic attractor representing an erratically oscillating soliton. When the pump field increases further, a crisis of the chaotic attractor occurs, and more complicated chaotic states in which many degrees of freedom are excited arise.

To summarize, by means of direct numerical simulations, Nozaki and Bekki detected the *period-doubling* transition to chaos, and thereby it was demonstrated that generic routes to chaos occur in soliton-bearing systems. Also they were first to derive a set of ordinary differential equations (ODEs) which model transition to chaos in a perturbed soliton system in terms of parameters of solitons and radiation. They found a good agreement between the modelled partial differential equation (PDE) (1.46) and the reduced system of ODEs.

The paper of Nozaki and Bekki [70] has stimulated many authors to investigate similar problems all the more two basic questions remained unanswered. Is the period-doubling route to chaos the only generic scenario for the driven damped NLS ? When reducing to low-dimensional models, does a systematic procedure exist to find the relevant modes?

The first answers came from Bishop *et al* [91] who studied the damped driven sine-Gordon equation,

$$u_{tt} - u_{xx} + \sin u = -\lambda u_t + f\sin(\Omega t). \tag{1.47}$$

When the driver's frequency, Ω, is near but less than unity ($\Omega \approx 1, \Omega < 1$) and the amplitude of the solution is small, one can use singular perturbation methods [73, 6, 5] similar to those described in the previous section to reduce eq. (1.47) to the externally driven damped NLS equation (1.46). We mention, en passe, that this fact extends the applicability of NLS. We have already mentioned that the NLS arises in plasma, in the description of one-dimensional condensate with the ac field applied; now we can add to this list the dynamics of small-amplitude breathers of the easy axis ferromagnet in the rf field and long Josephson junctions.

Bishop *et al* studied the damped driven sine-Gordon equation (1.47) in the above mentioned NLS regime, and consequently their results translate to the case of the damped driven NLS (1.46). Their numerical simulations have furnished a particularly beautiful example of *quasiperiodic* route to chaos in a PDE. They observed that the chaotic regime is strongly intermittent, with the quasiperiodic regions distinguished from the chaotic bursts by a change in spatial symmetry. Temporally, the route exhibits one frequency, then two, and lastly temporal chaos. Bishop *et al* used the associated Inverse Scattering transform to precisely identify the nonlinear modes which comprise the attractors and found that interaction of coherent modes with radiation modes takes place with only a few (~ 3 or 4) nonlinear modes being appreciably excited — even when the attractor is chaotic. This simply means that only a small number of nonlinear modes of the underlying integrable system are needed for a "description" of all the attractors. Most importanly, they identified and showed

that (unperturbed) homoclinic states are crossed repeatedly in these regimes. It must be emphasized that the homoclinic states [74] have infinite temporal periods under unperturbed dynamics and frequently separate in the phase space states with distinct spatial structures (e.g., spatially localised modes from extended, radiation modes), and play a central role in generating chaos [75, 14].

A theoretical interpretation of the results obtained by Bishop *et al* is due to Terrones *et al* [76] whose analytical study establishes the existence of several metastable states (unstable states with small growth rates), which consist of spatially localised coherent excitations and differ from each other by the location of these excitations. In addition, it was shown that very unstable states (states with large growth rates) are present, along with their associated homoclinic orbits, and that instability occurs through a Hopf bifurcation and therefore there are two unstable modes. Thus, they provided the ingredients for a description of one type of chaotic attractor of the NLS (and of the sine-Gordon in the NLS regime).

The same damped driven sine-Gordon equation in the NLS regime was studied by Spatschek *et al* [92] and, for a different parameter range and a larger length of the system, a period-doubling route to temporal chaos was found. In this case too, the numerical calculations showed that only few modes dominate the dynamics of the system. By means of linear stability analysis combined with Inverse Scattering diagnostics, Grauer and Birnir [77] showed that *three* modes are relevant for the dynamics. In addition, through a series of experiments whose purpose was to understand the influence of the length of the system on the bifurcation sequences, they found that in the same parameter regime a decrease in the length results in the bifurcation sequence described by Terrones [76] and Bishop [91], while an increase of the length leads to the period doubling route.

Thus, depending on the parameter range and the system length, the sine-Gordon equation in *the NLS regime* exibits all the generic routes to temporal chaos known for low-dimensional systems.

The results for the sine-Gordon equation in the NLS regime are in an excellent agreement with what the analysis of the NLS equation displays. More specifically, Eickermann *et al* [71] proved that besides the period-doubling observed by Nozaki and Bekki, the NLS (1.46) exhibits intermittency and period-n windows in the chaotic regime. Intermittency was observed at the border of the period-3 window while for shorter system length quasiperiodic states arise, still with the (perturbed) soliton dominating the behaviour. They showed that the whole scenario is consistent with results obtained by means of a variety of approaches (Kahunen-Loève, perturbed IST in the periodic setting, Bäcklund transformation).

While the externally driven damped NLS equation was extensively studied, very little was known until recently about an equally important system: the *parametrically* driven damped NLS equation [79, 80, 58]:

$$i\psi_t + \triangle\psi + 2|\psi|^2\psi = -i\gamma\psi + h\psi^* e^{2i\Omega t}, \quad h, \gamma > 0. \tag{1.48}$$

Similarly to the *externally* driven NLS, this equation describes a large number of nonlinear resonant phenomena in various physical media. These include the Faraday resonance in fluid dynamics [81, 80, 82], parametric generation of spin waves in ferro and antiferromagnets [79, 83] [58, 84], parametric instabilities in plasma [85, 86, 87], and amplitude modulation in

long Josephson junctions [89, 90]. In all these cases, a strong parametric excitation of the system can produce and sustain solitonic waves.

Stability of the parametrically excited solitons heavily depends on the dimensionality of space and geometry of the problem at hand. In the two and three-dimensional *infinite* media the soliton was shown to be unstable and to collapse in a finite time [79]. However, if the system is bounded in one or two directions (consider, for instance, a long narrow rectangular water tank [81]), a stable soliton can be experimentally observed. This soliton is exponentially localised only in one direction, so it is effectively a one-dimensional object [80]. There are also a number of genuinely one-dimensional systems such as the one-dimensional ferro and antiferromagnets and long Josephson junctions where the existence of the parametrically driven soliton was predicted [88, 58]. All this motivates the study of the one-dimensional version of eq. (1.48) which this work is devoted to.

By means of a simple scaling, one can always arrange that $\Omega = 1$ in eq. (1.48):

$$i\psi_t + \psi_{xx} + 2|\psi|^2\psi = -i\gamma\psi + h\psi^* e^{2it}, \quad h, \gamma > 0, \tag{1.49}$$

As was shown in [58], soliton solutions can be found exactly — even for nonzero dissipation. Namely, eq. (1.49) has two solitons, ψ_+ and ψ_-,

$$\psi_\pm = A_\pm \frac{e^{i(t-\theta_\pm)}}{\cosh(A_\pm x)}, \tag{1.50}$$

where $A_\pm > 0$ and

$$\begin{aligned} A_+^2 &= 1 + (h^2 - \gamma^2)^{1/2}, \quad 2\theta_+ = \arcsin(\gamma/h), \\ A_-^2 &= 1 - (h^2 - \gamma^2)^{1/2}, \quad 2\theta_- = \pi - \arcsin(\gamma/h). \end{aligned} \tag{1.51}$$

The soliton ψ_+ exists above the line $h = \gamma$ in Fig. 1. The ψ_- exists between the lines $h = \gamma$ and $h = \sqrt{1+\gamma^2}$. Barashenkov *et al* [58] examined stability of these solitons against small perturbations and found that the ψ_- soliton is unstable for any h and γ. The stability of the ψ_+ soliton turned out to be a more subtle and difficult question. It was relatively straightforward to demonstrate that for $h > (1+\gamma^2)^{1/2}$ the ψ_+ is unstable with respect to the continuous spectrum waves which are excited by the parametric pumping. (Since the solution $\psi = 0$ is unstable for $h > (1+\gamma^2)^{1/2}$, the soliton solution is also unstable with respect to a continuum of modes.) Furthermore, the linearised stability analysis has revealed that the soliton has two internal ocillation modes the resonance of which produces Hopf bifurcation and instability. In ref. [58] it was suggested that this is the first bifurcation in a sequence leading to a chaotic behaviour[1].

[1]It is interesting to note that the same mechanism of the soliton instability occurs in the *directly* driven NLS [78].

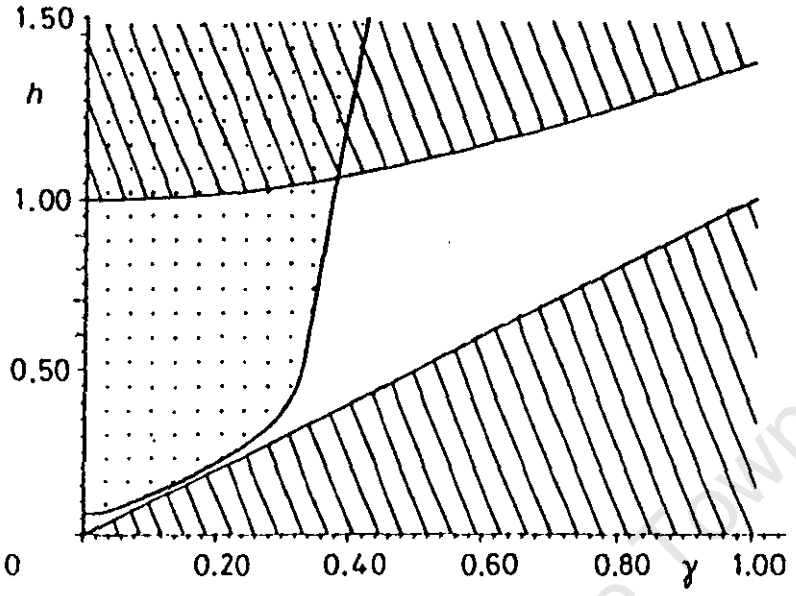

Fig.1

Stability diagram of the phase-locked soliton. Dashed is the domain $h < \gamma$ where no solitons exist and the region $h > (1+\gamma^2)^{1/2}$ where the soliton is unstable w.r.t. continuous spectrum. In the dotted region the soliton is unstable w.r.t. a local mode; in the empty wedge the soliton is stable.

A natural question arises: what happens to the soliton in the region where it is unstable? What attractors replace the stationary phase-locked soliton, what structures dominate the dynamics in the *dotted* area in Fig. 1? It is this question that we try to answer to in our numerical study.

We start by presenting our numerical algoritm.

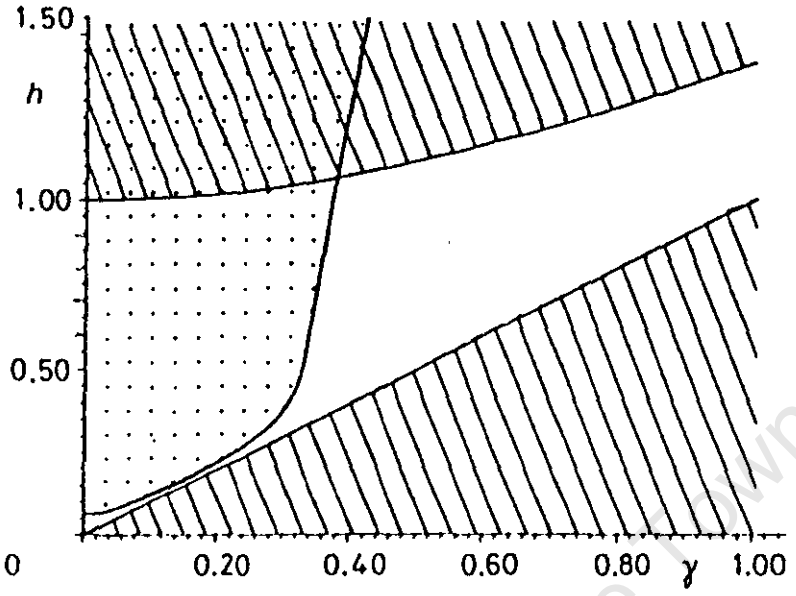

Fig.1

Stability diagram of the phase-locked soliton. Dashed is the domain $h < \gamma$ where no solitons exist and the region $h > (1+\gamma^2)^{1/2}$ where the soliton is unstable w.r.t. continuous spectrum. In the dotted region the soliton is unstable w.r.t. a local mode; in the empty wedge the soliton is stable.

A natural question arises: what happens to the soliton in the region where it is unstable? What attractors replace the stationary phase-locked soliton, what structures dominate the dynamics in the *dotted* area in Fig. 1? It is this question that we try to answer to in our numerical study.

We start by presenting our numerical algoritm.

Chapter 2

Numerical Method

"... the justification of such a mathematical construct is solely and precisely that is expected to work."
John von Neumann

2.1 Why split-step Fourier method ?

Apart from its physical significance the NLS equation presents a considerable interest for numerical analysis. Various instabilities and recurrence, interacting solitons and their bound states whose steep spatial and temporal gradients pose a real challenge to numerical methods [95] are some of the features which attract the numerical analyst. Thus, it is not surprising that there is a rich literature on numerical methods and stability of the NLS equation.

Among the earlier methods used for solving the NLS numerically, are split-step and Fourier methods, for example the methods employed by Lake *et al* [96] and Tappert [97]. Some of the more recent references to numerical solutions of the NLS include [98]—[107]. These authors used mainly finite difference or finite element methods to discretize the space variable. For the discretization of the time variable, Sanz-Serna [98, 99] employed an explicit, variable time step leap-frog scheme, Delfour *et al* [100] a modified Crank-Nicholson scheme, Griffits *et al* [101] a predictor-corrector method, and Herbst *et al* [95] the midpoint rule. Most recently, Fei *et al* [107] utilised a non-selfstarting globally linear implicit scheme which uses the Crank-Nicholson to provide a starting.

Taha and Ablowitz [108] conducted extensive computations in which the split-step Fourier method of Tappert [97] was compared with several finite difference, pseudospectral and even global methods, including some of the numerical schemes described in [98]—[107]. In the majority of their experiments, the split-step method turned out to be superior. The method owes part of its success to the fact that it avoids solving a nonlinear algebraic system at each time level. Thus high accuracy may be obtained at comparatively low computational cost. In their review of pseudospectral methods for solving PDEs, Fornberg and Sloan [23] also showed that in the context of solving time-dependent PDEs, the finite difference or

finite element methods do not even come close in efficiency.

An important theoretical analysis of split-step (finite difference and Fourier) methods was performed by Weideman and Herbst [110]. Under the approach that the salient physical properties of the NLS should also be reflected in the numerical schemes, their investigations were concerned with number of particles conservation, the nonlinear dispersion relation and the (linearized) stability of the numerical methods.

It was shown that both methods conserve number of particles exactly. Also the discrete form of the nonlinear dispersion relation proved to be exact in the case of the Fourier method. Recalling that the specific type of the solution of the NLS (number of solitons, occurence of bound states, etc.) depends on the balance between dispersion and nonlinearity, this quality of the split-step Fourier method is especially relevant since the accuracy of the approximation of the nonlinear dispersion by the numerical method is an indication of its ability to maintain this balance. Weideman and Herbst have also shown that the method is able to simulate closely the analytical instability properties of the NLS.

Despite the advantages over its rivals, the split-step Fourier method has not yet been applied to the perturbed NLS. Neither anything is known about its theoretical behaviour in this case. The aim of the next several sections is to design a version of the split-step Fourier method for the solution of the parametrically driven damped NLS (1.49), and analyze its properties.

We begin by discussing some of the relevant analytical properties of our perturbed NLS equation (1.49).

2.2 Analytical properties of the parametrically driven damped NLS equation

It appears convenient to transform eq. (1.49), by means of the substitution $\psi e^{it} \to \psi$, to a two-parameter autonomous equation,

$$i\psi_t + \psi_{xx} - \psi + 2|\psi|^2\psi = h\psi^* - i\gamma\psi, \quad h, \gamma > 0, \tag{2.1}$$

where h and γ are the driver's strength and dissipation coefficient, respectively.

2.2.1 Spatially uniform attractors and their stability

We begin our analytical study [112] by first constructing "flat" solutions of (2.1), i. e., solutions that are uniform in space and do not depend on time. In addition, we study eq. (2.1) subject to periodic boundary condition as is appropriate for comparison to the numerical solutions.

Static, spatially homogeneous solutions

We seek an x- and t-independent solution ψ_0 of

$$i\psi_t + \psi_{xx} - \psi + 2|\psi|^2\psi = h\psi^* - i\gamma\psi. \tag{2.2}$$

Let $\psi_0 = ae^{-i\alpha}$ for some constants $a > 0$ and α which denote the amplitude and phase of the solution respectively; they satisfy the following equation :

$$-1 + 2a^2 = he^{2i\alpha} - i\gamma. \tag{2.3}$$

Equating real and imaginary parts, one obtains

$$2a^2 - 1 - h\cos 2\alpha = 0 \tag{2.4}$$

$$\gamma - h\sin 2\alpha = 0, \tag{2.5}$$

and hence the amplitudes and phases of the two flat solutions of (2.2) are given by

$$a_+^2 = \frac{1 + \sqrt{h^2 - \gamma^2}}{2}, \quad \alpha_+ = \frac{1}{2}\arcsin\frac{\gamma}{h} \tag{2.6}$$

and

$$a_-^2 = \frac{1 - \sqrt{h^2 - \gamma^2}}{2}, \quad \alpha_- = \frac{\pi}{2} - \frac{1}{2}\arcsin\frac{\gamma}{h}, \tag{2.7}$$

respectively. Note that the flat states have the same phases as the $\psi_\pm$ solitons, and their amplitudes are related as $\sqrt{2}a_\pm = A_\pm$, where $A_\pm$ are the soliton amplitudes given by (1.51).

Linear stability analysis

Next we investigate stability of these flat states [112]. Setting

$$\psi(x,t) = \psi_0 + \delta\psi(x,t), \tag{2.8}$$

where

$$\delta\psi = e^{-i\alpha_\pm - \gamma t}\{f(x,t) + ig(x,t)\} \tag{2.9}$$

is a small perturbation, and linearising with respect to $\delta\psi$ gives

$$-g_t - \gamma g = \{-d^2/dx^2 + 1 - 6a_\pm^2 + h\cos(2\alpha_\pm)\}f, \tag{2.10}$$

$$f_t - \gamma f = \{-d^2/dx^2 + 1 - 2a_\pm^2 - h\cos(2\alpha_\pm)\}g. \tag{2.11}$$

Transforming to $T = a_\pm^2 t$ and $X = a_\pm x$, and defining $\tilde{\gamma} = \gamma/a_\pm^2$, one gets

$$\begin{aligned} -g_T - \tilde{\gamma}g &= \mathbf{L_1}f, \\ f_T - \tilde{\gamma}f &= \mathbf{L_0}g, \end{aligned} \tag{2.12}$$

with

$$\begin{aligned} \mathbf{L_0} &= -d^2/dX^2 \mp \epsilon_{\pm}, \\ \mathbf{L_1} &= -d^2/dX^2 - 4, \\ \epsilon_{\pm} &= 2\sqrt{h^2 - \gamma^2}/a_{\pm}^2 \quad \Big(0 \leq \epsilon \leq 4\Big). \end{aligned} \tag{2.13}$$

The flat solution will appear unstable if eqs. (2.12) have solutions growing faster than $\exp[\tilde{\gamma}T]$.

It is sufficient to consider separable solutions of the form

$$f(X,T) = e^{\eta T} f(X), \quad g(X,T) = e^{\eta T} g(X), \tag{2.14}$$

where

$$\eta = \nu + i\omega, \tag{2.15}$$

and $f(X)$ and $g(X)$ are complex functions. Substituting into (2.12), we obtain

$$\begin{aligned} \mathbf{L_1} f = & - (\eta + \tilde{\gamma}) g, \\ \mathbf{L_0} g = & \quad (\eta - \tilde{\gamma}) f. \end{aligned} \tag{2.16}$$

Defining λ as

$$\lambda^2 \equiv \eta^2 - \tilde{\gamma}^2 \tag{2.17}$$

and $\tilde{g}(X)$ as

$$\tilde{g}(X) \equiv (\eta + \tilde{\gamma})\lambda^{-1} g(X), \tag{2.18}$$

eqs. (2.16) become

$$\begin{aligned} \mathbf{L_1} f &= -\lambda \tilde{g}, \\ \mathbf{L_0} \tilde{g} &= \lambda f. \end{aligned} \tag{2.19}$$

Eqs. (2.19) do not contain $\tilde{\gamma}$. Thus we have reduced the stability problem for the damped system to the one for dissipation-free case.

Let us start with the stability of a_+ solution. For the notational convenience, we shall denote the amplitude a_+ by a.

Having in mind the analysis of the Fourier numerical method, which imposes the periodic boundary conditions, we consider periodic perturbations f and $\tilde{g}$:

$$f(X) = f(X + aL), \quad \tilde{g}(X) = \tilde{g}(X + aL), \tag{2.20}$$

with L being the length of the system. Expanding

$$f(X) = \sum_{n=-\infty}^{\infty} f_n e^{i\tilde{k}_n X},$$
$$\tilde{g}(X) = \sum_{n=-\infty}^{\infty} g_n e^{i\tilde{k}_n X}, \tag{2.21}$$

where the wavenumbers $\tilde{k}_n$ are given by

$$\tilde{k}_n = \frac{2\pi n}{aL}, \tag{2.22}$$

eq. (2.19) reduces to the following linear algebraic system :

$$\begin{aligned} (\tilde{k}_n^2 - 4)f_n + \lambda g_n &= 0, \\ (\tilde{k}_n^2 - \epsilon)g_n - \lambda f_n &= 0 \quad (n = -\infty, \ldots, \infty). \end{aligned} \tag{2.23}$$

The eigenvalues λ_n are given by

$$\lambda_n^{\pm} = \pm\sqrt{-(\tilde{k}_n^2 - 4)(\tilde{k}_n^2 - \epsilon)}. \tag{2.24}$$

Clearly, the eigenvalues are either real or pure imaginary,

$$\lambda_n = \begin{cases} \lambda_n^R & \text{when } \epsilon < \tilde{k}_n^2 < 4 \\ i\lambda_n^I & \text{otherwise.} \end{cases} \tag{2.25}$$

Coming back to (2.15) and (2.17) this means that either $\nu = 0$, in which case the solution is stable, or $\omega = 0$ in which case we may have instability provided $\nu^2 > \tilde{\gamma}^2$, i.e. if $\lambda_n^2 > 0$. On the other hand, we know from (2.25) that $\lambda_n^2 > 0$ holds true when at least one of the $\tilde{k}_n^2$ falls into the window $(\epsilon, 4)$:

$$\epsilon < \tilde{k}_n^2 = \left(\frac{2\pi n}{aL}\right)^2 < 4. \tag{2.26}$$

One can easily obtain conditions under which at least one of the $\tilde{k}_n^2$ falls into the window $(\epsilon, 4)$. To this end, one picks up $\tilde{k}_n^2$ closest to 4 on the right-hand side ($\tilde{k}_n^2 > 4$:

$$n = \text{int}\left[\frac{aL}{\pi}\right] + 1. \tag{2.27}$$

Then if $\tilde{k}_{n-1}^2 < \epsilon$, the homogeneous solution is stable; otherwise it is unstable. Thus the instability occurs if

$$\frac{\pi}{aL}\text{int}\left[\frac{aL}{\pi}\right] > \frac{\epsilon^{1/2}}{2}. \tag{2.28}$$

Let, for instance, $\gamma = 0.27$ and $h = 0.9$. For this choice of parameters, $a = 0.964$ and $\epsilon = 1.9253$. If we choose $L = 50$, eq. (2.27) gives us $n = 16$. Hence, the most unstable mode could be the one with $n = 15$. And indeed, $\tilde{k}_{15}^2 = 3.8234$ so it falls into the window $(\epsilon, 4)$. One may check that there are altogether five unstable modes in the regime we chose.

In general the condition for stability,

$$\tilde{k}_{n-1}^2 < \epsilon < 4 < \tilde{k}_n^2, \tag{2.29}$$

amounts to

$$n - 1 < \frac{L}{2\pi}(2\sqrt{h^2 - \gamma^2})^{1/2} < \frac{L}{2\pi}(2\sqrt{h^2 - \gamma^2} + 2)^{1/2} < n. \tag{2.30}$$

The necessary condition for this is

$$\frac{L}{2\pi}(2\sqrt{h^2 - \gamma^2} + 2)^{1/2} - \frac{L}{2\pi}(2\sqrt{h^2 - \gamma^2})^{1/2} < 1. \tag{2.31}$$

Consequently, for the flat solution a_+ to be *unstable*, it is sufficient that the length of the interval exceed certain critical value :

$$L > \frac{\sqrt{2}\pi}{(\sqrt{h^2 - \gamma^2} + 1)^{1/2} - (h^2 - \gamma^2)^{1/4}}. \tag{2.32}$$

In the case of the a_- solution, we should only substitute $\epsilon \to -\epsilon$ in eq. (2.23) which yields

$$(\tilde{k}_n^2 - 4)(\tilde{k}_n^2 + \epsilon) + \lambda^2 = 0. \tag{2.33}$$

Instability occurs if $\lambda^2 > 0$, i.e. if (at least one) $\tilde{k}_n^2$ falls into the window $(-\epsilon, 4)$. And there always are $\tilde{k}_n^2$ falling into this window, in particular $\tilde{k}_n^2 = 0$. Consequently, a_- is *always* unstable.

To summarize, several points should be emphasized.

- The zero solution proves to be stable for $h < (1 + \gamma^2)^{1/2}$ and therefore, acts as an attractor in this region for which reason we shall refer to it as the *zero attractor.*
- Like the ψ_- soliton (see [58]) the a_- flat solution is always unstable.
- The a_+ solution is unstable to modes with wavenumbers in the band $\epsilon < \tilde{k}_n^2 < 4$.
- Identification of the unstable modes can be accomplished using the relation (2.26).
- Modes with sufficiently high wavenumbers are always stable.
- For any γ and h, the spatial period L can be chosen so large that the a_+ solution is unstable (see eq. (2.32)).

It is appropriate to mention that these results are similar to the ones obtained by Terrones *et al* [76] for the externally driven damped NLS equation.

We are now prepared to discuss the numerical solution of the parametrically driven NLS. We start with the presentation of our numerical scheme.

2.3 The split-step Fourier method

In order to derive a numerical scheme for the damped driven NLS equation (2.1), it is convenient to rewrite (2.1) as

$$\psi_t = i\mathbf{L}\psi + i\mathbf{N}(\psi)\psi, \quad -\infty < x < \infty, \tag{2.34}$$

with the operators $\mathbf{L}$ and $\mathbf{N}$ defined by

$$\mathbf{L}\psi = \psi_{xx} - \psi - h\psi^* + i\gamma\psi, \quad \mathbf{N}(\psi)\psi = 2|\psi|^2\psi. \tag{2.35}$$

We start with the discretization of the time variable.

2.3.1 Time discretization

The solution of (2.35) may be advanced from one time level to the next one by means of the formula

$$\psi(x, t+\tau) = e^{i\tau(\mathbf{L}+\mathbf{N})}\psi(x,t) + \mathcal{O}(\tau^2), \tag{2.36}$$

where τ denotes the time step. The right-hand side of (2.36) can now be replaced by

$$e^{i\tau(\mathbf{L}+\mathbf{N})} = e^{i\tau\mathbf{L}}e^{i\tau\mathbf{N}}\psi(x,t) + \mathcal{O}(\tau^2). \tag{2.37}$$

Eq. (2.37) is exact whenever $\mathbf{L}$ and $\mathbf{N}$ commute. In general, however, $\mathbf{L}$ and $\mathbf{N}$ do not commute and so eq. (2.37) is only first order accurate in τ. The splitting (2.37) can be improved to the accuracy $\mathcal{O}(\tau^3)$ and higher. This, however, makes little sense as the representation (2.36) (which is basic for our purposes) is first order accurate itself. We refer to Appendix A for details.

Combining (2.36) and (2.37), we have

$$U(x, t+\tau) = e^{i\tau\mathbf{L}}e^{i\tau\mathbf{N}}U(x,t), \tag{2.38}$$

where $U(x,t)$ denotes the approximation to $\psi(x,t)$.

Incidentally, some authors find it convenient to view the scheme (2.38) as succesively solving the equations

$$\psi_t = i\mathbf{N}(\psi)\psi, \quad \phi_t = i\mathbf{L}\phi \tag{2.39}$$

employing the solution of former equation as initial condition for the latter.

First, the solution is advanced using only the nonlinear part :

$$V^m = e^{i\tau\mathbf{N}(U^m)}U^m, \tag{2.40}$$

with $U^m = U(t = m\tau)$. Then, the split-step scheme (2.38) may be written as

$$U^{m+1} = e^{i\tau \mathbf{L}} V^m. \tag{2.41}$$

Weideman and Herbst [110] refer to the quantity V^m as an intermediate solution — although it, of course, cannot be considered an approximation to the theoretical solution. For simplicity, we shall do the same. If U^m is L-periodic, so is V^m, and therefore the boundary conditions are not violated by the introduction of V^m as an intermediate step.

Since the operator $\mathbf{N}$ does not involve derivatives, no further time approximation to (2.40) need to be made. On the other hand, the formula (2.41) involves the second spatial derivative and so approximation in space is required for the computation. So, we turn to the discretization of the space variable, and consider a Fourier method for this purpose.

2.3.2 Space discretization

At this point, one recalls that although the NLS equation is defined over the real line, one needs to impose conditions at finite boundaries when it is solved numerically. Also, we have to keep in mind that the Fourier method is only applicable to periodic problems. This may sound disturbing and look inappropriate when a problem with soliton solutions has to be solved. In practice, however, it is sufficient to place the boundaries far enough apart so that they do not interfere with the wave motion [110].

We first review a few well-known results concerning discrete Fourier transform (see Brigham [20], Canuto [22], Conte and deBoor [21]). Let $\mathrm{w}(x)$ be an L-periodic function, i. e. $\mathrm{w}(x) = \mathrm{w}(x + L)$. The Fourier series of $\mathrm{w}(x)$ reads

$$\mathrm{w}(x) = \sum_{n=-\infty}^{\infty} \hat{\mathrm{w}}_n e^{ik_n x}, \tag{2.42}$$

where $k_n = \frac{2\pi n}{L}$ and the Fourier coefficients $\hat{\mathrm{w}}_n$ are given by

$$\hat{\mathrm{w}}_n = \frac{1}{L} \int_{-L/2}^{L/2} \mathrm{w}(x) e^{-ik_n x} dx. \tag{2.43}$$

In deriving (2.43) from (2.42), or vice-versa, one uses the orthogonality condition

$$\int_{-L/2}^{L/2} e^{i(k_n - k_m)} dx = L\delta_{n,m}. \tag{2.44}$$

Here δ denotes the Kronecker symbol. The interval $[-L/2, L/2]$ is divided into N equal subintervals with grid spacing Δx and grid points x_j :

$$\Delta x = \frac{L}{N}, \quad x_j = j\Delta x, \quad j = -N/2, \ldots, N/2. \tag{2.45}$$

On the grid (2.45) the discrete Fourier transform of a discrete function

$$W = (W_{-N/2}, \ldots, W_{N/2-1})^T \tag{2.46}$$

is defined by

$$\hat{W}_n = \frac{1}{N} \sum_{j=-N/2}^{(N/2)-1} W_j e^{-\imath k_n x_j}, \quad n = -N/2, \ldots, N/2-1. \tag{2.47}$$

The inverse formula is

$$W_j = \sum_{n=-N/2}^{(N/2)-1} \hat{W}_n e^{\imath k_n x_j}, \quad j = -N/2, \ldots, N/2-1 \tag{2.48}$$

and so the orthogonality condition becomes

$$\sum_{j=-N/2}^{(N/2)-1} e^{\imath(k_n - k_m)x_j} = N\delta_{n,m(\mathrm{mod}N)}. \tag{2.49}$$

Comparing (2.44) with (2.49), we see that the discrete N-grid cannot distinguish between wavenumbers k_n and $k_{n(\mathrm{mod}N)}$, and although the small wavelength components may have been generated by nonlinear interactions [111], at a later stage they may be interpreted as long wavelength components. This phenomenon is called *aliasing* and its origin lies in the right-hand side of (2.49) [105].

Thus, whenever we do sampling of $\mathrm{w}(x)$, $W_j = \mathrm{w}(x_j)$, the exact Fourier amplitude $\hat{\mathrm{w}}_n$ and the aliased discrete amplitude $\hat{W}_n$ are related by

$$\hat{W}_n = \hat{\mathrm{w}}_n + \sum_{j=1}^{\infty} \hat{\mathrm{w}}_{n \pm jN}. \tag{2.50}$$

One may note that for a sufficiently smooth function the aliasing contribution in (2.50) becomes neglijeble as $N \to \infty$. The relation (2.50) also explains the absence of the amplitude $\hat{W}_{N/2}$ from (2.47) and (2.48). In this formulation $\hat{W}_{-N/2}$ represents the approximation to both $2\hat{\mathrm{w}}_{-N/2}$ and $2\hat{\mathrm{w}}_{N/2}$. In addition if $\mathrm{w}(x)$ has $p-1$ continuous derivatives and piecewise continuous p-th derivative then

$$\hat{W}_j = \hat{w}_j + \mathcal{O}((\Delta x)^p). \tag{2.51}$$

Turning back to our problem, the first step in the Fourier split-step scheme consists in replacing $V^m(x)$ and $U^{m+1}(x)$ in (2.41) by their Fourier series. This yields

$$\hat{u}_n^{m+1} = f(h, k_n^2, \tau)\hat{v}_n^m, \quad n = -\infty, \ldots, \infty \tag{2.52}$$

where $\hat{v}_n^m$ and $\hat{u}_n^{m+1}$ are the Fourier coefficients of the continuous functions $V^m(x)$ and $U^{m+1}(x)$, and $f(h, k_n^2, \tau)$ some complex function. Equation (2.52) may now be "discretized" by replacing $\hat{v}_n^m$ by $\hat{V}_n^m$ where

$$\hat{V}_n^m = \frac{1}{N} \sum_{j=-N/2}^{(N/2)-1} V_j^m e^{-ik_n x_j}, \quad n = -N/2, \ldots, N/2-1, \tag{2.53}$$

and V_j^m is the intermediate solution given by

$$V_j^m = e^{2i\tau|U_j^m|^2} U_j^m. \tag{2.54}$$

Thus, (2.52) becomes

$$\hat{U}_n^{m+1} = e^{-\gamma\tau} G(h, k_n^2, \tau), \quad n = -N/2, \ldots, N/2-1. \tag{2.55}$$

When the driver's strength h satisfies the condition $h < 1 + k_n^2$, the real and imaginary parts, A_n and B_n, of the complex function $G(h, k_n^2, \tau)$ are given by

$$\begin{aligned} A_n &= y_n \cos\omega_n\tau + \alpha_n z_n \sin\omega_n\tau, \\ B_n &= z_n \cos\omega_n\tau - \alpha_n^{-1} y_n \sin\omega_n\tau \end{aligned}$$

with ω_n and α_n denoting

$$\omega_n = |h^2 - (1+k_n^2)^2|^{1/2}, \quad \alpha_n = \left|\frac{1+k_n^2-h}{1+k_n^2+h}\right|^{1/2}, \tag{2.56}$$

and y_n and z_n being given by combinations of the real and imaginary parts of $\hat{V}_j^m$. For details of calculation we refer to the next section.

For $h > 1 + k_n^2$, A_n and B_n take the form

$$\begin{aligned} A_n &= \frac{y_n - \alpha_n z_n}{2} e^{\omega_n\tau} + \frac{y_n + \alpha_n z_n}{2} e^{-\omega_n\tau}, \\ B_n &= \frac{z_n - \alpha_n^{-1} y_n}{2} e^{\omega_n\tau} + \frac{z_n + \alpha_n^{-1} y_n}{2} e^{-\omega_n\tau}. \end{aligned}$$

Finally, the approximation at the next time level is calculated from the inverse transform

$$U_j^{m+1} = \sum_{n=-N/2}^{(N/2)-1} \hat{U}_n^{m+1} e^{ik_n x_j}, \quad j = -N/2, \ldots, N/2-1. \tag{2.57}$$

Summarizing, the method consists of three steps. First, the nonlinearity is inexpensively computed in the physical space using (2.54), then transposed into Fourier space by (2.53) and finally the Fourier space solution (2.55) is transformed back to the physical space by another Fourier transform (2.57).

In order to render the method competitive in terms of the speed of computation, the transformations (2.53) and (2.57) should be performed by Fast Fourier techniques [20]. This reduces the number of operations from $\mathcal{O}(N^2)$ to $\mathcal{O}(N \log N)$. As we discussed above, the penalty one may think we pay, however, is that aliasing errors are introduced into the approximation. In their review [23], Fornberg and Sloan showed that such fears seem to arise mainly from shortsighted analysis. They proved that even in the case of non-smooth functions the pseudospectral method sometimes performs much better than current theory would suggest and one of the most important strengths of pseudospectral methods is that relatively large errors cancel systematically over time. Still, several procedures exist by means of which the aliasing error can be removed (for more details on aliasing we refer to [22, 23, 111, 109, 105]). Moreover, the equation (2.50) shows that if solution is band-limited, i. e. if there exists an n_0 such that

$$\hat{\psi}_n^m = 0, \quad |n| > n_0, \tag{2.58}$$

then the Fourier discretization is exact provided $N \geq 2n_0$.

2.4 Derivation of the numerical solution for parametrically driven damped NLS

According to the split-step method discussed in Sec.2.2, the solution of parametrically driven damped NLS (2.1) may be advanced as

$$\psi(x, t+\tau) \approx e^{i\tau \mathbf{L}} e^{i\tau \mathbf{N}} \psi(x,t), \tag{2.59}$$

where

$$\mathbf{N}\psi = 2|\psi|^2\psi, \quad \mathbf{L}\psi = \psi_{xx} - \psi - h\psi^* + i\gamma\psi. \tag{2.60}$$

The function $e^{i\tau \mathbf{N}}\psi(x,t)$ can be seen as the solution $v(x,t)$, at $t = \tau$, of the equation

$$v_t = i\mathbf{N}(v)v, \quad \mathbf{N}(v)v = 2|v|^2 v \tag{2.61}$$

with the initial condition

$$v(x,0) = \psi(x,t). \tag{2.62}$$

Indeed, solving (2.61) with the initial condition (2.62) one gets at $t = \tau$

$$v(x,\tau) = \psi(x,t) e^{2i\tau|\psi(x,t)|^2}, \tag{2.63}$$

which is nothing but $e^{i\tau \mathbf{N}}\psi(x,t)$. Returning to (2.60), we have

$$\psi(x, t+\tau) \approx e^{i\tau \mathbf{L}} v(x,\tau). \tag{2.64}$$

Analogously, the right-hand side of (2.64) can be seen as a solution $u(x,t)$ of the initial-value problem

$$u_t = i\mathbf{L}u, \quad u(x,0) = v(x,\tau). \tag{2.65}$$

Thus, to evaluate $e^{i\tau\mathbf{L}}$ we must solve (2.65), that is

$$iu_t + u_{xx} - u + i\gamma u - hu^* = 0, \quad h,\gamma > 0. \tag{2.66}$$

We write u in the form

$$u(x,t) = e^{-\gamma t} f(x,t), \tag{2.67}$$

with $f(x,t)$ a complex function, $f = a + ib$. When substituting in (2.66), the exponential factors cancel and both real and imaginary components can be equated to obtain

$$\begin{aligned} -b_t + a_{xx} - a - ha &= 0, \\ a_t + b_{xx} - b + hb &= 0. \end{aligned} \tag{2.68}$$

Now, we expand a and b in Fourier series and (2.68) becomes

$$\begin{aligned} -\dot{B}_n + (ik_n)^2 A_n - A_n - hA_n &= 0, \\ \dot{A}_n + (ik_n)^2 B_n - B_n + hB_n &= 0. \end{aligned} \tag{2.69}$$

In (2.69) k_n is given by $k_n = (2\pi n/L)$, A_n and B_n are the Fourier coefficients of a and b respectively, and overdot denotes differentiation with respect to time.

Next, we rearrange (2.69) as

$$\begin{aligned} \dot{B}_n &= -(k_n^2 + 1 + h)A_n, \\ \dot{A}_n &= (k_n^2 + 1 - h)B_n, \end{aligned} \tag{2.70}$$

and look for a solution of the form

$$\begin{pmatrix} A_n(t) \\ B_n(t) \end{pmatrix} = \begin{pmatrix} \xi_n \\ \zeta_n \end{pmatrix} e^{i\Omega t}, \tag{2.71}$$

where ξ_n and ζ_n are constants. This gives

$$\begin{aligned} i\Omega\zeta_n &= -(k_n^2 + 1 + h)\xi_n, \\ i\Omega\xi_n &= (k_n^2 + 1 - h)\zeta_n. \end{aligned} \tag{2.72}$$

Nontrivial solutions exist if

$$\Omega_{1,2} = \pm\sqrt{(1 + k_n^2)^2 - h^2}. \tag{2.73}$$

For $(1 + k_n^2)^2 - h^2 > 0$, we obtain then

$$\begin{aligned} A_n &= c_n \cos\omega_n t + d_n \sin\omega_n t, \\ B_n &= \frac{\omega_n}{1 + k_n^2 - h}(-c_n \sin\omega_n t + d_n \cos\omega_n t), \end{aligned} \tag{2.74}$$

where $\omega_n = |(1+k_n^2)^2 - h^2|^{1/2}$ and c_n, d_n are arbitrary real coefficients. Otherwise, for $(1+k_n^2)^2 - h^2 < 0$,

$$\begin{aligned} A_n &= c_n e^{\omega_n t} + d_n e^{-\omega_n t}, \\ B_n &= \frac{\omega_n}{1+k_n^2-h}\Big(c_n e^{\omega_n t} - d_n e^{-\omega_n t}\Big). \end{aligned} \tag{2.75}$$

Note that we discard the case of the so-called resonances when $(1+k_n^2)^2 - h^2 = 0$.

The coefficients c_n and d_n can be fixed from the initial condition (2.65). We expand the real and imaginary parts of (2.65) in Fourier series, to get

$$A_n(0) = y_n, \quad B_n(0) = z_n, \tag{2.76}$$

where y_n and z_n represent the Fourier coefficients of the real and imaginary parts of $v(x,\tau)$.

From (2.74) and (2.76) we have, for $(1+k_n^2)^2 - h^2 > 0$

$$c_n = y_n, \quad d_n = \alpha_n z_n, \tag{2.77}$$

with

$$\alpha_n = \left|\frac{1+k_n^2-h}{1+k_n^2+h}\right|^{1/2}. \tag{2.78}$$

For $(1+k_n^2)^2 - h^2 < 0$, eqs. (2.75) and (2.76) yield

$$c_n = \frac{1}{2}(y_n - \alpha_n z_n), \quad d_n = \frac{1}{2}(y_n + \alpha_n z_n). \tag{2.79}$$

Thus we find that

$$\begin{aligned} A_n &= y_n \cos\omega_n t + \alpha_n z_n \sin\omega_n t, \\ B_n &= z_n \cos\omega_n t - \alpha_n^{-1} y_n \sin\omega_n t, \end{aligned} \tag{2.80}$$

when $(1+k_n^2)^2 - h^2 > 0$, and

$$\begin{aligned} A_n &= \frac{y_n - \alpha_n z_n}{2} e^{\omega_n t} + \frac{y_n + \alpha_n z_n}{2} e^{-\omega_n t}, \\ B_n &= \frac{z_n - \alpha_n^{-1} y_n}{2} e^{\omega_n t} + \frac{z_n + \alpha_n^{-1} y_n}{2} e^{-\omega_n t}, \end{aligned} \tag{2.81}$$

for $(1+k_n^2)^2 - h^2 < 0$.

Recalling that A_n and B_n are the Fourier coefficients of the real and imaginary parts of $f(x,t)$ in (2.67), we find that under the Fourier transform eq. (2.67) becomes

$$\hat{u}_n(t) = e^{-\gamma t}(A_n + iB_n). \tag{2.82}$$

The inverse Fourier tranform of (2.82) gives us the numerical solution of parametrically driven damped NLS :

$$u(x,t) = \sum_{n=-\infty}^{\infty} \hat{u}_n e^{ik_n x}. \tag{2.83}$$

We close this section with a brief comment on the method used to find y_n and z_n. The most straightforward way is to obtain them through Fourier transforms both of real and imaginary parts of $v(x,\tau)$. This would imply 3 fast Fourier transforms per time step altogether. Highly unwanted, since we need a very low CPU time consuming code. Fortunately, this can be avoided if we write $v(x,\tau)$ as

$$v(x,\tau) = \text{Re } v(x,\tau) + i\text{Im } v(x,\tau), \tag{2.84}$$

and Fourier-expand each term of (2.84) to obtain

$$p_n + iq_n = y_n + iz_n. \tag{2.85}$$

In (2.85), p_n and q_n are the real and imaginary parts of the Fourier coefficients of $v(x,\tau)$. Re $v(x,\tau)$ and Im $v(x,\tau)$ are real quantities and therefore their complex Fourier coefficients (y_n and z_n, respectively) have the property that

$$y_n^* = y_{-n}, \quad z_n^* = z_{-n}. \tag{2.86}$$

Using (2.86) in (2.85), we arrive at the following relation for y_n and z_n :

$$y_n = \frac{p_n + p_{-n}}{2} + i\frac{q_n - q_{-n}}{2}, \tag{2.87}$$

$$z_n = \frac{q_n + q_{-n}}{2} - i\frac{p_n - p_{-n}}{2}. \tag{2.88}$$

Thus, eqs. (2.87)-(2.88) bring down the total number of fast Fourier transforms per time step to 2 FFT and render a 50% faster computational code. (We must mention also that the equations are discretized and therefore the index n ranges from $-N/2, \ldots, N/2-1$.)

Since in practice computational errors are expected, in the next section we turn to a stability analysis in order to establish under which conditions perturbations, e. g. numerical errors, may grow.

2.5 Numerical stability

We consider [112] the stability of the flat solution

$$\overset{\circ}{U}{}^m = ae^{-i\alpha} \tag{2.89}$$

in the framework of the split-step Fourier method. Since the solution (2.89) is x- and t-independent we keep the notation $\overset{\circ}{U}$. We perturb (2.89) to

$$U_j^m = (1 + \varepsilon_j^m)\,\overset{\circ}{U}, \tag{2.90}$$

where ε_j^m is assumed to be an L-periodic function [110]. The discrete Fourier expansion of the perturbation is

$$\varepsilon_j^m = \sum_{n=-N/2}^{(N/2)-1} \hat{\varepsilon}_n^m e^{ik_n x_j}, \quad j = -N/2, \ldots, N/2-1, \tag{2.91}$$

with k_n given by $k_n = 2\pi n/L$.

Substituting (2.90) into (2.40) and retaining first order terms ε_j^m, we arrive at the linearized version of the intermediate solution

$$V_j^m = \overset{\circ}{U}\, e^{2i|\overset{\circ}{U}|^2\tau}[1 + \varepsilon_j^m + 2i|\,\overset{\circ}{U}\,|^2\tau(\varepsilon_j^m + \varepsilon_j^{m^*})]. \tag{2.92}$$

From (2.53) and (2.92) it follows that

$$\hat{V}_n^m = \begin{cases} \overset{\circ}{U}\, e^{2i|\overset{\circ}{U}|^2\tau}\Big[1 + \hat{\varepsilon}_0^m + 2i|\,\overset{\circ}{U}\,|^2\tau(\hat{\varepsilon}_0^m + \hat{\varepsilon}_0^{m^*})\Big], & n = 0, \\ \overset{\circ}{U}\, e^{i2|\overset{\circ}{U}|^2\tau}\Big[\hat{\varepsilon}_n^m + 2i|\,\overset{\circ}{U}\,|^2\tau(\hat{\varepsilon}_n^m + \hat{\varepsilon}_{-n}^{m^*})\Big], & n \neq 0. \end{cases} \tag{2.93}$$

Next, $\hat{U}_n^{m+1}$ is computed from (2.55), (2.89) and (2.93), to give

$$\begin{aligned} \hat{U}_n^{m+1} &= e^{-\gamma\tau} a\{\hat{\varepsilon}_n^m[(a_n(1+c_n) - ib_nc_n) - (a_n^*c_n + ib_n^*(1+c_n))] \\ &+ \hat{\varepsilon}_{-n}^{m^*}[(a_nc_n + ib_n(1-c_n)) + (a_n^*(1-c_n) - ib_n^*c_n)]\}, \quad n \neq 0, \end{aligned} \tag{2.94}$$

where we denoted

$$a_n \equiv (\cos\omega_n\tau - i\cosh\rho_n \sin\omega_n\tau)e^{2i|\overset{\circ}{U}|^2\tau},$$

$$b_n \equiv \sin\omega_n\tau \sinh\rho_n e^{-2i|\overset{\circ}{U}|^2\tau + 2i\alpha},$$

$$c_n \equiv 2i|\,\overset{\circ}{U}\,|^2\tau$$

and

$$\cosh\rho_n = \frac{\alpha_n + (\alpha_n)^{-1}}{2}, \quad \sinh\rho_n = \frac{\alpha_n - (\alpha_n)^{-1}}{2}, \tag{2.95}$$

with α_n and ω_n given by (2.56). In deriving eq. (2.94) we have assumed that $h < 1 + k_n^2$. The situation with $h > 1 + k_n^2$ may arise only at the border of our region of interest.

On the other hand, from (2.90) and (2.91) we have

$$\hat{U}_n^{m+1} = \begin{cases} \overset{\circ}{U}\,(1 + \hat{\varepsilon}_0^{m+1}), & n = 0, \\ \overset{\circ}{U}\,\hat{\varepsilon}_n^{m+1}, & n \neq 0. \end{cases} \tag{2.96}$$

A comparison of (2.94) and (2.96) yields

$$\begin{pmatrix} \hat{\varepsilon}_n \\ \hat{\varepsilon}^*_{-n} \end{pmatrix}^{m+1} = A_n \begin{pmatrix} \hat{\varepsilon}_n \\ \hat{\varepsilon}^*_{-n} \end{pmatrix}^m, \quad n = -N/2, \ldots, N/2, \quad n \neq 0 \tag{2.97}$$

where the amplification matrices A_n are given by

$$A_n = e^{-\gamma\tau} \begin{pmatrix} a_n(1+c_n) - ib_n c_n & a_n c_n + ib_n(1-c_n) \\ -a^*_n c_n - ib^*_n(1+c_n) & a^*_n(1-c_n) - ib^*_n c_n \end{pmatrix}. \tag{2.98}$$

The eigenvalues of A_n are given by an expression of the form

$$\lambda_n = e^{-\gamma\tau}\Big(\beta_n \pm (\beta_n^2 - 1)^{1/2}\Big), \tag{2.99}$$

with

$$\beta_n = \frac{1}{2}\{(a_n + a^*_n) + (a_n - a^*_n)c_n - i(b_n + b^*_n)c_n\} \tag{2.100}$$

Exponential growth will be exhibited by $(\hat{\varepsilon}_n, \hat{\varepsilon}^*_{-n})^T$ whenever either of the eigenvalues given by (2.99), satisfies

$$|\lambda_n| > 1. \tag{2.101}$$

It is easy to see [110] that this is equivalent to

$$|\beta_n| > \cosh\gamma\tau. \tag{2.102}$$

Let us have a closer look at β_n. By means of algebraic manipulations and Taylor expansion to the second order in $A\tau$ with $A \equiv 2|\,\mathring{U}\,|^2$, one gets

$$\beta_n = (1 - \frac{3}{2}A^2\tau^2)\{\cos\omega_n\tau + \tan\theta\sin\omega_n\tau\}, \tag{2.103}$$

where

$$\tan\theta = \frac{\eta_n(A\tau) + \sinh\rho_n \sin 2\alpha(A\tau)^2}{1 - \frac{3}{2}(A\tau)^2} \tag{2.104}$$

and

$$\eta_n \equiv 2\cosh\rho_n + \sinh\rho_n\cos 2\alpha. \tag{2.105}$$

Thus, the condition (2.102) for instability becomes

$$|\cos(\omega_n\tau - \theta)| > \cosh(\gamma\tau)(1 + \frac{3}{2}A^2\tau^2)\cos\theta \tag{2.106}$$

with

$$\cos\theta = \frac{1}{\sqrt{1+\tan^2\theta}}. \tag{2.107}$$

We shall discuss the instability condition in two regimes: far enough and close to the resonance between the soliton's internal frequency ω_n and driver's frequency Ω ($\Omega = 1$ in our case; in Sec. 1.4 we mentioned that we can always arrange that $\Omega = 1$ in (1.48)). Hence, at resonance $h = 1 + k_n^2$.

For values of h not too close to a resonance $1 + k_n^2$, i. e. for $\alpha_n \sim 1$, the relation (2.106) can be reduced to

$$|\cos(\omega_n\tau - \theta)| > \cos(s_n\tau), \tag{2.108}$$

where

$$s_n^2 \equiv (\eta_n^2 - 3)A^2 - \gamma^2. \tag{2.109}$$

Here, we must point out that instability may occur only when $(\eta_n^2 - 3)A^2 - \gamma^2 > 0$ which we therefore assume. It was found that this assumption holds true for $\alpha_n > 1/\sqrt{3}$ which places us far enough from resonance. First order Taylor series expansions of both sides in eqs. (2.107)-(2.108) lead to

$$\eta_n A - s_n < \omega_n < \eta_n A + s_n. \tag{2.110}$$

In the regime $\alpha_n \sim 1$, one gets $\eta_n \sim 2$, $s_n \sim A$, $\omega_n \sim 1 + k_n^2$ and $A \sim 1$; hence, we can (roughly) approximate (2.110) by $1 < 1 + k_n^2 < 3$ which shows that only low wavenumber modes become unstable. This is in complete agreement with the analytical instability. It is necessary to note here that this is a very rough estimate and therefore one cannot expect to obtain the analytical result exactly. The fact that eq. (2.110) is the counterpart of the analytical instability condition (2.26), is confirmed by a more accurate calculation.

Because of the oscillatory nature of the instability condition (2.108) some high frequency modes may be unstable in addition to the low modes given by (2.110). To check this, we considered [112] A, h, γ and τ fixed, and defined a function

$$g(\omega) = \cos(\omega\tau - \theta). \tag{2.111}$$

It was convenient to consider ω as a continuous variable, even though the wavenumbers present in computation can only assume discrete values $k_n = 2\pi n/L$. (This idea belongs to Herbst and Weideman [110].) The function g has turning points at

$$\omega = \omega_p = \frac{\theta + p\pi}{\tau}, \quad p = 0, 1, \ldots \tag{2.112}$$

It follows that the inequalities

$$|g(\omega)| > \cos(s\tau) \tag{2.113}$$

and

$$|\omega - \omega_p| < s, \quad p = 0, 1, \ldots \tag{2.114}$$

are equivalent. Thus, whenever $\omega = \omega_n$ satisfies (2.114) for some p, the n-th mode becomes unstable.

We saw earlier that the instability resulting from $p = 0$ corresponds to the analytical instability (see (2.110)). However, for $p > 1$ the scheme's finite time step τ comes into play and high wavenumber instabilities, which have no analytical conterparts, may set in. These should be avoided. Accordingly, we need to derive a condition ensuring that the inequality (2.114) may hold true for no any $p > 0$. Considering $p = 1$ and bearing in mind that the highest values of k^2 and therefore of ω, present in the computation are

$$k^2_{-N/2} = \left(\frac{2\pi(-N/2)}{L}\right)^2 = \frac{\pi^2}{(\Delta x)^2} \tag{2.115}$$

and

$$\omega = \left(\left(\frac{\pi^2}{(\Delta x)^2} + 1\right)^2 - h^2\right)^{1/2} \sim \frac{\pi^2}{(\Delta x)^2} + 1, \tag{2.116}$$

one finds that (2.114) becomes

$$\tau < \frac{(\Delta x)^2}{\pi}. \tag{2.117}$$

(Here $\Delta x \equiv L/N$.) Hence, as long as (2.117) is satisfied the solution is stable against high frequency perturbation. Note that an identical relation was derived by Herbst and Weideman [110] for the unperturbed NLS.

We point out that eq. (2.117) is sufficient but not necassary. From (2.114), it follows that if s is small, the range of ω values for which (2.114) is satisfied is small. It could therefore be that no higher wavenumbers k_n fall inside this range even when (2.117) is violated. In this case, of course, the instability will not show up.

Assume now we are close to a resonance, i. e. $\alpha_n^{-1} \gg 1$. If $\eta_n \tau \ll 1$, it can be shown that no numerical instability arises [112]. If, on the contrary, $\alpha_n^{-1} \gg 1$ and $\eta_n \tau \gg 1$, the condition (2.106) takes the form

$$|\cos(\eta_n A \tau)| > \frac{\cosh \gamma\tau}{\eta_n A \tau} \approx \frac{1}{\eta_n A \tau}, \tag{2.118}$$

and we are doomed to have multiple numerical instabilities. These can be avoided by choosing a sufficiently small time step τ, $\tau ll \eta_n^{-1}$. We are not elaborating here on *how* small τ should be since we did not have to carry out simulations for resonant values of h.

Up until now we have been considering stability of the flat nonzero solution. In a similar way one can analyse stability of the zero solution. This turns out to be a rather trivial exercise; no numerical instability occurs in this case.

We close this section by pointing out that our stepsize restrictions correspond to the flat solution of the perturbed NLS. Strictly speaking, it is not clear how these restrictions will modify when a localised (soliton) solution is simulated. Another, not necessarily unrelated question concerns the relevance of linear stability analysis for a nonlinear equation.

These questions refer to any numerical scheme, of course, and usually remain unanswered. Consequently, the obtained stepsize restrictions should always be supplemented by an *ad hoc* stability analysis; for instance, one should watch for the excitation of the Fourier modes with high wavenumbers. (One should take care, however, because it could happen that the small wavelength components may have been generated by nonlinear interactions [111].) The value of the above restrictions is that they provide at least a start-up idea on the choice of the time step. It is interesting to note here that in our simulations of soliton dynamics the numerical instability did not arise whenever the restriction $\tau < (\Delta x)^2/\pi$ was in place.

Chapter 3

Numerical results

"There were things which he stretched,
but mainly he held the truth"
Mark Twain, *Huckleberry Finn*

In this chapter we present numerical studies of nonlinear oscillations and chaotic temporal behaviour of the soliton solution ψ_+ of the parametrically driven damped NLS,

$$i\psi_t + \psi_{xx} - \psi + 2|\psi|^2\psi = h\psi^* - i\gamma\psi, \tag{3.1}$$

above the Hopf bifurcation curve (i. e. in the region where the stationary soliton is unstable). We also uncover other attractors in that region and consequently, reconstruct the attractor chart on the (h, γ)-plane.

3.1 Topography of attractors of the parametrically driven, damped nonlinear Schrödinger equation

We used the method described in the previous chapter to simulate the evolution of the (unstable) stationary soliton (1.50-1.52). We took 1024 Fourier modes with the time increment[1] $\Delta t = 2\pi \times 10^{-3}$. The interval length was chosen to be $L = 50$.

The main results of this work are summarised in Fig. 2. This is the attractor chart of the parametrically driven NLS on the (h, γ) plane. The region where the stationary soliton is stable was discussed in Sec. 1.4, while in the unstable region, the following subregions were

[1]The integration was verified by decreasing the time increment, Δt, to $\Delta t = 2\pi \times 10^{-4}$ and also by using a different method — a finite difference scheme [113].

identified.

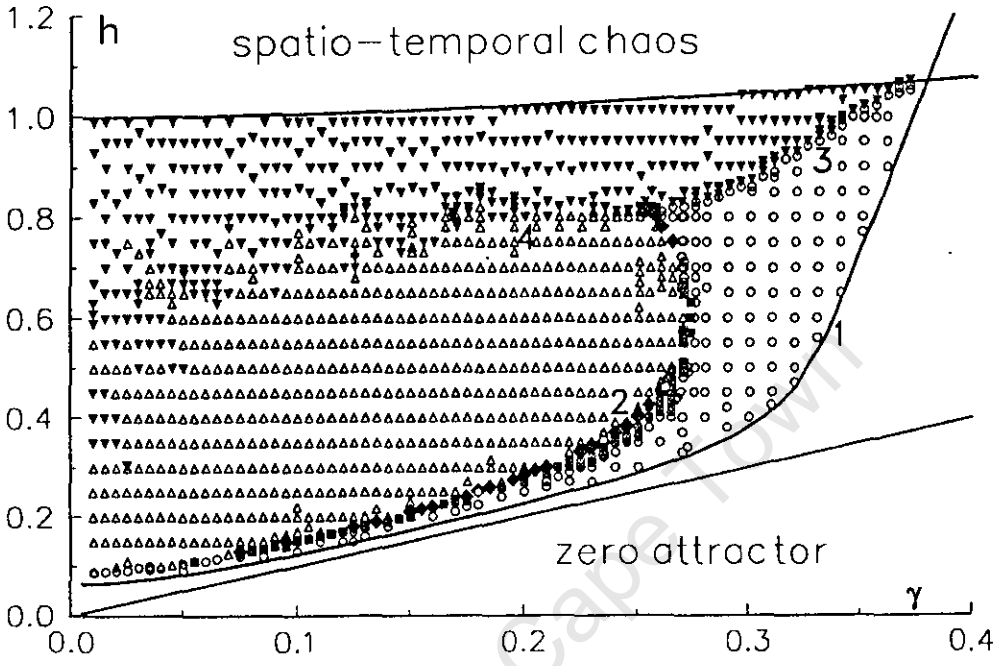

Fig.2

The attractor chart of eq.(2) on the (h, γ)-plane. Empty circles denote period-1 solutions and shadowed boxes periods-2, 4, and 8. Small white blobs indicate period-6, period-7 and period-10 solitons observed at $(\gamma = 0.262, h = 0.46)$, $(\gamma = 0.235, h = 0.355)$ and $(\gamma = 0.18, h = 0.251)$, respectively. Shadowed diamonds stand for type-I and type-II strange attractors observed at $(\gamma = 0.18, h = 0.253)$ and $(\gamma = 0.26, h = 0.4530)$, respectively, as well as for complex cycles. The region of stable stationary solitons is left blank; empty triangles mark the area where the only attractor is $\phi \equiv 0$, and the domain of spatio-temporal chaos is marked by black triangles. Note an unexpectedly complex, "shark jaw" shape of the interface between the regions of spatio-temporal chaos and zero attractor.

First of all, clearly seen is the domain where the period-doubling route to (temporal) chaos takes place. Above the line 1, in the domain marked by open circles, the nontrivial attractor is temporally periodic. Very roughly one may think of it as a soliton with periodically varying amplitude and phase. (However, unlike the stationary soliton (1.50)–(1.52), this periodic soliton has undulations on its spatial "tails".) In the vicinity of the curve 1 the frequency of the periodic solution, ω_1, was seen to be in a good agreement with $\mathrm{Im}\,\lambda$ where λ is the complex eigenvalue of the operator arising in the linearisation of eq. (3.1)

around the stationary soliton (1.50)–(1.52) [58]. In Fig. 2 attractors resulting from subsequent period-doubling (2-periodic, 4-periodic, 8- and higher periodic, and finally, complex cycles and strange attractors) occupy a narrow band of "boxes", "diamonds" and white blobs. The curve 2 is a boundary of the period-doubling sequence and separates the region of strange attractors from the region where only zero attractor exists. The latter region is marked by empty triangles.

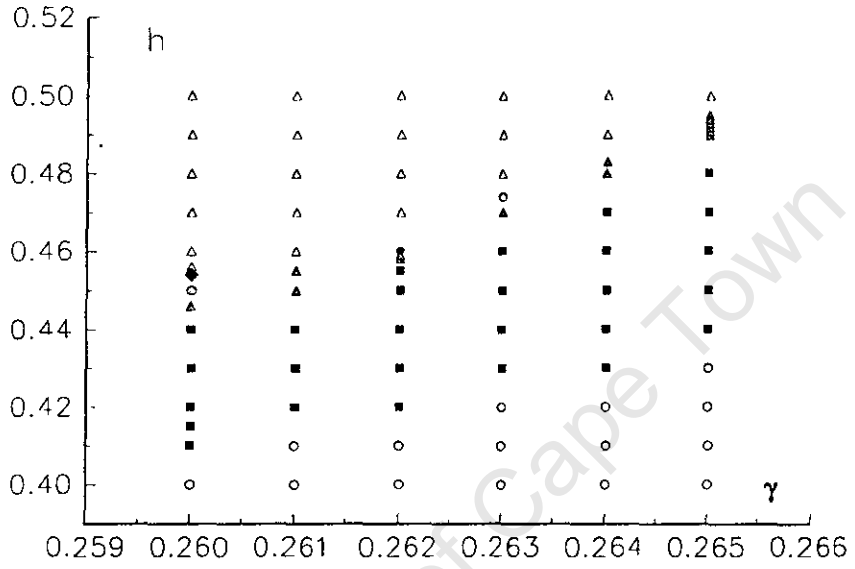

Fig.3

An enlarged portion of Fig.2 displaying the period-doubling route to chaos. Notation is as in Fig.2 with the exception that shadowed boxes, triangles, and circles stand for periods-2, 4, and 8, respectively. The black blob at $\gamma = 0.262, h = 0.46$ marks a period-6 solution. (Note the appearance of odd periods and their doublings in the neighbourhood of the upper boundary of the period-doubling sequence.) .

Crossing the bifurcation line 3, the limit cycle is replaced by the spatio-temporal chaos. As opposed to the period-doubling scenario, there are no intermediate attractors here which corresponds to the quasiperiodic transition. The line 4 separates spatio-temporal chaos from the region of the zero attractor. The lines 2, 3, and 4 meet at a "tricritical" point $h_c = 0.812$, $\gamma_c = 0.2525$ which separates the period-doubling and quasiperiodic routes.

Details of the period-doubling transition are presented in Figs. 3 and 4. Fig. 3 displays an enlarged portion of the attractor chart exhibiting the period-doubling sequences for the fixed γ and varied h. (Note the appearance of odd periods and their doublings in the

neighbourhood of the upper boundary of the period-doubling sequence.)

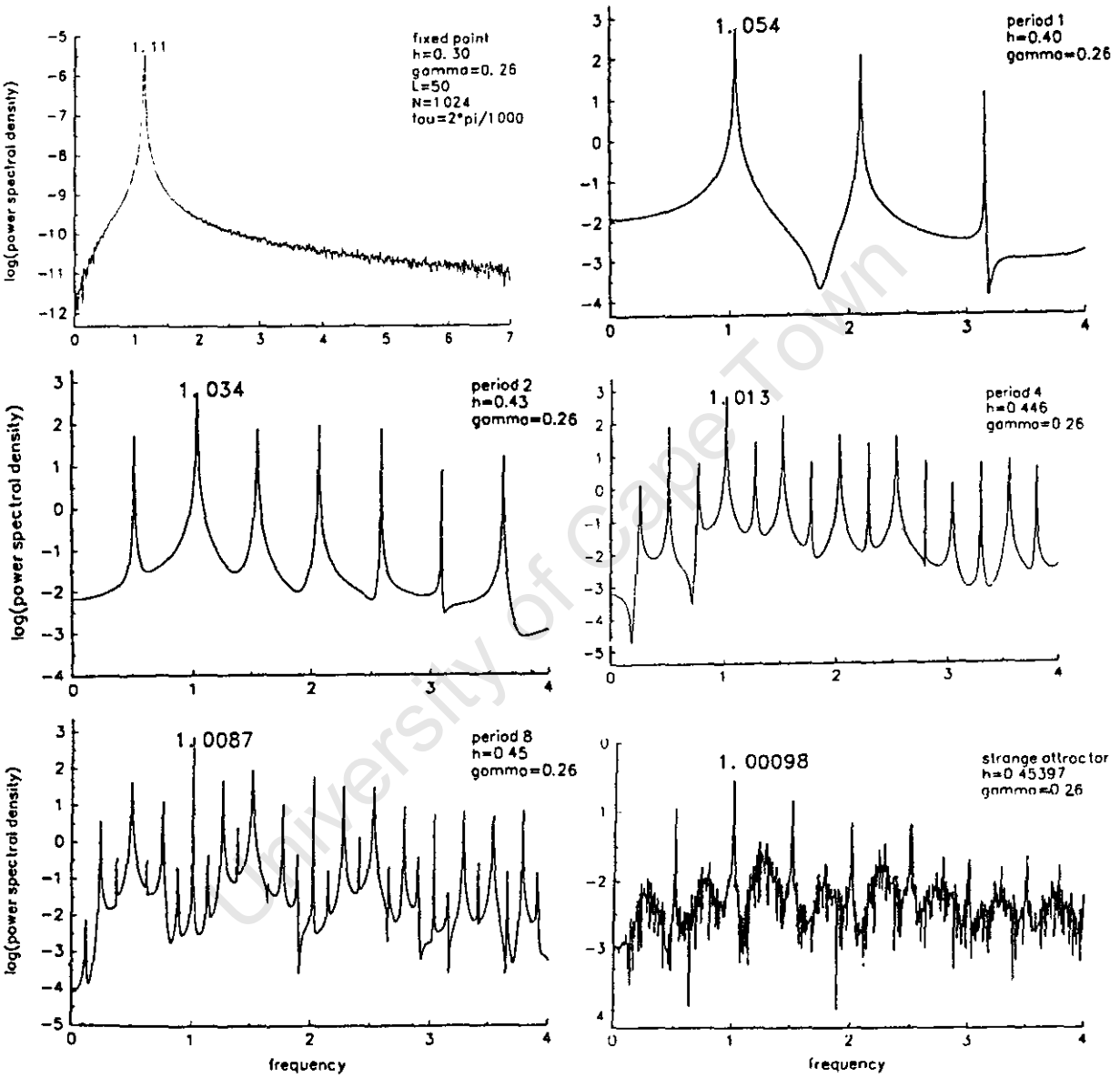

Fig.4

a: The power spectral density of the stable stationary solution during the start-off transient ($1000 \leq t \leq 2000$). b-f: Power spectral densities of the time-dependent solitons. b-e: periods-1,2,4,8 ; f: two-band strange attractor.

In Fig. 4, typical attractors are illustrated by their power spectra. As an example, we have chosen a sequence arising along the line $\gamma = 0.26$. Below the curve 1 the attractor is the stable stationary soliton, $\psi(x,t) = \psi_+(x)$. Fig. 4a shows the power spectrum of the transient solution in this region. (We have picked up a point close to the curve 1.) Before settling down to the stationary attractor, the solution oscillates with the frequency $Im\lambda$. (λ is the eigenvalue of the linearised problem described above.) As we cross the curve 1 in Fig. 2, the Hopf bifurcation occurs and this frequency becomes the main harmonic frequency of the period-1 solution. (We denote the latter ω_1.) In the immediate vicinity of curve 1 the frequency is $\omega_1 = 1.105$ which practically coincides with $Im\lambda$. Here the amplitude of the oscillation is small and the contribution of higher harmonics negligible. As h is increased, the main frequency decreases (Fig. 4 d-f); on the other hand we know that the $Im\lambda$ grows. This discrepancy is caused, of course, by the growth of anharmonicity effects. Finally, the period-doubling can be seen from the appearance of subharmonics in Fig. 4.

In order to emphasize the existence of the entire Feigenbaum sequence of direct and reverse bifurcations, we plot the phase portrait of a two-band strange attractor arising for $\gamma = 0.26$, $h = 0.4539$ (Fig. 5a). The two-band structure is explicitly illustrated by a one-dimensional map $X_{n+2} = f(X_n)$ (Fig. 5b). Here $\{X_n\}$ is the sequence of the maximum values of $\mathrm{Im}\,\psi(0,\mathrm{t})$ on the phase portrait (Fig. 5a).

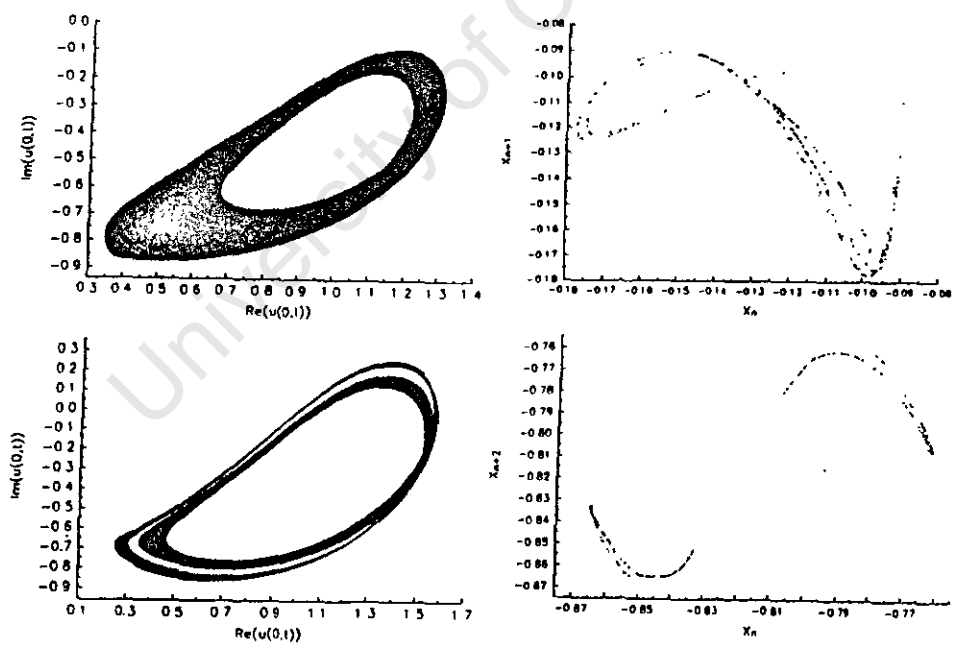

Fig.5

a,b: type-I (two-band) strange attractor, $\gamma = 0.26, h = 0.453974$. *c,d: type-II strange attractor,* $\gamma = 0.18, h = 0.253$.

The band of strange attractors borders the region of the zero attractor. As we approach the border between the two regions, the structure of the strange attractor becomes more complex. This is exemplified by a phase portrait and one-dimensional map of a complex attractor for $\gamma = 0.18$ and $h = 0.253$ (Fig. 5, c-d). As h is increased, the strange attractors undergo a crisis (Fig. 6) and we find ourselves in the zero attractor domain. Thus, the final stage of the soliton's instability following the period-doubling sequence, is its decay to zero. If we increase h for a fixed γ (provided γ is smaller than $\gamma_c = 0.2525$ so as not to cross the upper part of the period-doubling band), the zero attractor becomes unstable and a spatio-temporal chaotic state emerges.

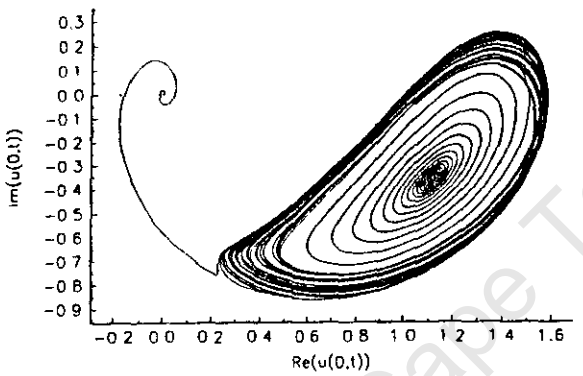

Fig.6

Crisis of the attractor; $\gamma = 0.26, h = 0.453975$

For all $\gamma > \gamma_c$ and $h > h_c$, the transition to chaos is via the quasiperiodic route. In terms of the equation (1.5) this implies the sequence "stationary soliton → period-1 soliton → spatio-temporal chaos". In terms of eq. (1.48), the stationary soliton (1.50)–(1.52) becomes periodic with the frequency of the driver, $\Omega = 1$, while the period-1 soliton becomes quasiperiodic with two frequencies, Ω and ω_1. (Hence the name of the route.) In the vicinity of the curve 3 (the curve of the quasiperiodic transition), an additional low frequency $\tilde{\omega}$ is excited in the power spectrum. Below the curve the low frequency oscillation dies off as a transient. For example, for $\gamma = 0.34$ and $h = 0.993443329$, the frequency $\tilde{\omega} \approx 0.06$ disappeared from the spectrum after $t \sim 2000$. Above the curve 3, the $\tilde{\omega}$ is also excited in the spectrum at the first instance of time — together with combinations of $\tilde{\omega}$ and ω_1, the main frequency of the cycle. Soon after that a chaotic structure nucleates in the core of the soliton and subsequently spreads over the entire axis. (The same sequence "period-1 → spatio-temporal chaos" was observed for larger systems, e. g. $L = 200$. We kept the time step unchanged and increased N to 4096 so that to preserve the spatial resolution. Here the spatio-temporal chaos sets in at a slightly smaller[2] h, i. e. for $h = 0.98925$.) Fig. 7 shows a

[2]In a similar way, the curve 4 (Fig. 2) shifts towards smaller h when L is increased.

typical evolution of the soliton in the spatiotemporal chaotic domain.

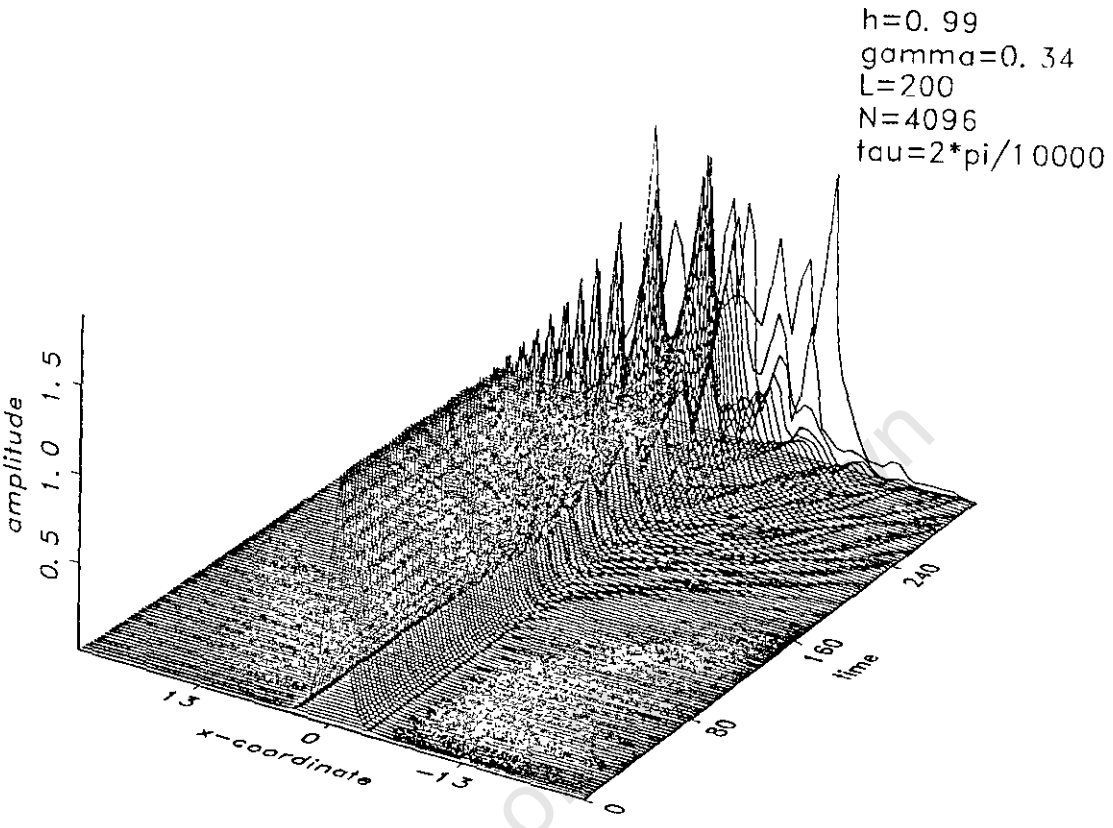

Fig.7
Spatio-temporal chaos seeded by the soliton.
Only (-25,25) part is shown

In the region to the right of curve 1 and above the line $h = (1+\gamma^2)^{1/2}$ (Fig. 2), the unstable soliton evolves into a cnoidal wave. It is merely a bifurcation *in space* that occurs here along the line $h = (1+\gamma^2)^{1/2}$. Fig. 8 shows how this cnoidal wave attractor emerges from the decay of the unstable soliton. Note the creation and annihilation of soliton-like structures occuring while the solution settles down.

Fig.8
Cnoidal wave emerging from the decay of the unstable soliton.

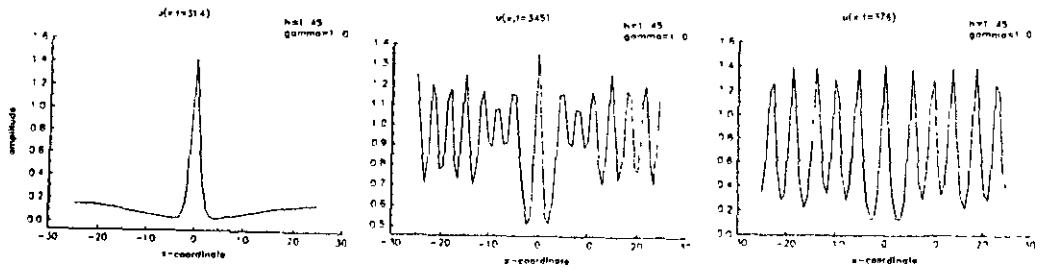

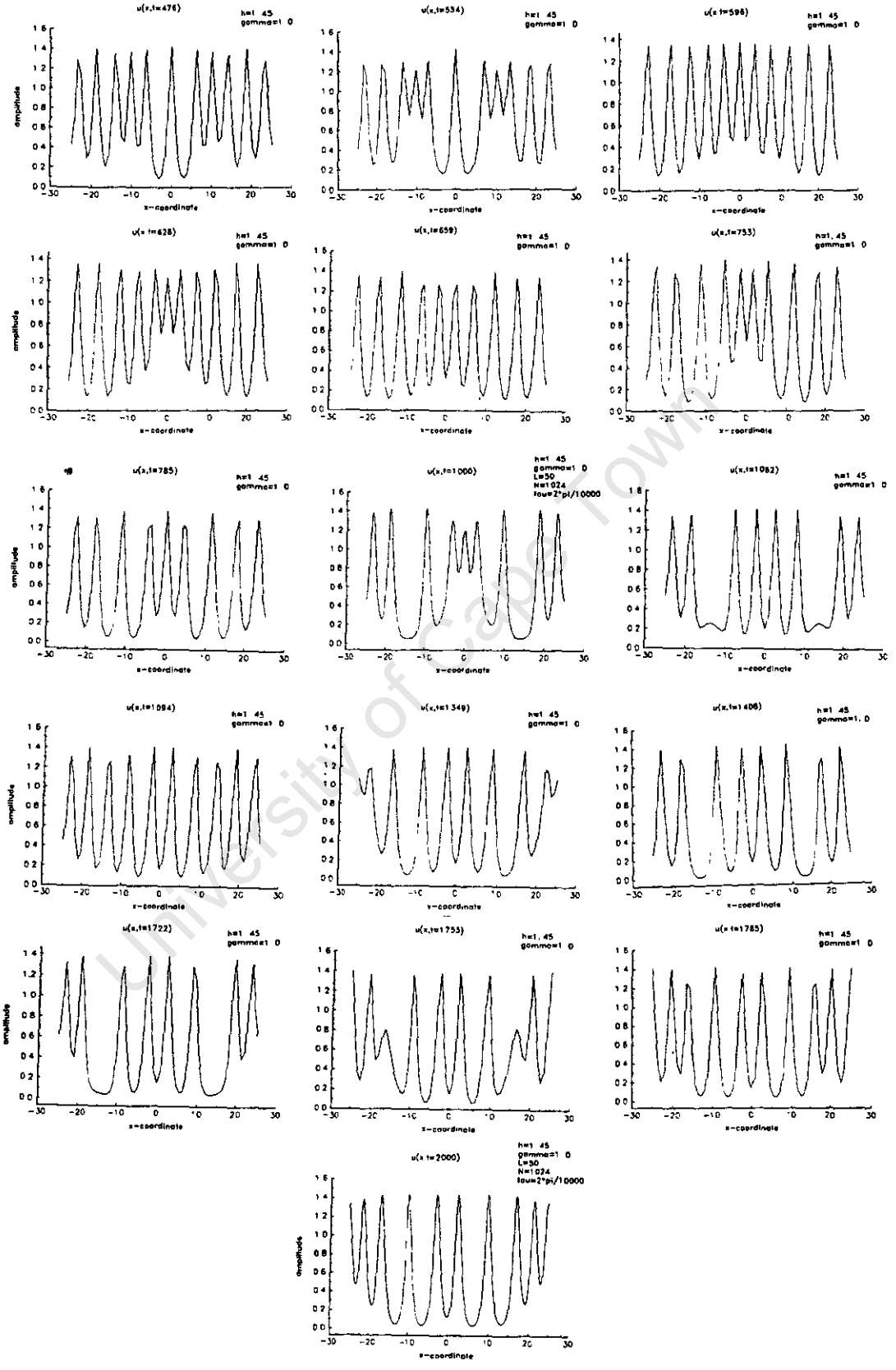

We conclude the discussion of the observations by mentioning a few curious phenomena. First, it is worth noticing an unusual, "shark jaw" shape of the boundary between the regions of the zero attractor and spatio-temporal chaos. Second, for some values of h and γ the setting-in of the spatio-temporal chaos was preceded by the appearance of what can be interpreted as a bound state of two solitons: a finite lifetime state in the form of two solitons with overlapping tails (see Fig. 9).

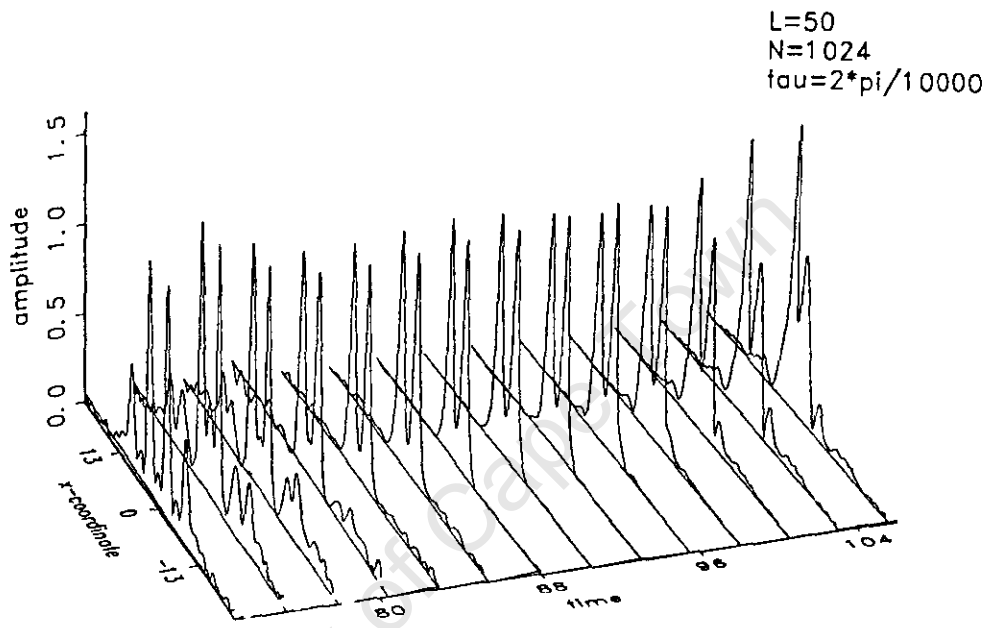

Fig.9
'Bound state' of two solitons which precedes the appearance of spatio-temporal chaos.
h=*0.84*, $\gamma = 0.24$

Finally, we have simulated the evolution of the unstable *homogeneous* solution of eq. (3.1) at some points along the lines $\gamma = 0.26$ and $\gamma = 0.34$ on the (h, γ) plane. Surprisingly, for points on the line $\gamma = 0.26$ this evolution results in the formation of two solitons of which only one survives finally. (The other one dies off to zero.) As we increase h, the surviving soliton exhibits period-doubling sequence followed by zero attractor and spatio-temporal chaos.

The decay of the flat solution for $\gamma = 0.34$ resulted in the creation of two solitons as well. (This was seen for instance, at $h = 0.7$.) In this case, they approach each other to merge finally into a period-1 soliton. As we increase h to $h = 0.8$, the emerging spatial pattern consists of two (double-peaked) structures centered at $x = 0$ and $x = L/2$, each of which could be interpreted as two strongly overlapping solitons oscillating periodically in time (see Fig. 10 for the profile of this structure). A further increase of h leads to spatio-temporal chaos.

The evolution of the unstable homogeneous solution was also simulated in the region to the right of curve 1 on Fig. 2. In this region the attractor is the stationary soliton ψ_+. We picked up a point close to the curve 1: $h = 0.7, \gamma = 0.35$. Again two solitons emerged. After transients died off we were left with two stationary solitons (positioned at arbitrary points in space).

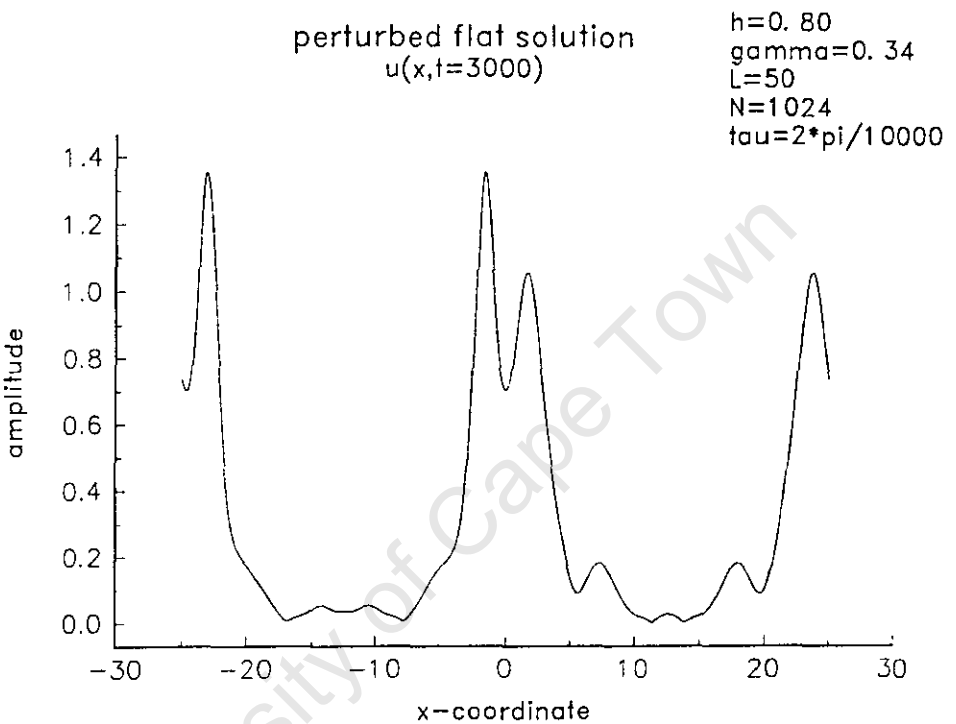

Fig. 10

Double-peaked structures resulting from the decay of the homogeneous solution.

To summarize, the parametrically driven damped NLS was numerically simulated in the neighbourhood of its exact solution. We obtained the attractor chart on the control parameter plane in the domain of the soliton's instability. Regions of the period-doubling and quasiperiodic transitions are found, and the existence of a critical point where the two scenarios meet, is demonstrated. Above the line $h = (1+\gamma^2)^{1/2}$ where the soliton is unstable w.r.t. a continuum of modes excited by parametric pumping, two types of bifurcations occur. In the region situated to the left of curve 1 in Fig. 2 (here instability w.r.t. a local mode is also present, see Fig. 1), the soliton evolves into a spatio-temporally chaotic state, while in the region placed to the right of curve 1 the soliton develops into a cnoidal wave.

We close this section with a few remarks. Our simulations for larger systems ($L = 200$) showed that the main results of this work are insensitive to the change of the interval length.

En passe, we mention that it is only for small γ's ($\gamma = 0.01 - 0.02$) along the line $h = 0.35$ that there is a discrepancy between the results obtained for $L = 200$ and those for $L = 50$. Namely, for this particular h, in larger systems there are solutions describing a wandering type motion of the soliton over a background radiation. Shorter intervals ($L = 50$) exhibit spatio-temporal chaos. For $h > 0.35$ this discrepacy did not arise.

It is interesting to note a striking similarity between the bifurcation sequence arising, for instance, along the line $\gamma = 0.1$ in our system, and the one detected by Nozaki and Bekki [70] in a related equation, the *externally* driven damped NLS. In their case the period-doubling sequence is followed by what Nozaki and Bekki call an attractor crisis (the flat attractor) and then spatio-temporal chaos. Furthermore, the structure of the attractor chart Spatschek *et al* [92] suggested[3] for the externally driven damped NLS, also with the structure of our attractor chart. In both cases, for some γ's ($\gamma \geq 0.17$ for externally driven damped NLS and $\gamma \geq 0.275$ in our case) no period-doubling bifurcations occur and the limit cycle is stable up to the value of h where the solutions become spatially incoherent. Also the reocurrence of a limit cycle after a period-doubling sequence was observed in both cases. The latter phenomenon was detected for $h = 0.245, \gamma = 0.16$ in the externally driven case [92], and $0.813 < h < 0.67$, $0.2525 < \gamma < 0.273$ in our case.

Possibly the most fascinating feature of the parametrically driven, damped NLS is the strength of its solitonic attractor. Even if we start with initial conditions which are far from the unstable ψ_+ soliton (in particular, if we start with the homogeneous solution), we end up with precisely the same asymptotic state as if we started with ψ_+. This is not surprising when h and γ are small and so the system is in the near-integrable limit. However, by no means would one expect that even far from integrability, decay of the unstable soliton and flat solution would produce the same solitonic attractor. Here we refer, for instance, to the results obtained for $(h = 0.7, \gamma = 0.26)$, $(h = 0.7, \gamma = 0.34)$, $(h = 0.7, \gamma = 0.35)$. Thus we are tempted to believe that our main conclusions presented here remain in place even beyond the neighbourhood of the exact soliton solution. However, it is interesting to verify within what limits this assertion is valid. This work is in progress.

In the next sections we discuss several curious phenomena observed in our numerical simulations.

[3]Rigorously speaking, the attractor chart of Ref. 92 is the chart not for the partial differential equation but for a reduced 4-dimensional system. This fact makes the mentioned resemblance even more interesting.

3.2 Period-1 → spatio-temporal chaos transition

In this section we discuss an interesting peculiarity of the transition from the period-1 soliton to the spatio-temporal chaos. This transition occurs upon crossing the line 3 on the attractor chart (Fig. 2). Namely, as we have already mentioned, an *additional* frequency is excited in the spectrum of the oscillating soliton in the vicinity of the curve 3.

We detected this frequency for h *below* the curve 3, i.e. in the region where the attractor is period-1 soliton. Initially we used the temporal step $\tau = 2\pi \times 10^{-3}$ but then verified the results by decreasing τ 10 times.

Figs. 11, a-c show the power spectrum of the oscillating soliton for $\gamma = 0.34$ and $h = 0.993443329$. (The parameters of the numerical scheme here are $L = 50$, $N = 1024$, and $\tau = 2\pi \times 10^{-4}$.) This value of h was chosen close to the onset of the spatio-temporal chaos ($h_{STC} = 0.993443330$.)

Fig.11

Power spectral densities in the period-1 region close to the onset of spatio-temporal chaos ($\gamma = 0.34, h = 0.993443329$). a: $0 \le t \le 500$. b: $500 \le t \le 1100$. c: $2000 \le t \le 2500$.

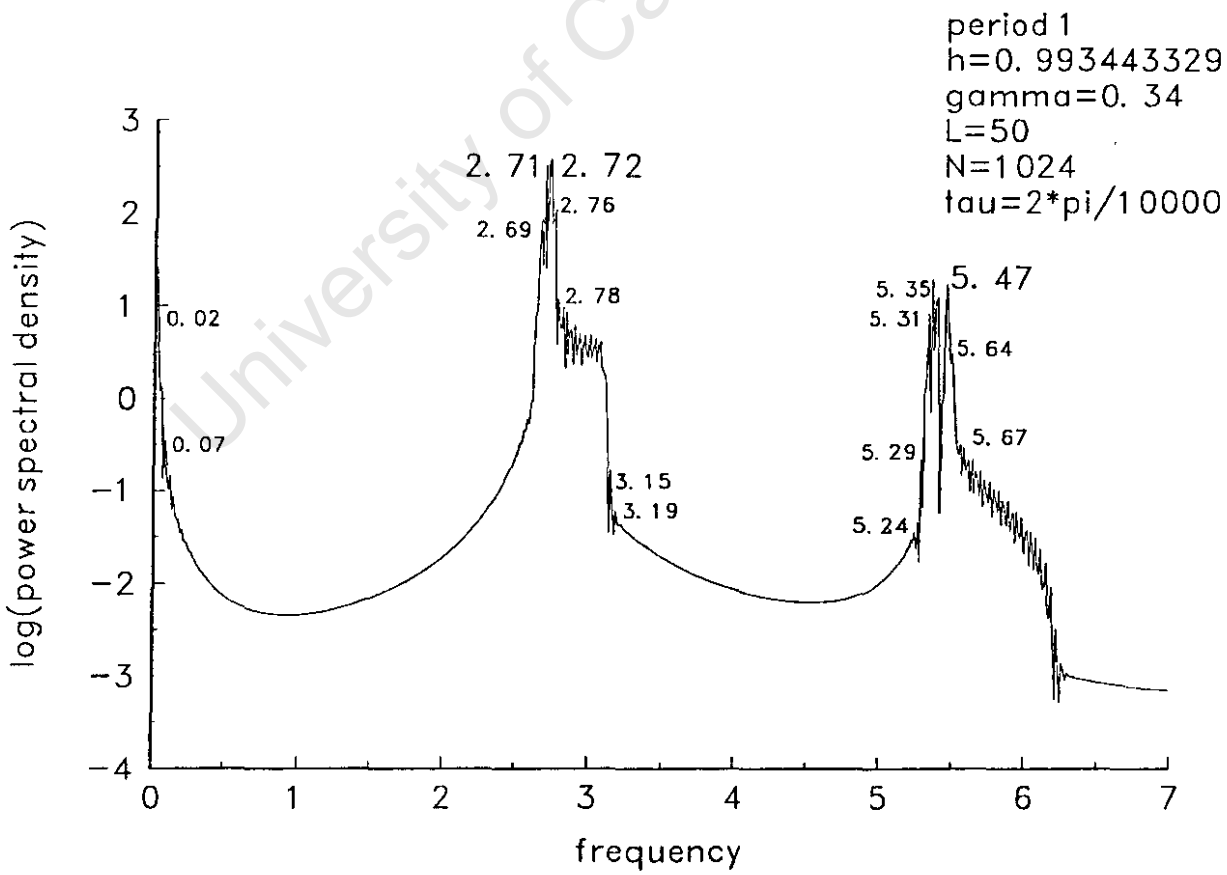

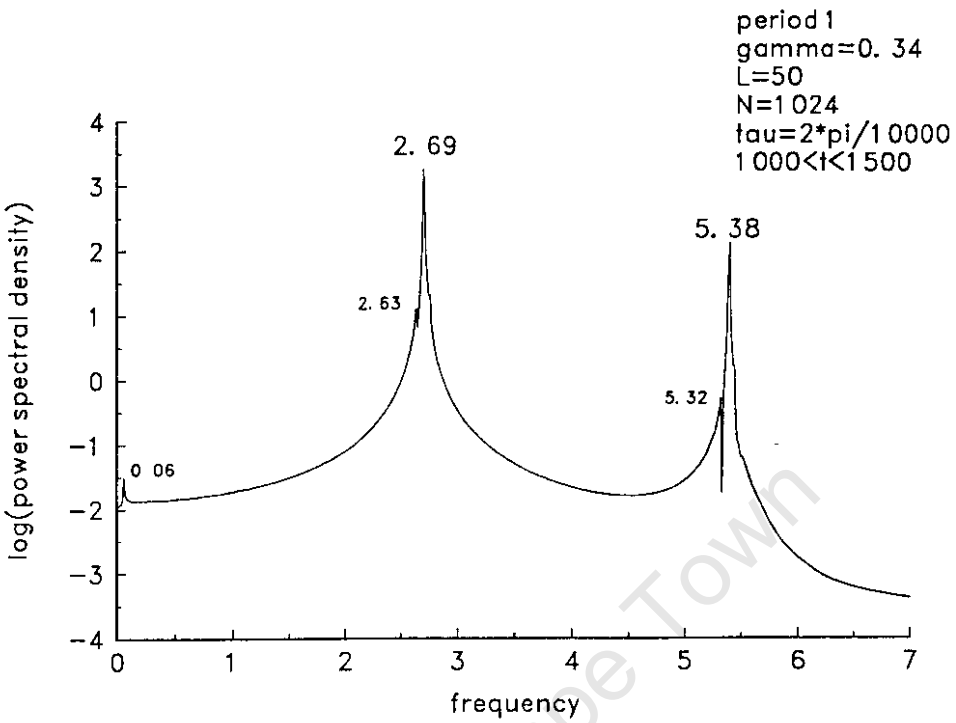

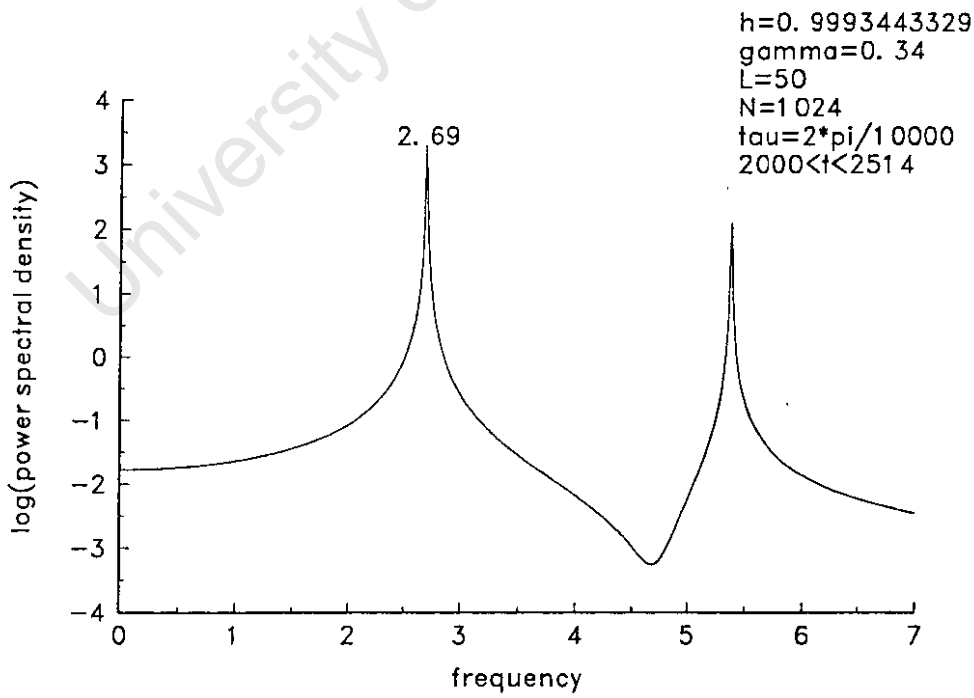

Fig. 11a displays a host of frequencies excited in the temporal interval $0 \leq t \leq 500$, i.e. during the rapid formation of the limit cycle out of the unstable start-off state.

Next, Fig. 11b shows that all these frequencies but one, are short-lived. Here $500 \leq t \leq 1100$. Large peaks in Fig. 11b correspond to the main frequency of the soliton, $\omega_1 \approx 2.69$ and its higher harmonics $2\omega_1, 3\omega_1$ *etc.* In addition to these, clearly seen is the peak at $\tilde{\omega} \approx 0.06$ as well as combinations of $n\omega_1$ and $\tilde{\omega}$. At this stage rapid processes have been over, and the only transient frequency persisting in the spectrum, is $\tilde{\omega} = 0.06$.

Finally, the spectrum of Fig. 11c has been measured for $2000 \leq t \leq 2500$. The $\tilde{\omega}$-oscillation has decayed, and the solution has settled down to the stable limit cycle of frequency ω_1.

We attempted to detect the frequency $\tilde{\omega}$ above the onset of chaos as well. Fig. 12a shows the spectrum of the start-up transient in the spatio-temporal chaotic region. Here $\gamma = 0.34$, $h = 0.993443330$, and the temporal interval is $t = 0$ to $t = 102$. This is the initial stage of instability. The amplitude of soliton's ocillations is small but growing slowly. In this case it takes the instability about the same time to reach the developed stage as in the case of the period-1 solution.

Fig. 12b displays a host of frequencies excited in the temporal interval $102 \leq t \leq 283$ when a configuration resembling a limit cycle is forming out of the the unstable start-off state. At this stage, the amplitude of the soliton's oscillations has become quite large.

Finally, Fig. 12c corresponds to the break up of the soliton and an early stage of the spatio-temporal chaos, with a characteristic continuous power spectrum. The spectrum of Fig. 12c has been measured for $411 \leq t \leq 514$. One can clearly see that all frequencies excited in the spectrum are multiples of $\tilde{\omega}$. The reason why $\tilde{\omega}$ itself is "absent" from the spectrum is simply that the spectral resolution is fairly rough ($\Delta\omega \approx 0.06$ at Fig. 12c).

Fig.12

Power spectral densities in the chaotic region ($\gamma = 0.34, h = 0.993443330$). a: $0 \leq t \leq 102$. *b:* $102 \leq t \leq 283$. *c:* $411 \leq t \leq 514$.

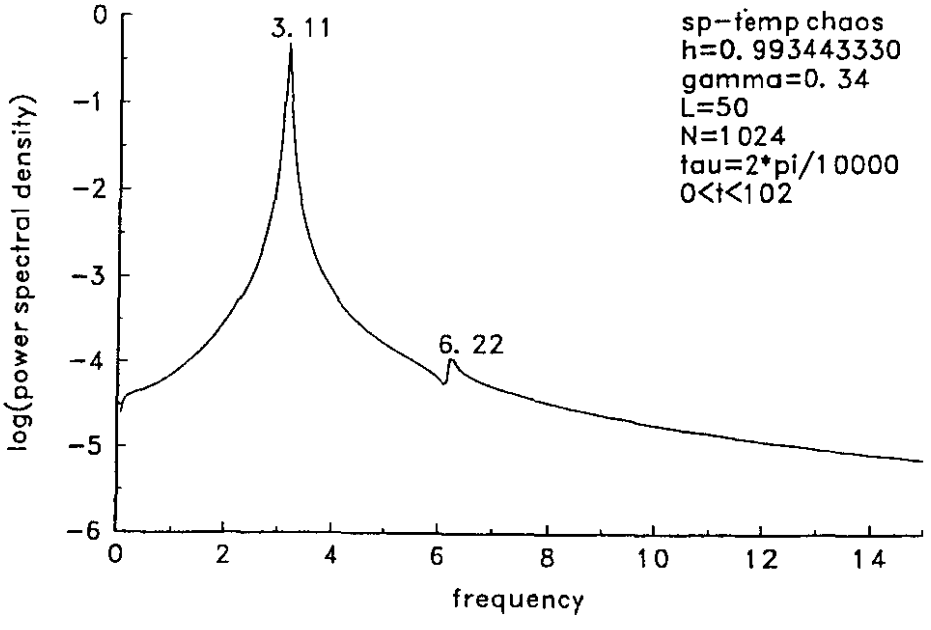

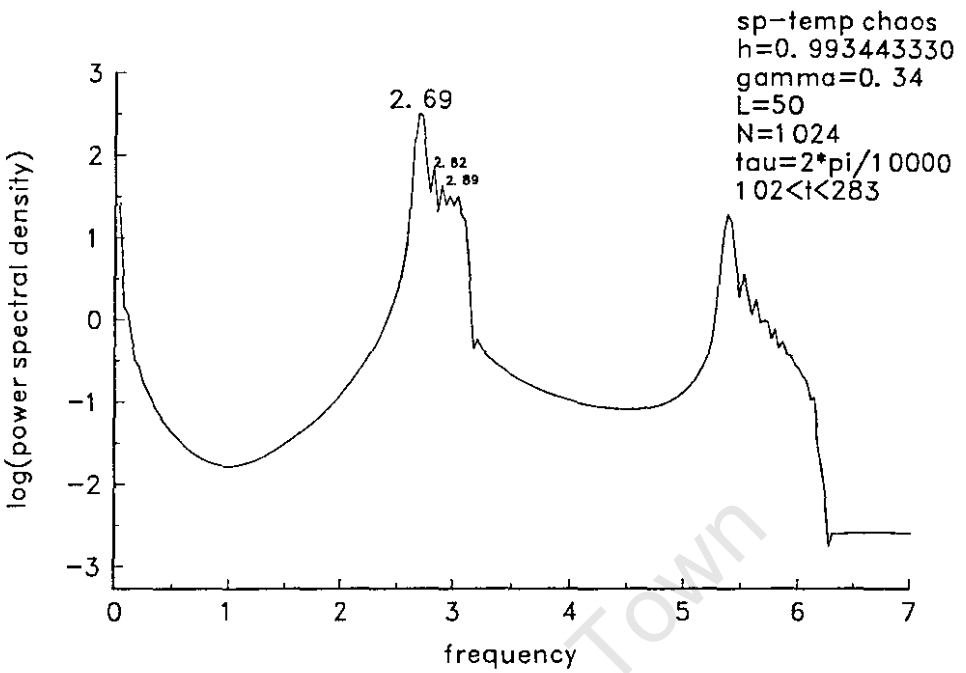

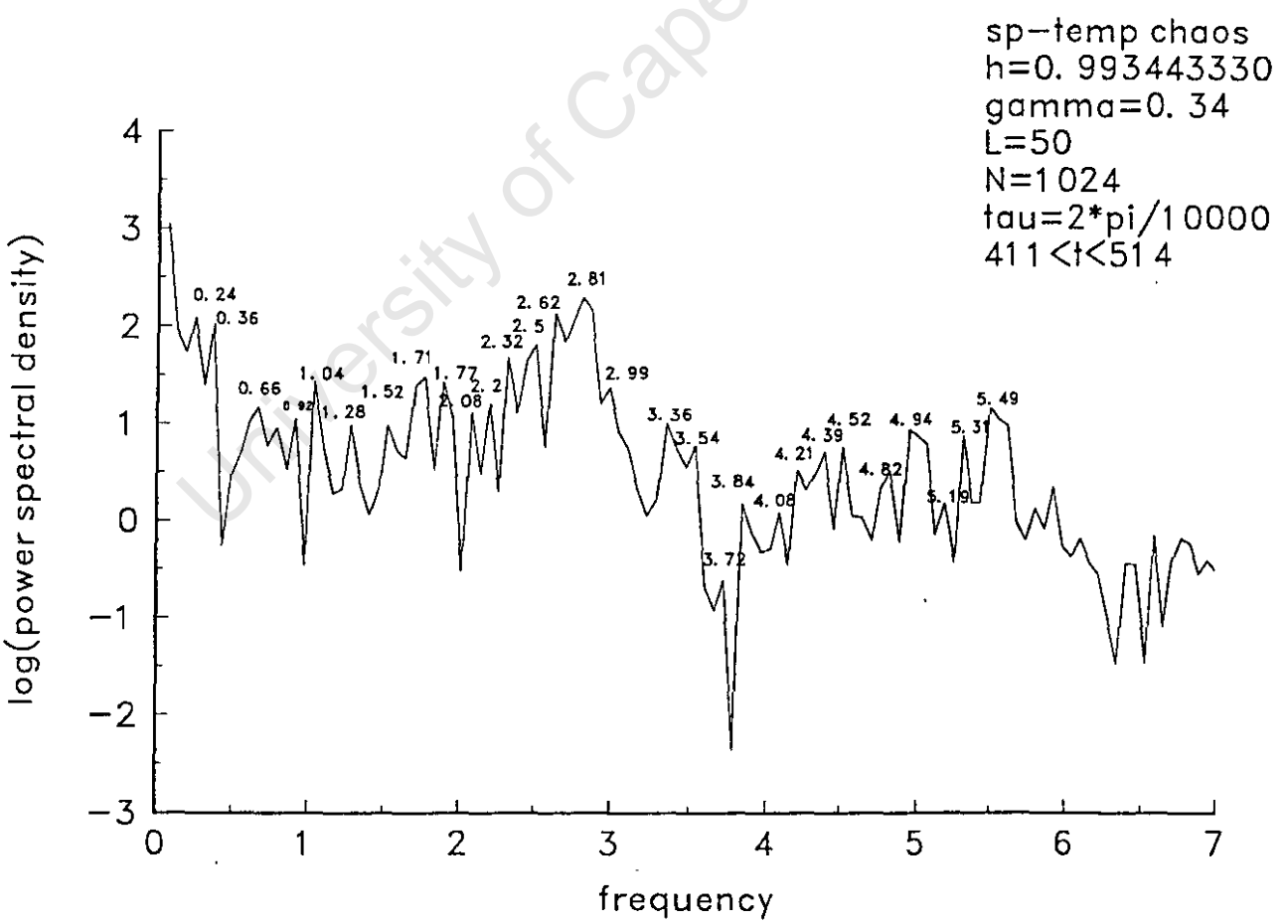

What is the origin of the frequency $\tilde{\omega}$ in the spectrum *below* the curve 3? One possible explanation could be that it results from the circular motion of the radiation over the ring from $x = -L/2$ to $x = L/2$. If this were the case, the frequency $\tilde{\omega}$ would have no relation with the appearance of spatio-temporal chaos. (Indeed, it would have to disappear as we send $L \to \infty$ whereas the chaos survives the increase of the interval length.) However, as we will now demonstrate, this possibility can be ruled out.

The dispersion law for small amplitude linear waves in eq. (2.66) was derived in Sec. 2.3:

$$\omega(k) = [(1+k^2)^2 - h^2]^{1/2}. \tag{3.2}$$

Consequently, radiations with the wavenumber k travel at the group velocity

$$v_{gr}(k) = \frac{d\omega}{dk} = 2\frac{k(1+k^2)^2}{\sqrt{(1+k^2)^2 - h^2}}. \tag{3.3}$$

The radiation wave with the wavenumber $k_n = 2\pi n/L$ will take $T = L/v_{gr}(k_n)$ to travel around the ring of the length L. Assuming that the motion is periodic, we obtain

$$\tilde{\omega}(k_n) = \frac{2\pi}{T} = \frac{4\pi}{L}\frac{k_n(1+k_n^2)^2}{\sqrt{(1+k_n^2)^2 - h^2}}. \tag{3.4}$$

The frequencies for the first few modes are

$$\begin{aligned} \tilde{\omega}(k_1) &= 0.1513976, \\ \tilde{\omega}(k_2) &= 0.1773451, \\ \tilde{\omega}(k_3) &= 0.1920447, \\ \tilde{\omega}(k_4) &= 0.2073937, \end{aligned} \tag{3.5}$$

and so on. The $\tilde{\omega}$'s corresponding to higher wavenumbers will be even larger since, as one can easily verify, $\tilde{\omega}(k) = (2\pi/L)v_{gr}(k)$ is a monotonously growing function of k.

A striking discrepancy between the theoretical values eq. (3.5) and the experimentally observed $\tilde{\omega} = 0.06$, clearly rules out the "circulation of radiation" explanation for the frequency $\tilde{\omega}$.

These results suggest that another, second Hopf bifurcation occurs along the line 3: a pair of complex-conjugate eigenvalues $\lambda = \nu \pm i\tilde{\omega}$ crosses the imaginary axis at $h = h_{STC}$, the threshold of chaos. For values $h < h_{STC}$ the amplitude of the corresponding perturbation $e^{\nu t}$ should decrease e times after the time $t \sim -1/\nu$. Consequently, the transient times should scale as $(h_{STC} - h)^{-1}$ in the vicinity of h_{STC}. The verification of this scaling law will constitute one of the directions of future research.

3.3 The travelling soliton

Another interesting phenomenon was observed for small values of the dissipation coefficient. After several hundreds units of time since the beginning of the simulation, the soliton was seen to start moving steadily over a rapidly oscillating background. This was observed, for instance, for ($\gamma = 0.01, h = 0.087$); ($\gamma = 0.015, h = 0.089$); ($\gamma = 0.02$, $h = 0.08$ and $h = 0.09$). The parameters of these simulations were $L = 50$, $N = 1024$, and $\tau = 2\pi \times 10^{-3}$.

Increasing the spatial interval the motion of the soliton persisted. We have re-examined the case $\gamma = 0.02$, $h = 0.09$ with $L = 200$. (We kept the time step unchanged, $\tau = 2\pi \times 10^{-3}$, and increased N to 4096 so that to preserve the spatial resolution.) The soliton did travel — though its velocity decreased drastically. (For $L = 200$ the velocity was $\sim 10^{-4}$ while for shorter interval $L = 50$ the soliton travelled at $v \sim 0.04$). Therefore one could expect that when $L \to \infty$, the motion will disappear completely. However other runs with the interval $L = 200$ exhibited a very lively soliton; for instance for ($\gamma = 0.02, h = 0.35$) and ($\gamma = 0.01, h = 0.35$)[4] the velocity was ~ 0.2.

It must be emphasized straight away that theoretical studies [114] proved that the parametrically driven damped NLS *does not* possess soliton solutions travelling over the zero background. (The only exception is the undamped case, $\gamma = 0$.) Therefore it is natural to assume that the observed motion is a numerical artefact, and we are now going to demonstrate that this is indeed the case.

From the previous chapter we know that the condition of the instability of the n-th Fourier mode, $e^{ik_n x}$, reads

$$|\cos(\omega_n \tau - \theta)| > \cos(s_n \tau). \tag{3.6}$$

Here

$$\omega_n = |(1 + k_n^2)^2 - h^2|^{1/2}; \tag{3.7}$$

θ and s_n are given by eqs. (2.104) and (2.109). For small τ the right-hand side of (3.6) is close to 1 and so $(\omega_n \tau - \theta)$ must be close to one of the values πm, with m integer. The case $m = 0$ corresponds to the analytic instability for which we have $0 < \omega_n \tau - \theta < s_n \tau$ and so the analytically unstable modes have wavenumbers with $n \leq 40$. On the other hand, $m = 1, 2, \ldots$ pertain to spurious, numerical instabilities. The smallest ω_n (and therefore, the smallest wavenumber k_n) that can be numerically unstable corresponds to $m = 1$:

$$\omega_n \tau - \theta \approx \pi. \tag{3.8}$$

Consequently $\omega_n \tau$ must be greater than π. (θ is positive.) Eq.(3.7) implies then that potentially unstable wavenumbers are only those with $n \geq 178$.

Coming back to our simulations, the travelling soliton was always accompanied by a very rapidly oscillating background (Fig. 13a). In its turn, the appearance of this rapidly

[4]Notice that for $L = 50$ these two sets of h and γ correspond to the spatio-temporal chaos.

oscillating background was always synchronized with the excitation of the *high wavenumber* Fourier modes (Fig. 13b). As we have just mentioned, this implies the *numerical* instability.

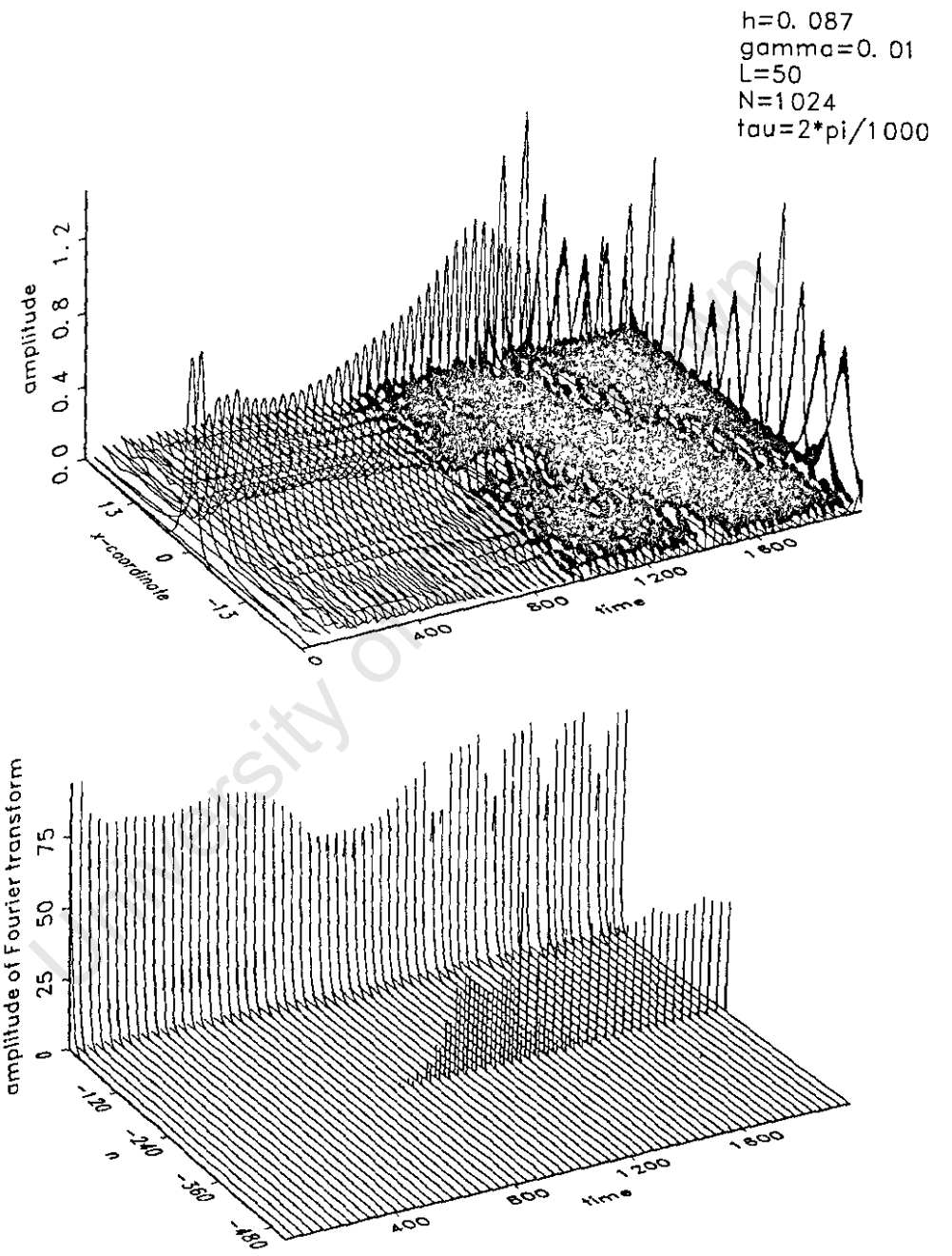

Fig.13

a: Travelling soliton. b: Amplitudes of Fourier modes as functions of time.

Thus, the steady motion of the soliton is a purely numerical artefact: the conservation of momentum forces it to travel against the flow of short wavelength, rapidly oscillating ripples which are excited due to the instability of the scheme. Decreasing the time step, $\tau \to \tau/10$, resulted in that the high wavenumber instability disappeared — together with the steady motion of the soliton.

We must make it clear that we make a distinction between the *steadily travelling* soliton and the soliton that wanders back and forth within some limited interval of x. The latter effect will be discussed in the next section. Here we only mention that the steadily travelling and wandering soliton are different, but not unrelated phenomena. Namely, the fast soliton observed for $\gamma = 0.02, h = 0.35$ and $L = 200$ turned into the wanderer as the temporal step was decreased from $\tau = 2\pi \times 10^{-3}$ (numerically unstable τ) to $2\pi \times 10^{-4}$ (numerically stable τ).

It is probably worth mentioning here that all our results were tested against the numerical instabilities similar to the one described above. We observed that these instabilities set in only for very small γ's. In such instances we have always been able to eliminate them by decreasing τ.

3.4 The wanderer

As we have demonstrated in the previous section, the steady motion of the soliton is a consequence of the numerical instability. This numerical artefact disappears when the temporal step is reduced. In this section we discuss another dynamical effect which *is not* related to the numerical instability. This phenomenon is the *wandering* soliton, and it was observed in simulations with $0.01 \leq \gamma \leq 0.02$, $h = 0.35$, and $L = 200$. The temporal step was chosen to be $\tau = 2\pi \times 10^{-4}$ which prevents the appearance of any numerical instability.

In the case under consideration, the soliton performs irregular walks, back and forth, over a limited spatial interval, see Fig. 14a. (For $\gamma = 0.01$ the interval was $-25 \leq x \leq +27$; for $\gamma = 0.02$ the soliton wandered over $-7 \leq x \leq 2$.) Also seen in this picture is a considerable amount of ripples which are "in thermodynamical equilibrium" with the soliton.

The fact that the observed behaviour is not a numerical artefact, follows from the spatial Fourier spectrum at Fig. 14b. No higher Fourier modes are seen to be excited, and therefore the ripples seen in Fig. 14a do not originate from numerical instabilities.

Fig.14

a: Wandering soliton. b: Time evolution of Fourier amplitudes.
c,d: Creation of ripples and the corresponding evolution of Fourier amplitudes.

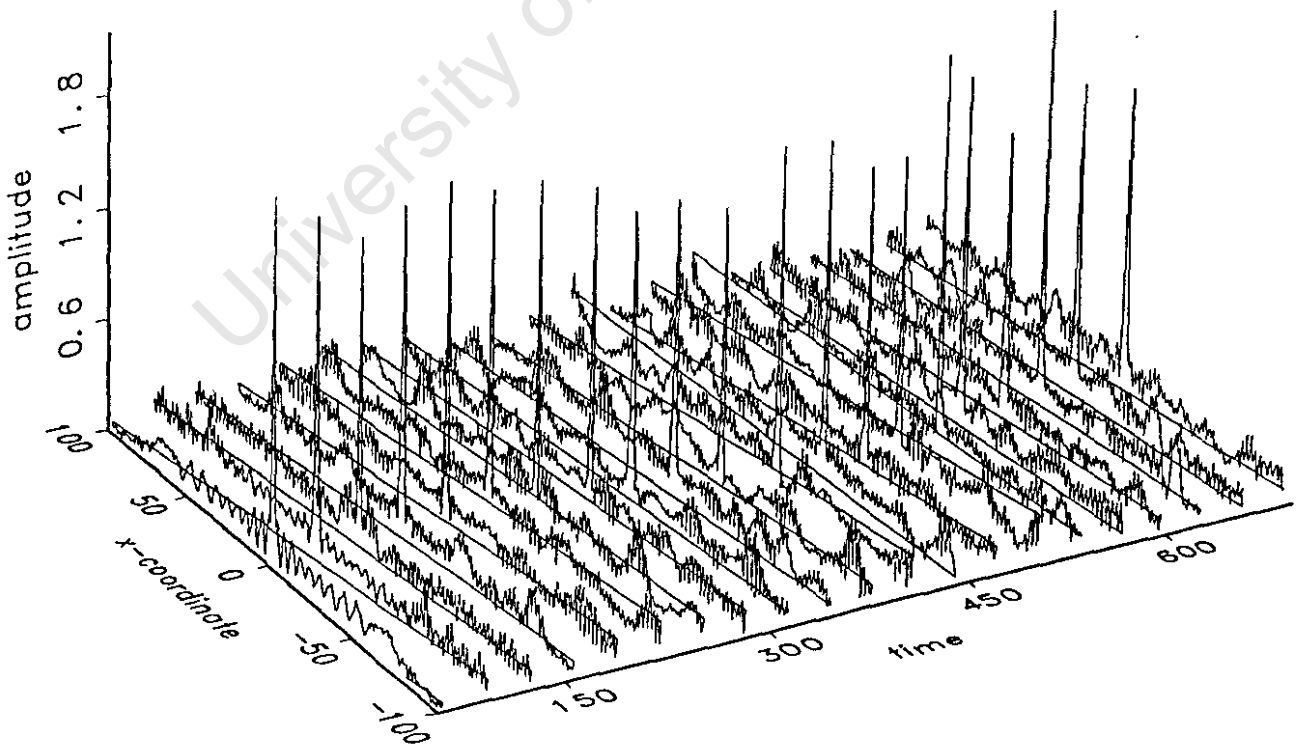

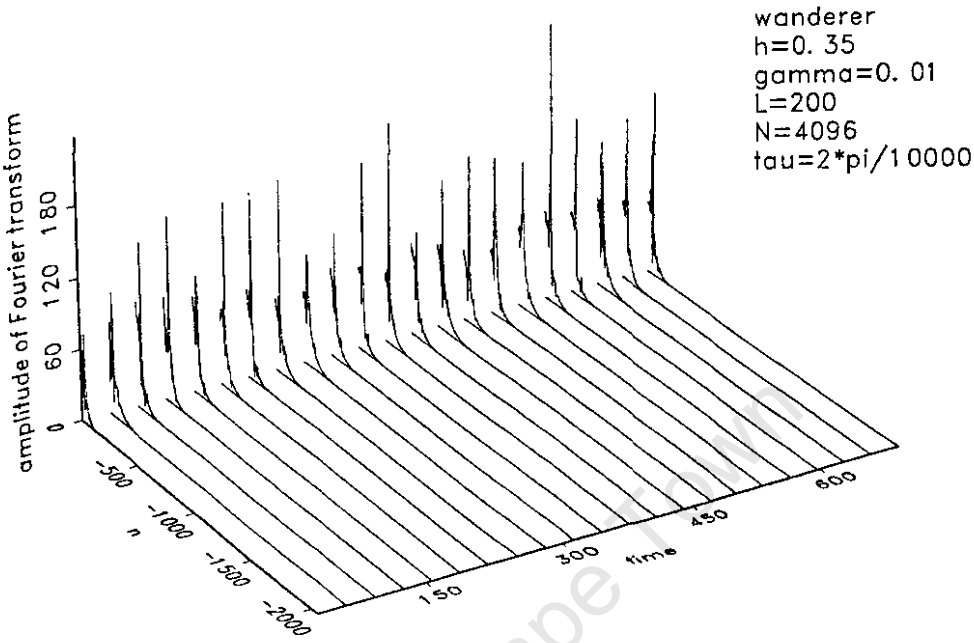

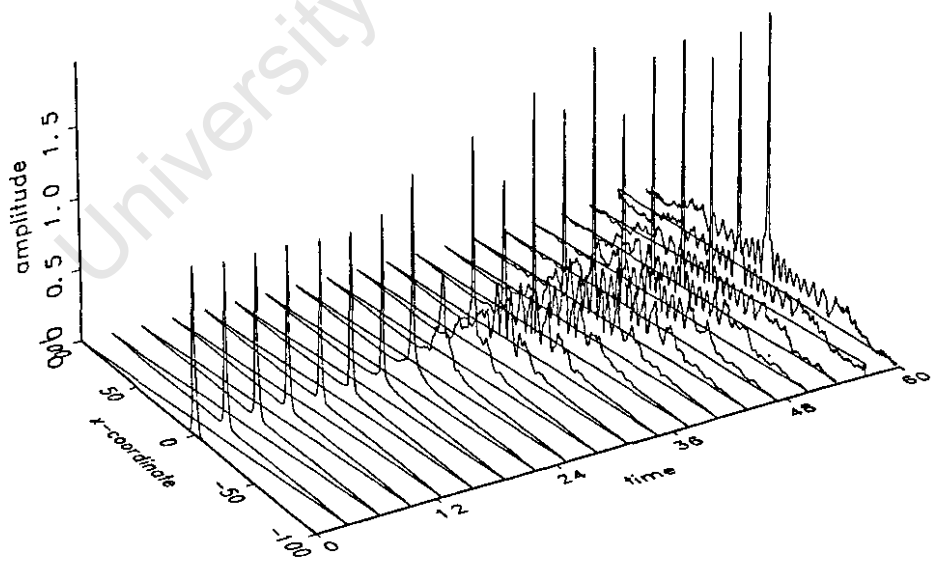

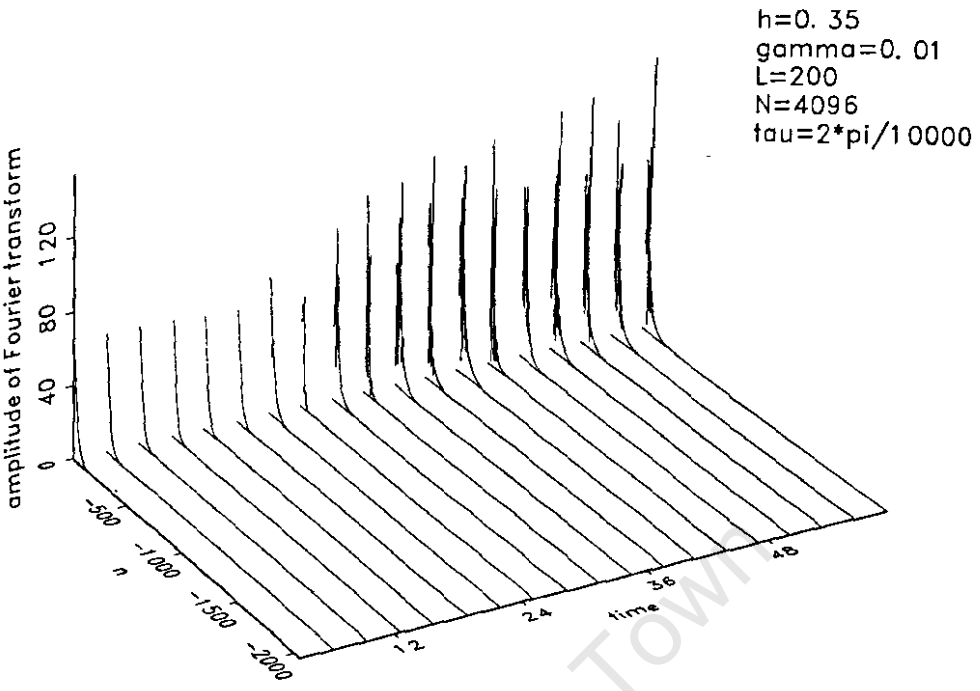

In Fig. 14c we attempt to trace the source of these ripples; it is clearly seen that they originate from the soliton. Fig. 14d shows the evolution of the corresponding Fourier spectrum.

How can these observations be reconciled with the theoretical conclusions on the nonexistence of the moving solitons? The clue is possibly the presence of a large amount of radiation which forms a nontrivial background for the soliton. First of all, it is clear *why* the radiation is so intensive. The reason is that the dissipation coefficient γ is so small in the case at hand that the radiation simply does not have enough time to decay. The linear wave is attenuated exponentially, as $\phi \sim e^{-\gamma t}$. Hence after having travelled around the ring of the length L the amplitude of the wave will be $\sim e^{-\gamma T}$ of its initial value. Here $T = L/v_{gr}$ and $v_{gr} = v_{gr}(k_n)$ is the group velocity of the wave with the wavenumber $k_n = 2\pi n/L$, given by eq.(3.3). For instance, the k_1 harmonic will take $T = 166$ to return to the initial point and so it will be attenuated to $e^{-0.01\times 166} = 19\%$ of its initial value. High wavenumber waves travel faster (recall that v_{gr} is a monotonously growing function of k) and will be even less attenuated. Consequently, the radiation will persist in the system.

A possible explanation of soliton's wandering could be that the system "soliton + intensive radiation" is unstable with respect to small asymmetric perturbations. We plan to come back to the analysis of this instability in future studies.

3.5 Quasiperiodic transition at small γ

The main results of this work proved to be insensitive to the change of the interval length, L. The reason for this is that the length $L = 50$ is sufficient for the emitted radiations to decay and not affect the dynamics on its way back to the soliton. However, as we have already mentioned in the previous section, when the dissipation coefficient γ is small, the attenuation of radiations may be not sufficient and the length L may come into play. In this section we will discuss another anomalous effect that occurs for small γ and therefore may be caused by the finiteness of the interval.

One of our principal results was that there are two scenarios of transition to chaos, period-doubling in the left-hand part of the attractor chart and quasiperiodic in the right-hand part. Surprisingly we have not been able to observe the period-doubling for *very small* γ. In the region of $\gamma \sim 0.01 - 0.035$, increasing h resulted in that the period-1 soliton was suddenly replaced by the zero attractor — instead of becoming 2-periodic. For $\gamma = 0.01$, the driver $h_1 = 0.090890$ supported a period-1 soliton, while at $h_0 = 0.090895$ the attractor was $\phi = 0$. For $\gamma = 0.035$, the period-1 and zero attractors were seen at $h_1 = 0.09885$ and $h_0 = 0.09890$, respectively. (Other parameters: $L = 50$, $N = 1024$, and $\tau = 2\pi \times 10^{-4}$.) It is probably worth mentioning here that for these small γ, same as in the case of quasiperiodic transition occurring at large γ, all transient frequencies but one, are short-lived. The only transient frequency persisting in the spectrum disappears after $t \sim 2000$. (Our simulations with $L = 200$ revealed the same type of bifurcation.)

One explanation for this phenomenon can be that for small γ the finiteness of the interval length becomes very important. We intend to verify this hypothesis in future; here we can only refer to the work of Birnir and Grauer on the (externally) driven sine-Gordon equation [77]. These authors demonstrated that decreasing the interval length, the period-doubling transition is replaced by the quasiperiodic route.

We close this section by emphasizing that this behaviour occurs in a very small range of γ's. For $\gamma = 0.055$, for instance, the transition is already via period doubling. (The period-2 soliton was detected at $h = 0.11$.)

Chapter 4

Conclusions

"The tale of Math is a complex one, and it resists both a simple plot summary and a concise statement of its meaning"
Patrick K. Ford

4.1 Summary

The study results of which are presented in this thesis, consisted of two main parts.

First, we designed a fast numerical algoritm for the simulation of the parametrically driven, damped NLS equation. The algoritm is a split-step pseudospectral method which reduces, when γ and $h \to 0$, to the split-step Fourier scheme of Herbst and Weideman. (The latter is known to be the fastest algoritm for the unperturbed NLS equation.)

We have analysed the stability of the numerical method designed. Similarly to the case of the unperturbed NLS, for certain time steps and spatial resolutions, the method exhibits numerical instabilities which have no analytical counterpart. We have obtained a sufficient criterium for stability which allows one to always avoid numerical instabilities.

After having thoroughly tested the algoritm, we employed it to simulate nonlinear oscillations and chaotisation of the parametrically driven soliton. Results of this simulation comprise the second part of this work. Before proceeding to summarise these results, we would like to mention that the aforementioned numerical instabilities showed up only for very small dissipation coefficients. (We immediately eliminated these instabilities by decreasing the temporal step.)

In our numerical simulations we were mostly interested in the region where the stationary soliton ψ_+ is unstable. Using this soliton as initial condition we found a variety of spatially localised and extended attractors, obtained their quantitative characteristics, and compiled the attractor chart on the (h, γ)-plane. Our principal results here are as follows.

- When γ is smaller than a certain critical value, the increase of h results in the period-doubling transition to chaos. The stable static soliton ψ_+ becomes periodic, then

double-periodic, 4-periodic, and so on; finally, we have a spatially localised solution whose temporal evolution is described by the strange attractor. Increasing h further, the chaotic attractor undergoes a cascade of reverse bifurcations which is followed by the crisis of the attractor. That is, above a certain critical h only the trivial attractor is present, $\psi(x,t) \equiv 0$. The trivial attractor occupies a finite band of h values. If we, however, raise h even further, we find ourselves in the region of spatio-temporal chaos.

- When γ is larger than the aforementoned critical value, there is no period doubling. After the first Hopf bifurcation soliton becomes periodic, and remains periodic in a large band of h values. Increasing h, no other localised states appear; there is no window of the trivial attractor either. Instead, for h greater than a certain h_c a *spatio-temporal* chaotic state sets in.

- Thus we have the coexistence of the period-doubling and quasiperiodic transitions to chaos on the attractor chart. These two scenarios meet at a certain "tricritical point".

- The transition from periodic soliton to the spatio-temporal chaotic state was studied in detail. We were able to detect an additional small frequency which is excited in the spectrum in the immediate vicinity of the transition curve.

- For very small γ's the transition is not via period-doubling but via quasiperiodicity — similarly to the region of large γ's. A possible explanation for this behaviour is related to the finiteness of the interval of integration.

- Other anomalous effects observed include asymmetric instabilities producing wandering solitons and formation of solitonic bound states.

- We examined the region in the (h,γ)-plane where the trivial solution is unstable with respect to the countinuos spectrum excitations. The decay of the unstable soliton resulted in the formation of a cnoidal wave here.

- Finally, we simulated the evolution of the unstable flat solution. In most cases the final product of this evolution was precisely the same as in the case of the solitonic initial condition.

4.2 Possible directions of future research

- It is natural to expect that our results will remain valid for small-amplitude breathers of the parametrically driven, damped Landau-Lifshitz and sine-Gordon equations [88, 58]. In particular, we know that the sine-Gordon equation

$$u_{\tau\tau} + \lambda u_\tau - u_{zz} + (1 - f\cos 2\omega\tau)\sin u = 0 \tag{4.1}$$

with the driving frequency ω such that $1-\omega^2 \equiv \epsilon^2 \ll 1$, reduces [58] to eq. (2.1) with $x = \epsilon z$, $t = \epsilon^2\tau/2$, $h = f/(2\epsilon^2)$, $\gamma = \lambda/\epsilon^2$, and $u(\tau,z) = -4\epsilon \mathrm{Re}\left[\mathrm{i}\phi(\mathrm{t},\mathrm{x})\mathrm{e}^{-\mathrm{i}\omega\tau}\right]$. Note that the length of the sine-Gordon interval of integration, L_{SG}, and the NLS interval

L_{NLS} are related as $L_{SG} = (1/\epsilon)L_{NLS}$. Consequently, our NLS results with $L_{NLS} = 50$ correspond to the integration of the sine-Gordon equation (4.1) with e. g. $\omega = 0.98$ on the interval $L_{SG} \approx 250$.

- At this point, it is interesting to make contact with two closely related systems, namely the *directly* driven sine-Gordon and NLS equations. Different groups reported observations of different scenarios of transition to chaos in these systems [70, 91, 92, 76]. In the case of the driven sine-Gordon in the NLS limit[1] , for instance, Taki *et al* [92] observed the period-doubling route while Bishop *et al* [30] reported the quasiperiodic transition. The difference in the observed scenarios has been generally attributed to the fact that the values of the driver's strength and dissipation coefficient examined in [30] and [92], differ by order of magnitude. Consequently, the question of the interface between the two scenarios did not arise. However transforming the sine-Gordon to NLS as it was done above, one can easily verify that in terms of the NLS control parameters the period-doubling and quasiperiodic transitions occur in a close proximity. (Namely, the line of the period doublings observed in [92] corresponds to $\gamma \approx 0.1$ whereas the quasiperiodic transition of [30] pertains to $\gamma \approx 0.16$.) Therefore finding the mutual arrangement and interface between the regions of the two types of transition on the attractor chart of the above equations becomes an important problem. Figure 2 gives a complete solution to a similar problem in the case of the *parametrically* driven NLS. Given the fact that the two equations have the same mechanism of soliton instability [78, 58], it would be interesting to check whether the period-doubling and quasiperiodic routes meet at a "tricritical" point in the directly driven NLS as well. This work is in progress.

- In their study of the *directly* driven sine-Gordon equation, Grauer and Birnir [77] found that period-doubling bifurcations occur either when the frequency of the driver goes to 1 ($\omega \approx 0.98$) for fixed L ($L_{SG} = 80$) or for fixed ω ($\omega \approx 0.94$ or $\omega \approx 0.96$) letting the length L go to infinity ($L \geq 480$). These results are in agreement with those obtained by Grauer and Kivshar [115] when studying the *parametrically* driven sine-Gordon system. It is interesting to note that in both systems, in terms of the (corresponding) NLS control parameters, the quasiperiodic scenario (which changes to period-doubling when L is increased) occurs at very small γ's. ($\gamma = 0.034$ and $\gamma = 0.05$ correspond to the lines of quasiperiodic transition in the directly driven sine-Gordon, and $\gamma = 0.026$ and $\gamma = 0.03$ correspond to the lines of quasiperiodicity in the parametrically driven sine-Gordon; in both systems, $\gamma = 0.1$ corresponds to the period-doubling when L is fixed.)

  Therefore it would be worthwhile to check whether the quasiperiodic scenario we observed for very small γ's changes to period-doubling route when L is increased beyond $L = 200$. (One may recall that the quasiperiodic scenario survived the increase of L from 50 to 200.) Increasing L we would have a better understanding of the wandering soliton phenomenon as well.

[1] Here, we mention that the data available from various numerical studies indicate that the pattern "quasiperiodicity at very small γ's followed, as γ is increased, by period-doubling and again quasiperiodicity" was observed both in the directly driven NLS [92, 71] and directly driven sine-Gordon equation [77, 92, 30].

- The understanding of the mechanism of instability through which the spatio-temporal chaos sets in, is another aspect which requires further analysis. In Sec. 3.2 we suggested that a second Hopf bifurcation occurs along the line 3 in Fig. 2. If this to be the case the transient times should scale as $(h_c - h)^{-1}$, h_c being the threshold of chaos. The verification of this scaling law requires further research. At this stage it is not clear whether it is the interaction betwen the soliton and radiation that is responsible for this bifurcation, or rather soliton-soliton interaction. Some simulations revealed a very strong soliton-radiation interaction; yet in other cases the spatio-temporal chaos was preceded by the splitting of the soliton into a pair. Finally, we still do not have a satisfactory explanation for the "shark-jaw" shape of the boundary between the regions of the zero attractor and spatio-temporal chaos.

  Therefore, further analysis is necessary. One possible line of attack would be to extract the energetically most dominant modes from the numerically obtained solutions by making use of the so-called Kahunen-Loève expansion. (Using these modes as the variational trial functions, one can construct a simplified low-dimensional model described by ODEs.) Incidentally, we mention that in the case of the parametrically driven sine-Gordon equation studied by Grauer and Kivshar [115], the Kahunen-Loève method showed excellent agreement with direct numerical simulations of the corresponding PDE. In addition, one can make use of the fact that the parametrically driven NLS is integrable for $h = \gamma = 0$ and utilize IST diagnostics to study the marginal modes around the soliton. The radiation modes can then also be related to the Kahunen-Loève modes.

- Last, but not least, it is worthwhile to study in more detail the evolution of the unstable homogeneous solutions. This would allow to realise the limits of applicability of the attractor chart beyond the neighbourhood of the solitonic initial condition.

Appendix A

Discussion on the order of time approximation in the split-step method

In Sec. 2.2 we replaced $e^{i\tau(\mathbf{L}+\mathbf{N}(\psi))}\psi$ by $e^{i\tau\mathbf{L}}e^{i\tau\mathbf{N}}\psi$. One can easily show that our replacement is only first order accurate in time, i.e., it holds true *only* for a first order Taylor series expansion of both sides. Thus, one can write

$$e^{i\tau(\mathbf{L}+\mathbf{N}(\psi))}\psi = e^{i\tau\mathbf{L}}e^{i\tau\mathbf{N}}\psi + \mathcal{O}(\tau^2) \tag{A.1}$$

One way to improve the accuracy of this splitting is to use the approximation

$$e^{i\tau(\mathbf{L}+\mathbf{N}}\psi = e^{i\frac{\tau}{2}\mathbf{N}}e^{i\tau\mathbf{L}}e^{i\frac{\tau}{2}\mathbf{N}}\psi + \mathcal{O}(\tau^3). \tag{A.2}$$

Still, there will be no improvement if the formula (A.1), which advances the solution from one time-level to the next, proves itself not to be at least second order accurate in time.

Now, will shall check to what order eq. (A.1) proves to be accurate.

As in Sec. 2.2, we write our perturbed NLS (2.1) as

$$\psi_t = i\mathbf{L}\psi + i\mathbf{N}(\psi)\psi, \tag{A.3}$$

with

$$\mathbf{N}(\psi)\psi = 2|\psi|^2\psi, \quad \mathbf{L}\psi = \psi_{xx} - \psi - h\psi^* + i\gamma\psi. \tag{A.4}$$

A Taylor expansion of order two of $\psi(x,t)$ around $t = 0$ gives us

$$\psi(x,t) = \psi_0(x) + \psi_1(x)t + \frac{1}{2}\psi_2(x)t^2 + \mathcal{O}(t^3). \tag{A.5}$$

Differentiating (A.5) with respect to t, we get

$$\psi_t = \psi_1 + \psi_2 t + \mathcal{O}(t^2). \tag{A.6}$$

From (A.4) and (A.5) we have

$$\mathbf{N} = \mathbf{N}_0 + \mathbf{N}_1 t + \mathcal{O}(t^2), \tag{A.7}$$

where

$$\mathbf{N}_0 = 2|\psi_0|^2, \quad \mathbf{N}_1 = \psi_0\psi_1^* + \psi_0^*\psi_1. \tag{A.8}$$

Subsituting ψ_t and $\mathbf{N}$ back in (A.3), we obtain

$$\psi_1 = i\mathbf{L}\psi_0 + i\mathbf{N}_0\psi_0, \tag{A.9}$$
$$\psi_2 = i\mathbf{L}\psi_1 + i(\mathbf{N}_0\psi_1 + \mathbf{N}_1\psi_0), \tag{A.10}$$

and then

$$\psi_2 = (i\mathbf{L})^2\psi_0 + i\mathbf{L}i\mathbf{N}_0\psi_0 + i\mathbf{N}_0i\mathbf{L}\psi_0 + (i\mathbf{N}_0)^2\psi_0 + i\mathbf{N}_1\psi_0. \tag{A.11}$$

Thus, we can rewrite (A.5) as

$$\begin{aligned}\psi(x,t) = \psi_0(x) &+ it\Big[\mathbf{L} + \mathbf{N}(\psi_0)\Big]\psi_0(x) \\ &+ \frac{i}{2}t^2\Big[\mathbf{L} + \mathbf{N}(\psi_0)\Big]^2\psi_0(x) + \frac{i}{2}t^2\mathbf{N}_1\psi_0(x) + \mathcal{O}(t^3).\end{aligned} \tag{A.12}$$

On the other hand, we may write

$$\psi(x,t) = e^{it(\mathbf{L}+\mathbf{N}(\psi_0))}\psi_0(x) + \mathcal{O}(t^n), \tag{A.13}$$

with n unknown yet. To find n, we shall expand the right-hand side of (A.13) in Taylor series of order two first and compare it with right-hand side of (A.12) :

$$\begin{aligned}e^{it(\mathbf{L}+\mathbf{N}(\psi_0))}\psi_0(x) = \Big\{\mathbf{I} &+ it\Big[\mathbf{L} + \mathbf{N}(\psi_0)\Big] \\ &+ \frac{i}{2}t^2\Big[\mathbf{L} + \mathbf{N}(\psi_0)\Big]^2 + \mathcal{O}(t^3)\Big\}\psi_0(x).\end{aligned} \tag{A.14}$$

The right-hand side of the two equations (A.12) and (A.14) differ by a term $\frac{i}{2}\mathbf{N}_1\psi_0(x)t^2$. As one may easily check, this term is non-zero and, therefore, $n = 2$.

Thus, it is useless to improve the $e^{i\mathbf{L}t}e^{i\mathbf{N}t}$ approximation for $e^{i(\mathbf{L}+\mathbf{N})t}$ since $e^{i(\mathbf{L}+\mathbf{N})t}$ is itself accurate up to $\mathcal{O}(t^2)$.

Bibliography

[1] Henri Poincaré, *Science and Method.*

[2] G. B. Whitham, *Linear and Nonlinear Waves*, Wiley-Interscience, New York, 1974.

[3] M. Remoissenet, *Waves Called Solitons*, Springer-Verlag, 1994.

[4] G. L. Lamb, *Elements of Soliton Theory*, John Wiley, New York, 1980.

[5] R. K. Dodd, J. C. Eilbeck, J. D. Gibbon, H. C. Morris, *Solitons and Nonlinear Wave Equations*, 1984, Academic Press Inc., London, pp. 501-504.

[6] A. C. Newell, *Solitons in Mathematics and Physics*, SIAM CBMS-NSF Regional Conference Series in Applied Mathematics, 1985.

[7] M. J. Ablowitz and H. Segur, *Solitons and the Inverse Scattering Transform*, SIAM Studies in Applied Mathematics 4, Philadelphia, 1981.

[8] F. Calogero and A. Degasperis, *Solitons and the Spectral Transform*, North-Holland, Amsterdam,1982.

[9] J. M. T. Thompson and H. B. Stewart, *Nonlinear Dynamics and Chaos*, John Wiley and Sons, 1986.

[10] J. Moser, *Stable and Random Motions in Dynamical Systems*, 1973, Princeton University Press: Princeton, NJ.

[11] A. J. Lichtenberg and M . A. Lieberman, *Regular and Stochastic Motion*, 1982, Springer-Verlag: New York, Heilderberg, and Berlin.

[12] V. I. Arnold, *Mathematical Methods of Classical Mechanics*, 1978, Springer-Verlag, New York.

[13] H. L. Swinney and J. P. Gollub, eds., *Hydrodynamic Instabilities and the Transition to Turbulence*, Topics in Applied Physics 45, Springer Verlag, New York, 1981.

[14] J. Guckenheimer and P. Holmes, *Nonlinear Oscillations, Dynamical Systems and Bifurcations of Vector Fields*, Springer-Verlag, 1983.

[15] A. Hasegawa, *Optical solitons in fibers*, 1989 Springer-Verlag.

[16] G. P. Agrawal, *Nonlinear Fiber Optics*, 1989 Academic.

[17] A. C. Newell and J. V. Moloney, *Nonlinear Optics*, 1991 Addison-Wesley.

[18] *Optical Solitons-Theory and Experiment*, 1992 Cambridge Univ. Press, ed. J. R. Taylor.

[19] P. G. deGennes, *Superconductivity of Metals and Alloys*, New York: Benjamin, 1966, ch. 6.

[20] E. O. Brigham, *The Fast Fourier Transform*, Prentice-Hall, Englewood Cliffs, NJ, 1974.

[21] S. D. Conte and C. deBoor, *Elementary Numerical Analysis. An Algorithmic Approach*, third ed., McGraw-Hill, New York, 1980.

[22] C. Canuto, M. Y. Hussaini, A. Quarteroni, T. Zang, *Spectral Methods in Fluid Dynamics*, Springer-Verlag, New York, 1988.

[23] B. Fornberg and D. M. Sloan, *A review of pseudospectral methods for solving partial differential equations*

[24] A. C. Scott, F. Y. Chu, D. W. McLaughlin,*The Soliton: A new concept in applied science*, Proc. IEEE **61** (1973), pp. 1443-1483.

[25] R. Miura, *The Korteweg-de Vries equation, a survey of results*, SIAM Rev. **18** (1976), pp. 412-459.

[26] S. Takeno, In *Nonlinear Coherent Structures in Physics and Biology*, ed. by K. H. Spatschek and F. G. Mertens, NATO ASI Series, series B: Physics, Vol. 329 (1994), pp. 39-50.

[27] B. Holian, H. Flaschka and D. McLaughlin, Phys. Rev. **A24** (1981), p. 2595.

[28] A. Muto, A. Scott and P. Christiansen, Physica **D44** (1990), p. 75.

[29] G. L. Lamb,*Analytical descriptions of ultrashort optical pulse propagation in a resonant medium*, Rev. Mod. Phys. **43** (1971), pp. 99-124.

[30] A. R. Bishop, J. A. Krumhansl and S. E. Trullinger, *Solitons in condensed matter: A paradigm*, Physica **D1** (1980), pp. 1-44.

[31] B. M. Lake, H. C. Yuen, H. Rungaldier and W. E. Ferguson, *Nonlinear deep water waves: theory and experiment, Part 2*, J. Fluid Mech. **83** (1977), pp. 49-74.

[32] H. Hasimoto and H. Ono, *Nonlinear modulation of gravity waves*, J. Phys. Soc. Japan **33** (1972), pp. 805-811.
A. Davey *The propagation of weakly nonlinear wave*, J. Fluid Mech. **53** (1972), p. 769.

[33] D. J. Benney and G. J. Roskes, *Wave instabilities*, Stud. Appl. Math.**48** (1969), pp. 377-385.

[34] A. Davey and K. Stewartson, *On three-dimensional packets of surface waves*, Proc. Roy. Soc. (London) **A338** (1974), pp.101-110.

[35] A. S. Davydov, *The role of solitons in the energy and electron transfer in one-dimensional moleculer systems*, Physica **D3** (1981), pp. 1-22.

[36] V. I. Bespalov and V. I. Talanov, *Filamentary structure of light beams in nonlinear liquids*, JETP Lett. **3** (1966), pp.307-310.

[37] P. L. Kelley, *Self-focusing of optic beams*, Phys. Rev. Lett. **15** (1965), pp. 1005-1008.

[38] V. I. Talanov, *Self-focusing of wave beams in nonlinear media*, JETP Lett. **2** (1965), pp. 138-141.

[39] T. Taniuti and H. Washimi, *Self-trapping and instability of hydromagnetic waves along the magnetic field in a cold plasma*, Phys. Rev. Lett. **21** (1968), pp. 209-212.

[40] N. Asano, T. Taniuti and N. Yajima, *Perturbation method for nonlinear wave modulation,* II., J. Math. Phys. **10** (1969), pp. 2020-2024.

[41] V. I. Karpman and E. M. Kruskal, *Modulated waves in nonlinear dispersive media*, Sov. Phys. JETP **28** (1969), pp. 277-281.

[42] A. Hasegawa and F. Tappert, *Transmission of stationary nonlinear optical pulses in dispersive dielectric fibers*, Appl. Phys. Lett. **23** (1973), pp. 142-144.

[43] F. Tappert and C. M. Varma, *Asymptotic theory of self-trapping of heat pulses in solids*, Phys. Rev. Lett. **25** (1970), pp. 1108-1111.

[44] M. C. Cross and A. C. Newell, *Convection patterns in large aspect ratio systems*, Physica **D10** (1984), pp. 299-329.

[45] C. S. Gardner, J. M. Greene, M. D. Kruskal and R. M. Miura, *Method for solving the Korteweg-deVries equation*, Phys. Rev. Lett. **19** (1967), pp. 1095-1097.
———, *The Korteweg-deVries equation and generalizations.* VI. *Methods for exact solution*, Comm. Pure Appl. Math. **27** (1974), pp.97-133.

[46] J. Scott Russell, *The Modern System of Naval Architecture*

[47] N. J. Zabusky and M. D. Kruskal, *Interaction of "solitons" in a collisionless plasma and the recurence of initial states*, Phys. Rev. Lett. **15** (1965), pp. 240-243.

[48] P. D. Lax, *Integrals of nonlinear equations of evolutions and solitary waves*, Comm. Pure Appl. Math. **21** (1968), pp. 467-490.

[49] V. E. Zakharov and A. B. Shabat, *Exact theory of two-dimensional self focusing and one-dimensional self-modulation of waves in nonlinear media*, Soviet Phys. JETP **34** (1972), pp. 62-69.

[50] V. E. Zakharov and A. B. Shabat, *A scheme for integrating the nonlinear equations of mathematical physics by the method of the inverse scattering problem*, Funct. Anal. Appl. **8** (1974), pp.226-235.

[51] C. S. Gardner, *The Korteweg-deVries equation and generalizations.* IV. *The Korteweg-deVries equation as a Hamiltonian system*, J. Math. Phys. **12** (1971), pp. 1548-1551.

[52] V. E. Zakharov and L. D. Fadeev, *The Korteweg-deVries equation: a completely integrable Hamiltonian System*, Funct. Anal. Appl. **5** (1971), pp. 280-287.

[53] A. Fermi, J. Pasta and S. Ulam, *Studies of nonlinear problems*, Los Alamos Sci. Lab. Rep. LA-1940, 1955; also in Nonlinear Wave Motion, A. C. Newell, ed., Lectures in Applied Mathematics, 15, American Mathematical Society, Providence. RI, 1974, pp.143-196.

[54] M. D. Kruskal, *Asymptotology in numerical computation: Progress and plans on the Fermi-Pasta-Ulam problem*, Proc. IBM Scientific Computing Symposium on Large-Scale Problems in Physics, IBM Data Processing Division, White Plains, NY, 1965, pp. 43-62.

[55] M. D. Kruskal and N. J. Zabusky, *Progress on the Fermi-Pasta-Ulam non-linear string problem*, Princeton Plasma Physics Laboratory Annual Rept. MATT-Q-21, 1963, Princeton, NJ, pp. 301-308.

[56] N. J. Zabusky, *Computational synergetics and mathematical innovation*, J. Comp. Phys. **43** (1981), pp. 195-249.

[57] C. R. Doering, J. D. Gibbon, D. D. Holm and B. Nicolaenko, *Low-dimensional behaviour in the complex Ginzburg-Landau equation*, Nonlinearity **1** (1988), p. 279.

[58] I. V. Barashenkov, M. M. Bogdan, V. I. Korobov, Europhys. Lett. **15** (1991), pp.113-118.

[59] T. B. Benjamin and J. F. Feir, *The disintegration of wave trains on deep water*, J. Fluid Mech. **27** (1967), pp. 417-430.

[60] V. E. Zakharov, *Collapse of Langmuir waves*, Sov. Phys. JETP **35** (1972), pp. 908-914.

[61] V. E. Zakharov and V. S. Synakh, *The nature of self-focusing singularity*, Sov. Phys. JETP **41** (1976), pp. 465-468.

[62] D. J. Benney and A. C. Newell, *The propagation of nonlinear wave envelopes*, J. Math. and Phys. (now Stud. Appl. Math.) **46** (19670, pp. 133-139.

[63] A. Hasegawa and F. D. Tappert, Appl. Phys. Lett. **23** (1973), p. 171.

[64] V. E. Zakharov and A. B. Shabat, Sov. Phys. JETP **34** (1972), p. 62.

[65] K. J. Blow and N. J. Doran, *Non-linear propagation effects in optical-fibers: numerical studies.* In Optical Solitons-Theory and Experiment, 1992 Cambridge Univ. Press, ed. J. R. Taylor.

[66] A. Hasegawa, Appl. Opt. **23** (1984), p. 3302.

[67] L. F. Mollenauer and K. Smith, Opt. Lett. **13** (1988), p. 675.

[68] A. Hasegawa, M. Matsumoto, T. Yano and Y. Kodama, *Chaos and self-organization in optical solitons in fibers.* In *Nonlinear Coherent Structures in Physics and Biology*, ed. by K. H. Spatschek and F. G. Mertens, NATO ASI Series, series B: Physics, Vol. 329 (1994), pp. 335-341.

[69] K. Nozaki, Phys. Rev. Lett. **49** (1982), p. 1883.
K. Nozaki and N. Bekki, Phys. Rev. Lett. **50** (1983), p. 1226.

[70] K. Nozaki and N. Bekki, *Solitons as attractors of a forced dissipative nonlinear Schrödinger equation*, Phys. Lett. **A102** (1984), pp. 383-386.
———, *Low-dimensional chaos in a driven damped nonlinear Schrödinger equation*, Physica **D21** (1986), pp. 381-393.

[71] Th. Eickermann, R. Grauer and K. H. Spatschek, Proc. Conf. Lyngby; Phys. Lett. **A198** (1995), pp.383-388.

[72] D. J. Kaup and A. C. Newell, Phys. Rev. **B18** (1978), p.5162.

[73] D. J. Kaup and A. C. Newell, Proc. Roy. Soc. (London) **A361** (1978), p. 413.

[74] N. Ercolani, M. G. Forest and D. W. McLaughlin, *Geometry of the modulational instability*, Univ. of Arizona, preprint 1986.

[75] J. P. Eckmann and D. Ruelle, Rev. Mod. Phys. **57** (1985), p. 149.

[76] G. Terrones, D. W. McLaughlin, E. Overman and A. Pearlstein, SIAM J. Appl. Math. **50** (1990), p. 791-818.

[77] R. Grauer and B. Birnir, Physica **D56** (1992), pp. 165-184.

[78] I. V. Barashenkov, M. M. Bogdan and T. Zhanlav. In *Nonlinear World:* IV *International Workshop on Nonlinear and Turbulent Processes in Physics, Kiev, October 1989*, ed. V. G. Bar'iakhtar *et al.* (World Scientific, Singapore) 1990, Vol. **1**, p. 3.

[79] V. E. Zakharov, V. S. L'vov and S. S. Starobinets, Sov. Phys. Uspekhi **17** (1975), p. 896.

[80] J. W. Miles, J. Fluid Mech. **148** (1984), p. 451.

[81] J. Wu, R. Keolian and I. Rudnick, Phys. Rev. Lett. **52** (1984), p. 1421.

[82] E. W. Laedke and K. H. Spatschek, J. Fluid Mech. **223** (1991), p. 589.

[83] G. Wysin and A. R. Bishop, J. Magn. and Magn. Mater. **54-57** (1986), p. 1132.

[84] H. Yamazaki and M. Mino, Progr. Theor. Phys. Suppl. **98** (1989), p. 400.

[85] V. E. Zakharov, S. L. Musher and A. M. Rubenchik, Phys. Rep. **129** (1985), p. 285.

[86] N. Yajima and M. Tanaka, Progr. Theor. Phys. Suppl. **94** (1988), p. 138.

[87] M. V. Goldman, Rev. Mod. Phys. **56** (1984), p. 709.

[88] M. M. Bogdan, A. M. Kosevich and I. V. Manzhos, Sov. J. Low Temp. Phys. **11** (1985), p. 547.

[89] C. Vanneste, A. Gilabert, P. Sibillot and D. B. Ostrowsky, J. Low Temp. Phys. **45** (1981), p. 517.

[90] G. Cicogna and L. Fronzoni, Phys. Rev. **A42** (1990), p. 1901.

[91] A. R. Bishop, M. G. Forest, D. W. McLaughlin and E. A. Overman II, Physica **D23** (1986), p. 293; A. Mazor, A. R. Bishop and D. W. McLaughlin, Phys. Lett. **A119** (1986), p. 273; A. Mazor and A. R. Bishop, Physica **D27** (1987), p. 269.

[92] M. Taki, K. H. Spatschek, J. C. Fernandez, R. Grauer and G. Reinisch, Physica **D40** (1989), p. 65.
K. H. Spatschek, H. Pietsch, E. W. Laedke and Th. Eickermann. In: *Singular Behaviour and Nonlinear Dynamics.* T. Bountis and St. Pnevmatikos, Eds. World Sci. (1989).

[93] M. Bondila, I. V. Barashenkov and M. M. Bogdan, Physica **D87** (1995), pp. 314-320.

[94] J. W. Miles, SIAM J. Appl. Math., **41** (1981), pp.227-230.

[95] B. M. Herbst, J. Ll. Morris and A. R. Mitchell, J. Comp. Phys., **60** (1985), pp. 282-305.

[96] B. M. Lake, H. C. Yuen, H. Rungaldier and W. E. Ferguson, J. Fluid Mech., **83** (1977), pp. 49-74.

[97] F. D. Tappert, AMS Lecture Notes in Appl. Math., **13** (1974), pp. 215-216. See also R. H. Hardin, F. D. Tappert, SIAM Rev., Chronicle **15** (1973), p. 423.

[98] J. M. Sanz-Serna, J. Comp. Phys., **52** (1982), p. 273.

[99] J. M. Sanz-Serna and V. S. Manoranjan, J. Comp. Phys., **52** (1983), pp. 273-289.

[100] M. Delfour, M. Fortin and G. Payre, J. Comp. Phys., **44** (1981), pp. 277-288.

[101] D. F. Griffiths, A. R. Mitchell and J. Ll. Morris, Comp. Methods in Appl. Mech. and Eng., **45** (1984), pp. 177-215.

[102] B. M. Herbst, A. R. Mitchell and J. A. C. Weideman, J. Comp. Phys., **60** (1985), pp. 263-281.

[103] J. M. Sanz-Serna, Math. Comp., **43** (1984), pp. 21-27.

[104] A. R. Mitchell and J. Ll. Morris, Arab Gulf Journal of Scientific Research, **1** (1983), pp. 461-472.

[105] J. A. C. Weideman and B. M. Herbst, SIAM J. Sci. Stat. Comput., **8** (1987), pp. 988-1004.

[106] Y. Tourigny and J. Morris, J. Comp. Phys., **76** (1988), p. 103.

[107] Z. Fei, I. Martin, V. Perez-Garcia, F. Tirado and L. Vazquez. In *Nonlinear Coherent Structures in Physics and Biology*, ed. by K. H. Spatschek and F. G. Mertens, NATO ASI Series, series B: Physics, Vol. 329 (1994), pp. 287-298.

[108] T. R. Taha and M. J. Ablowitz, J. Comp. Phys., **55** (1984), pp. 203-230.

[109] G. S. Patterson Jr. and S. A. Orszag, Phys. Fluids, **14** (1971), pp. 2538-2541.

[110] J. A. C. Weideman and B. M. Herbst, SIAM J. Numer. Anal., **23** (1986), pp. 485-507.

[111] B. Fornberg and G. B. Whitham, Phil. Trans. Roy. Soc. Lond. **289** (1978), pp. 373-404.

[112] I. V. Barashenkov, M. Bondila and M. M. Bogdan, to be published

[113] M. M. Bogdan, private communication.

[114] A. Harin and I. V. Barashenkov, to be published

[115] R. Grauer and Y. Kivshar, Phys. Rev. **E48** (1993), pp. 4791-4800.

[116] B. A. Malomed, Phys. Rev. **E47** (1993), pp. 2874-2880.

[117] Y. Kivshar and B. A. Malomed, Rev. Modern Phys. **61** (1989), pp. 763-915.